STRUCTURAL DETERMINATION AND PHYSICO CHEMICAL STUDIES OF ZEOLITES

A Thesis
Submitted to

THE SWAMY RAMANAND TEERTH MARATHWADA

UNIVERSITY, NANDED

For the degree of

DOCTOR OF PHILOSOPHY

(IN PHYSICS)

By

K.U.GORE

DEPARTMENT OF PHYSICS

N.S.B.COLLEGE

NANDED

JULY-2001

DEDICTED TO MY BELOVED MOTHER

SHREEMATI DEOBAI UMAJIRAO

CERTIFICATE

Certified that the work incorporated in this thesis entitled "Structural Determination and Physico Chemical Studies of Zeolites" submitted by Mr. K U Gore for the degree of Doctor of Philosophy was carried out by the candidate under our supervision in the National Chemical Laboratory, Pune. Such material as has been obtained from other sources has been duly acknowledged in the thesis.

Dr. S G Hegde.
(Research Guide)

Dr. P L Kadam.
(Research Guide)

Declaration Statement

The work presented in this thesis was carried out by me in the Catalysis Division, National Chemical Laboratory, Pune under the guidance of Dr.S.G.Hegde, Scientist, Catalysis Division, and Dr P.L.Kadam, The Department of Physics,Yeshwant College, Nanded.

The experimental work, observations and interpretations of the data in connection with the studies are entirely my own. Such material as has been obtained from other sources has been duly acknowledged in the thesis.

The work reported in this thesis is original and has not been submitted in part or full for any degree or diploma to any other University or Institution.

K.U.GORE

(UGC Teacher Fellow)

ACKNOWLEDGEMENT

It gives me great pleasure in offering my deep sense of gratitude and indebtedness to my revered guides Dr.P L Kadam, Department of physics, Yeshwant College, Nanded and Dr. S G Hegde, Scientist, Catalysis Division, National Chemical Laboratory, Pune. It was a turning point in my life to get an opportunity to work in NCL with Dr.S G Hegde. The constant enthusiasm for research inspite of their busy schedule and an eye for perfection always kept me on my tows and made me explore newer and newer avenues in research. The inspiring guidance, keen interest and commitment to my work and constant encouragement and support all the time from them will be always remembered by me.

It is my pleasant duty to express my deep gratitude to Dr.S.Ganapathy, Head of the NMR group in NCL. In addition to invaluable scientific discussions and teachings, what touched me was his warm and caring personality at all the times of ups and downs, and was a moral booster for my present work. I have immensely benefited by his guidance during the present investigation.

I am indebted to Dr.A V Ramaswamy, Head of the Catalysis Division, NCL for his constant encouragement and co operation in completing this work successfully.

I wish to put my deep sense of gratitude to Dr.B S Rao for the valuable guidance, help and encouragement in my research work.

Dr.S Sivasanker, Dr.M K Dongare, Dr.S P Mirajker, Ms.M S Agashe, Dr.Mrs.V Ramaswamy, Dr.D Shrinivas, Dr.C V V Satyanarayan, Dr.H S Soni, Dr.Mrs A J Chandwadker, Mrs N E Jacob, Dr.Mrs.A A Belhekar, Dr.Ms S V Awate, Dr.P N Joshi Mr.G D Shahapure, Dr.Ms S S Deshpande, Dr.Mrs.M P Degaonkar, Dr.R A Sheikh, Dr.U R Kalkote, Dr.B M Bhaval and Dr.N P Argade have all helped me very much in completing this work successfully. I wish to thank them gratefully. I also thank T A B Mulla and all other scientific staff of Catalysis Division.

Financial assistance from The University Grants Commission, New Delhi, in the FIP 9th plan programme in the form of the award of teacher fellowship is gratefully acknowledged .It has helped me to achieve my dream of this challenging work in to reality.

I wish to put on the record the word of appreciation for the understanding, and encouragement offered by my wife Sangeeta, my children, brothers, sisters and other family members. My thanks are to my relatives Prof. J S Jadhav, Mr. S D Rasve, and Mrs. Nanda Rasve for their help on various occasions during my stay at NCL.

The help and support received from Dr. Janardhan Waghmare Ex.Vice Chancellor of my university, Dr.G D Deshpande, Exe. Principal of my College in my endeavor will always be remembered. My thanks are also to Dr.D P Vaidya, present Principal, Prof. C K Joshi,
Prof S P Pachling and other colleagues of my college for their whole hearted co-operation during the course of this work.

My Special words of thanks and admiration are due to my co-researchers Balakrushna Tope, R.Anand and Anuji Abraham whose helpful willing co-operation and cheerful company and sober attitude made my research tenure enjoyable. Thanks are also due to my other co-researchers Dr.D P Sabde, Rajaram Bal, Sivanand, Damodharan, Raina, Bennur, Tapas Sen, Vijay, Sharda, Monica, Suresh, Shiju, Shetty, Thomas, Gote, and the staff Manna Katti, Madhu and other staff and students of Catalysis Division.

It is my honor to gratefully acknowledge Dr.Paul Ratnasamy, Director, National Chemical Laboratory for giving me this opportunity to work in such internationally famous institute and for permitting me to present this work in the form of thesis.

K U GORE

CONTENTS

CHAPTER 1

1. INTRODUCTION

Zeolites have attracted widespread attention in scientific field as well as in industrial applications. It is a dynamic and rapidly growing field involving different branches of science like crystallography, theoretical physics, catalysis, inorganic, organic, physical, colloidal and biochemistry, environmental science, mineralogy, geology and oceanography. Zeolites are fascinating class of solids, which have played key role in the vigorously growing impact on the world economy in the twentieth century.

1.1: Zeolites

Zeolites are crystalline hydrated aluminosilicates having rigid three-dimensional infinitely extended framework structure. It encloses the cavities and channels of molecular dimensions. The framework structures are built from corner sharing of all four oxygens of the $[SiO_4]^{4-}$ and $[AlO_4]^{5-}$ tetrahedra as the primary-building units. The general empirical crystallographic unit cell formula of zeolite is expressed as (1)

$$M_{x/n}\,[(AlO_2)_x\,(SiO_2)_y]\,z\,H_2O$$

Where M is charge compensating cations of valence n, x and y represent the number of mols of AlO_2 and SiO_2 respectively, where $y \geq x$ and z is the number of water molecules. The Si-O bond in silicate tetrahedron has 50% covalent character and the bond is very much short (1.62 Å). Therefore even at standard temperature and pressure and easily in hydrothermal conditions, these tetrahedra can share vertices to form large varieties of polymeric zeolite structures. The $[AlO_4]^{-5}$ tetrahedron is also isostructural with $[SiO_4]^{-4}$ units and Al-O bond length is 1.75 Å. The most of the natural zeolites are aluminum isomorphs. Therefore zeolite is one of the most interesting classes of tectosilicate having open framework in which $[AlO_4]^{-5}$ is partially substituted for $[SiO_4]^{-4}$ in silicate polymorph. In nature, Al substitution up to an S i/ Al ratio of about 1:1 is observed. Al avoids Al-O-Al bonds as per Loewenstein's rule (2), therefore Al substitution generally does not occur below the ratio of 1:1.

1.2: Classification of Zeolites

Zeolites have been classified on the basis of their morphological characteristics (3), crystal structure (4), chemical composition (3), effective pore diameter (5) and natural occurrence (3). The classification of zeolites on the basis of morphology was

made initially by Bragg(6). On the basis of effective pore diameters they can be classified as

i. Small pore zeolites (diameter, d < 5 Å)
ii. Medium pore zeolites (d = 5.0-6.5 Å)
iii. Large pore zeolites (d = 6.5° A – 13.0 Å)
iv. Extra large pore zeolites (d =13.0-20 Å)
v. Mesoporous zeolites (d = 20.0-100 Å)

These pore openings are made up of 8-, 10-, 12-, 14-, 18-, and 24-membered oxygen rings and for mesoporous materials, the structure is not yet known. Table -1.1 represents some of the examples.

Zeolites are also classified on the basis of silica: alumina ratio (5) as follows.

i) Low Si: Al ratio, between 1 and 1.5 like Zeolite A, X and Sodalite.
ii) Intermediate Si: Al ratio, between 2 to 5 like Zeolite Y, L, Mordenite and Omega.
iii) High Si: Al ratio from 10 to several thousands like highly siliceous variants of Y, Erionite, Mordenite prepared by thermo chemical framework modifications, like EU-1, EU-2, ZSM-11, ZSM-5, ZSM-23, ZSM-48 prepared by direct synthesis and pure silica polymorphs, Silicalite-1 and Silicalite-2.

The Classification of zeolites according to structure types was also reported (4) as shown in the table-1.2.

Recently, Wilson et. al. (7) have reported a new class of molecular sieves called aluminophospate ($AlPO_4$) containing equal moles of Al^{3+} and P^{5+} ions in the lattice. Davis *et.al* (8) have discovered a new $AlPO_4$- type, 18 membered ring, large pore molecular sieve designated as VPI-5 having a pore diameter of 12 Å. Esterman et al (9) reported gallophosphate molecular sieve with a pore diameter of 29-30°Å. Most recently, a germanium silicate molecular sieve with 24-ring has also been discovered (10). The metal substitution in the aluminophosphate (MeAlPO) such as Si, Ti, V, Fe, Mg, Ga, Co, Zn, Mo and Cr have also been reported by different authors (11-13).

Table 1.1: Classification based on effective pore opening size of oxygen ring

Small Pore, 8-ring	Intermediate Pore, 10- ring	Large Pore, 12-ring	Extra large pore, 14-, 18-, and 24-ring.	Mesoporous Zeolites
Li-A	Dachiardite	Cancrinite	Cloverite,	MCM-41
Chabazite	Epistilbite	LindeX,Y,L	FDU-4	
Erionite	Ferrierite	Gmelinite		
ZK-5	Haulandite	Mazzite		
Linde-Y	Laumontite	Mordenite		
Natrolite	ZSM-5	Offretite		
Phillipsite	ZSM-11			
Rho	Stilbite			
Thomsonite				

Table -1.2: Classification of zeolites according to structure types

Structure type	Main representative species	Isostructural Species
Analcime group, Inter-connected 4- and 6-ring, ANA	Analcime	Ca-D, Na-B, Leucite, Viseitite, Pollucite
Natrolite group, fibrous, weakly cross linked chains of tetrahedra, NAT EDI,	Natrolite, Edingtonite Thomsonite	Mesolite, Scolecite, K-F Gonnardite
Chabazite group, Parallel 6-, 6-6-ring, CHA, ERI, LTL, SOD	Chabazit, Erionite, Linde-L Sodalite	Linde-D, Linde-R etc.
Phillisite group: Parallel 4-ring, PHI, ABW, MER	Phillipsite, Li-A, Merlinoite	Harmotome, Wellsite, ZK-19, $CsAlSiO_4$, $RbAlSiO_4$, K-M, Linde-W
. Heulandite group: 4- 5- rings, HEU, STI	Heulandite, Stilbite	Clinoptilolite, Barrerite, Desmine, Stellarite
Moredinite group: Each – Tetrahedron of the framework belongs at least one 5- ring. MOR, FER	Mordenite, Ferrierite	Na-D, Ptilolite, Zeolon. Sr-D, ZSM-21, ZSM-35
Faujasite groups,framework based on polyhedral cages of cubic or near cubic Symmetry FAU	Faujasite	. Linde-X, Linde-Y, ZSM-20
Lamontite group; LAU	Lamontite	Lconhardite
Pentasil group, MEL, MFI	ZSM-11, ZSM-5	
Clathrate group, MEP, MTN	Melanophlogite, ZSM-39	

1.3: Nomenclature

The international zeolite association structure commission and IUPAC have decided the structural codes to the synthetic and Natural zeolites (3,4). Designation consists of three capital letters, which are used to identify structure types. These codes are decided on the basis of the types of species and not on the number or composition, distribution of tetrahedral atoms (e.g., Ti, Be, Ge, Ga, P etc), cell dimensions or symmetry. Few of the examples (4,14) are given in the table-1.3.

1.4:Isomorphous Substitutions

The replacement of tetrahedral silicon or aluminum atoms by other elements is an interesting aspect of zeolites. Goldsmith reported first time, the isomorphous substitution in the zeolite framework in 1952 in the synthesis of Germanium containing thomsonite, in which Ge replaced Si in the lattice (15). The isomorphous substitution of tri, tetra and pentavalent ions like P^{5+}, Ge^{4+}, Fe^{3+}, Ti^{4+}, B^{3+}, Mo^{5+}, Ga^{3+}, $V^{4+/5+}$, Sn^{2+}, Cr^{5+} in various zeolite framework has been reported. The isomorphous substitution can be performed either during the primary synthesis (16-46), and post synthesis methods also have been used to incorporate Ti^{4+}, Ga^{3+}, Fe^{3+}, $V^{4+/5+}$ in to the zeolite framework (47-60).

Pauling predicted the possibility of isomorphous replacement and stability of the metal cations into the tetrahedral framework of the zeolite. According to this theory (55), metal cations having ρ (ρ = r_c /r_o, where r_c is the radius of cation and r_o is the radius of the oxygen) in the range of 0.225-0.414 are stable in the tetrahedral framework. Values of Pauling criteria for some of the metals are given in the table-1.4 .

If the cation for which ρ is out of the range of the possibility of lattice substitution or tetrahedral co-ordination, then as per Pauling's theory, substitution of it in the zeolite framework is not possible or takes place only on a limited scale.

1.5: Some Potential Applications of Zeolites

Zeolite molecular sieve is probably the most outstanding example of any framework structure, which is useful in diversity of purposes, in very simple to highly challenging circumstances. Some important applications of zeolites can be sited as follows.

Table 1.3: Accepted Nomenclature for some of the Zeolites

Structure type code	Species	Structure type code	Species
EUO	EU-1	AFI	ALPO-5
FER	Ferrierite	AFL	ALPO-11
ANA	Analcime	LTA	Linde Type A
HEU	Heulandite	LTL	Linde Type L
MTW	ZSM-12	LTT	Linde Type N
FAU	Faujasite		
LAU	Laumontite		
MEL	ZSM-11		
MFI	ZSM-5		
MOR	Mordenite		

Table 1.4: Pauling criteria for different coordinations

Critical Values, ρ (r_c/r_o)	Co-Ordination number	Corresponding cations
$\rho > 0.732$	8	$Bi^{3+/2+}$, Ti^{3+}, Nd^{3+}, Eu^{3+}, Pb^{2+}, Sn^{2+}, Ce^{3+}
$0.732 > \rho > 0.414$	6	In^{3+}, Mn^{2+}, Zn^{2+}, Hf^{4+}, Cu^{2+}, Sn^{4+}, Fe^{3+}, Mo^{6+}, Ti^{4+}, Pt^{4+}, Cr^{3+}, Ga^{3+}, Sb^{5+}, V^{4+}, Co^{2+}, Fe^{2+}
$0.414 > \rho > 0.2255$	4	Al^{3+}, Mn^{4+}, Ge^{4+}, V^{5+}, Si^{+4}, Cr^{6+}, P^{5+}, Se^{6+}, Be^{2+}, As^{5+}, Se^{6+},
$40.225 > \rho > 0.147$	3	B^{3+}

1.5.1: Zeolites as Molecular Sieves and Ion Exchangers

Both of these are classic examples. Steric hindrance, in which pore openings allow some molecules to pass while blocking others, can be used to separate molecules. For example, O_2 can be removed from air at ambient temperature by Na-A zeolite to yield a stream enriched in N_2 (61) and such separation finds use in state of the art air purifiers such as used in military applications. As N_2 and O_2 differ little in size, this indicates possible degree of selectivity. There are many other industrial applications of this "molecular sieve" property of zeolite. Zeolites were the first known ion exchangers and find application in detergents (62). Zeolites are characterized by a anionic framework that includes charge-compensating cations in the intracrystalline voids. These cations can exchange with others in solution and the selectivity of exchange can be high both because of steric selection and because of subtle differences in the electrostatic binding of different cations to the framework. Therefore the potential of such materials for the selective extraction of particular dissolved species are significant.

1.5.2: Zeolites as Solid Electrolytes:

Solid electrolytes conduct ions while remaining in solid state. They are useful for fuel cells because they can allow the intimate controlled reaction of fuel and oxidizer as charged species with out the need for a liquid phase. Zeolites have been investigated as alternative solid electrolytes (63) with ionic conductivity of metal cations. It seems likely that zeolites could be tailored so that ions would be much more mobile, and thus the solid electrolyte work at far lower temperatures than the currently known structures.

1.5.3: Zeolites as Catalysts:

This is probably the most important present day application of zeolites (64) and continues to motivate a great deal of research, especially in the petrochemical and refining industries. Active catalytic sites in the zeolite voids can only operate on molecules that can fit through the openings in to the zeolite structure. This yields catalytic specificity that can be compared with biological enzymes (65). Indeed, zeolites can be considered as analogous to proteins in providing a constrained environment for the controlled reaction of active molecules (66). More over, zeolites are potentially more practical for catalytic applications even in liquid phase reactions, because they remain separate and immobile and can be separated after the reaction. Indeed, some authors call

zeolitic pores as "nanoreactors" (67). Most such catalysts are "fixed " acids or bases in which charge-balancing cation can be acidic like H^+ or basic like Na^+ ionically bonded to a bridging oxygen of the frame work. (68). They have wide array of applications, especially in hydrocarbon refining (69). The cracking of specific alkanes (70), alkylation of phenol and aniline (71,72) and gasoline synthesis from methanol (73), are merely few examples. Although fixed acids dominate current catalytic applications, zeolite catalysts containing exchanged metal cations (M^+) rather than H^+ have been used (74) and remain promising for specialized applications (75).

Unfortunately, most of the zeolites are very unstable and loose their activity easily under the severe conditions of catalytic reactions and hydrothermal conditions of regenerations, because of extensive dealumination of zeolite framework. Ultimately, this leads to the collapse of the zeolite structure. In order to overcome this problem, as synthesized zeolites are dealuminated in a controlled manner and then resulting extra lattice Al species are extracted with acid. Literature is abundant with such studies related to type-Y zeolites because, it is the most promising zeolite due to the 3D pore structure which is best suited to produce very large numbers of important petrochemicals. Such catalysts are called “Ultra Stable Y (USY)”. Introduced in the year 1968 (76), it is the single largest zeolite in use even today in refining industries. Different types of dealumination procedures have been applied in the past, such as treatment with steam at elevated temperatures, with $SiCl_4$ vapor at moderate temperatures, with ammonium hexa fluoro silicate (77-80), with chelating agents like ethylene diamine tetra acetic acid (EDTA) at relatively low temperatures (81), with phosgene (82), with nitrosyl chloride (83), and with boron trichloride (84). In every method, the process has to be carefully controlled to prevent the silicon being withdrawn from the framework too quickly as this will result in the framework collapse and leads to poor crystallinity.

Despite these rapid progresses in the chemistry of zeolite catalysis, a real break through came only in 1983 when Taramoso et al (85) first reported the synthesis of TS-1, which is a Silicalite-1 zeolite containing Ti cations isomorphously substituted in the frame work. This material was shown to be highly active and selective catalyst for the hydroxylation of phenol and many other oxidation reactions with hydrogen peroxide (86). Since then, synthesis of other Ti-containing zeolites like TS-2 (with ZSM-11

structure)(87), Ti-ZSM-48 (88), Ti-ZSM-12 (89), Ti-Al-beta (90) and Ti-MCM-41 (91) has also been reported. These developments, no doubt, have expanded the scope of acid-base catalysts by incorporating simultaneous oxidizing activity. The synthesis of large pore Ti containing zeolites like Y, L and Mordenite which are large volume zeolite catalysts in use today and can find increasing use as oxidizing catalysts for bigger molecules have also been attempted. Where as the hydrothermal synthesis of all types of Ti-zeolite necessarily involves the use of organic templates, most useful large pore zeolites like Y, L and Mordenite can be synthesized without templates. Any attempt to synthesize such zeolites using organic templates meets with partial success and makes only the cost of the material prohibitively high. For that reason, it has been attempted to develop processes for the post synthesis incorporation of Ti in already synthesized zeolite framework. So far, three post synthesis Ti incorporation methods have been reported as follows,

(i) with $TiCl_4$ vapors (92-98), (ii) with ammonium hexaflorotitanate (98,99) and (iii) with ammonium titanyl oxalate (100). Such methods seem to be analogous to dealumination through isomorphous substitution of Si in Al-zeolites described earlier, but the details of the methods like the mechanism of titanation and the coordination of Ti cation in the sample are not studied. Of all the methods of Ti incorporation, the one using ammonium titanyl oxalate seems to be interesting because Ti is not only claimed to be incorporated in the lattice but is ion exchanged as TiO^+ species in the zeolite. This dual nature of Ti species makes the system more complex to characterize but provides a novel method of introducing TiO^+ species uniformly in the zeolite cavity making it a unique catalytic material. Such systems in which TiO^+ species is introduced in zeolite beta (101), zeolite Y, X and MCM-41 (102,103) have been reported. These studies amply demonstrate that zeolites with well-defined nano pore structures provide one of the most promising and suitable reaction spaces found in catalysts not only for general catalytic reactions but also for photo-catalytic reactions. In particular, Ti species in very low aluminum ultra stable zeolite type Y have shown very promising results in many use full oxidation reactions using hydrogen peroxide as well as for many photo catalytic decomposition reactions of environmentally hazardous chemicals (103).

1.6: Characterization of Zeolites

Different techniques can be applied to find out whether the dealumination of the zeolite as well as substitution of metal ions in the framework of molecular sieves has been really occurred or not. These techniques are also used to identify the material, its crystallinity and purity. They are discussed below.

1.6.1: X-ray Diffraction:

It is the most important technique used to study molecular sieves. It is used for (i) the identification of zeolite structure, (ii) determination of % crystallinity of the material, (iii) checking the purity (104) and (iv) determining the unit cell parameter. Isomorphic substitution of metal ions changes the unit cell volume, which provides the evidence of its lattice substitution in the zeolite (105). The correlation of the extent of the incorporation of Ti, Fe, Ga, V, Cr and B metals with the values of unit cell parameters has been reported (106-112,22). Depending upon the difference in the metal-oxide bond length of the substituted metal and that of Si-O, the shrinkage or the expansion in the unit cell volume is reported, for example, unit cell shrinkage was observed for B- substituted zeolite and, where as expansion in it is noticed in Fe-, Ti-, and V-forms (107,109,111). As the powder pattern is the characteristic feature of the individual zeolite structure, phase purity and percent crystallinity of the zeolite can be confirmed by comparing with standard pattern of the zeolite under investigation.

1.6.2: Infrared Spectroscopy

Infrared spectroscopy is a useful and sensitive technique for investigation of

i) The structural features of zeolites,
ii) The isomorphous substitution in zeolites (113),
iii) The acidic and basic properties of zeolites and
iv) The nature of adsorbate - zeolite interactions (114-116).

The zeolite lattice vibrations in the infrared spectra are observed in the mid ir region (400-1300 cm-1). These vibrations are classified in to two groups (111).

(i) Internal vibrations of the TO_4 units which are insensitive to structural vibrations and
(ii) Vibrations due to external linkages of the TO_4 units in the zeolite or structure sensitive vibrations (117,118).

The major infrared band assignments for internal and external vibrations are as shown in the table 1.5.

Systematic investigation of the framework vibrations of zeolites A, X, Y, ZK-5 and omega has been reported (116). The substitution of lighter elements such as B shifts the framework vibrations (Si-O-B) (119) to higher wave numbers, where as substitution of heavier metal ions such as Fe, Ga and Ti shifts the absorption bands to lower wave numbers than the corresponding aluminosilicats (120). Similar shifts have also been observed for Ferrisilicate analogues of molecular sieves (17,121,122). In the case of Titanium and Vanadium silicates, the additional symmetric stretching vibrations around 960 cm^{-1} has been reported. The presence of this band at 960 cm^{-1}in the case of metallosilicates (e.g. Ti, V and Sn) is a matter of debate. Originally, it was attributed to stretching vibrations of the Si-O bond in Si-O-M bridges (42,45,46). Later on, it has been suggested to the due to M=O (85) (especially in the case of Ti=O) and silanol groups (-Si-OH) (123) associated with defect centers.

In the case of titanium silicate with the MFI structures, Taramasso et al (85) observed asymmetric stretching vibrations at around 960 cm^{-1} and have ascribed it to the Si-O-Ti bond (or, Si-O-Ti=O). They have also correlated its intensity with the amount of titanium incorporated into the MFI structure.

In the case of large pore zeolites, Ward et al (123) observed hydroxyl stretching vibrations in the region 3700 to 3550 cm^{-1} and assigned them to bridging Si-OH-Al groups. Small pore and medium pore zeolites are found to exhibit similar –OH group vibrations at slightly lower wave numbers (124). Framework substitution of Ti, Fe or Ga in place of Al, shifts the –OH vibrations to higher wave numbers (17,125). Probe molecules like ammonia, pyridine and acetonitrile have been used to estimate and characterize Bronsted and Lewis acid sites in zeolites (115,125-128). Adsorption of water, alcohols, olefins, benzene and other hydrocarbons on zeolite surfaces have also been examined by IR spectroscopy (115,129-132).

Table 1.5: Frequencies of fundamental framework vibrations

	Mode of vibrations of framework	Frequency of vibration, cm^{-1}
(i)	Internal Tetrahedra	
	Asymmetric stretch	1250-950
	Symmetric stretch	720-650
	T-O bend	420-500
(ii)	External Linkages	
	Double ring	650-500
	Pore opening	300-420
	Symmetric stretch	750-820
	Asymmetric stretch	1050-1150

1.6.3: Nuclear Magnetic Resonance Spectroscopy

High-resolution Solid State Mass NMR spectroscopy has become powerful technique for the investigation of characteristics of solid-zeolite material. The central idea of NMR spectroscopy is that the chemical shift of magnetically active nucleus reflects its chemical environment in it's spectrum. The spectra for a complex solid will therefore consists of a number of spectral lines arising from chemical distinct centers for each type of nucleus examined. In order to derive structural information from such spectra, it is necessary to establish how the nuclei associated with different spectral lines are spatially related to each other (133-135). It is also used to determine the location of isomorphously substituted metal ions (136,137). Much attention has been focused towards ^{29}Si and ^{27}Al MAS NMR in order to investigate

i) Si and Al ordering in the zeolites (138),

ii) Crystallographically equivalent and nonequivalent Si and Al ions in various sites (139,140)

iii) Framework Si/Al ratio (141)

iv) The co-ordination number of Si (142) and Al (143)

v) Spectral correlations with Si-O-T bond angles (144) and Si-O bond lengths (145).

Further, the techniques like 2D NMR can be used to establish connectives in the solid state (146). Fyfe et al. (147-149) have demonstrated the three dimensional lattice connectivities in zeolite ZSM-5 (41,9)

The most frequently used NMR technique known as Bloch Decay (B.D) directly observes silicon or aluminum in a zeolite or a molecular sieves (150). In this technique, after the application of a short pulse of radio frequency at the resonance frequency of the given nucleus, its response is subsequently detected. The B.D ^{29}Si NMR spectrum of Faujasite zeolite contains five well resolved resonance that correspond to Si sites, which differ by the number of attached Al atoms, Si $(OAl)_n$ $(OSi)_{4-n}$ where n = 0 to 4. Various peak intensities can be used quantitatively to calculate Si/Al ratio (151) in the sample. The B.D ^{27}AL MAS NMR spectrum of Faujasite distinguishes among aluminum atoms in the tetrahedral, octahedral, penta-coordinated or amorphous sites (152).

1.6.4: Electron Spin Resonance Spectroscopy (ESR)

ESR spectroscopy is a sensitive tool to understand the environmental symmetry of paramagnetic metal ions. It is useful in finding the environment of isomorphously substituted framework metal ions and exchanged cations and metal oxides within the pores of the zeolite or on the external surface of the crystallites (147,148). Various paramagnetic metal ions such as Fe^{3+}, V^{4+} and Cr^{3+} have been studied extensively using ESR spectroscopy (149,153,154). The ESR technique (153) has been used to characterize solid-solid reactions between the zeolite and the metal oxide of elements such as Cu, Fe, Cr, Mo and V. The oxidation state, environment and redox property of V, in vanadium silicate molecular sieves with MFI and MEL and MCM-41 structures have been studied (154-156) by ESR spectroscopy. Electron spin echo modulation (ESEM) can provide quantitative data on the number of ligands to which the transition metal ion is co-coordinated and their interaction distances (134). Goldfarb et.al (135) have reported extensive ESR studies over iron containing sodalite by electron nuclear double resonance technique (ENDOR).

1.6.5: UV-Visible Spectroscopy

UV-visible diffuse reflectance spectroscopy is a very useful technique for identification of metal ion environments in the zeolite. The diffuse reflectance bands at different wavelength regions provide information about the environment of the metal ions

like Ti, Cr, Sn, and V etc in metallosilicate molecular sieves (157-160). The positions of the absorbance bands in the UV-visible region of some metal ions in different environments are given in the table 1.6.

1.6.6: Scanning Electron Microscopy (SEM)

Scanning electron microscopy (SEM) is a technique used to measure the particle size distribution and morphology of the crystals. The amorphous materials present can be detected from the micrographs.

Table 1.6: UV-Visible absorption region of various metal ions

Metal ion	Ionic environment	Absorbance, λ, nm
Ti	Td	212
Ti	Oh	240
V	Td	233 – 285
V	Oh	333 – 500
Sn	Sq Py	221 ± 3
Sn	Oh	255 ± 5

1.6.7: Thermal Analysis

The various physico-chemical changes occurring during the thermal treatments are observed in the DTA/TG/DTG curves. They are useful in evaluating thermal properties of zeolites (161,162). Due to loss of water and other physically adsorbed molecules, the thermogram indicates endothermic peak. The location of water molecules in hydrated zeolites is possible by analyzing the multiple endothermic (DTA) peaks due to dehydration (163). The thermogram indicates exotherm due to the structure collapse of zeolites. Therefore high temperature exotherm gives an indication of the thermal stability of the zeolite. The number of cations present in the zeolite and its nature affect significantly to the structural stability, which can be understood from the thermogram.

The importance of thermal stability and the interest in high temperature properties of zeolites is largely related to their use in petroleum catalytic cracking reactions. Thermal properties can be related to other physico-chemical characteristics of zeolites and thus provide some predictive utility. Flanigen and coworkers (164) have correlated the DTA structural collapse temperature of several stabilized type-Y samples to the frequency of

structure-sensitive stretching vibrations of zeolite framework in the infrared region. It is known that the thermal stability of zeolite framework structure increases with the Si / Al ratio (162).

1.6.8: Atomic Absorption Spectroscopy

Atomic absorption spectroscopy is used to determine the concentration of the following elements in the sample of given zeolite. These elements are Na, K, Fe, Al, Mg, Zn, Cd, Cu, Co, Ni, Mn, Ca, Sr, Ag, Pt, Au, etc. where as some of the elements which are not detectable by atomic absorption are Ti, Si, Ta, W, Mo, V, Ir and few others. This may be due to the fact that these elements form oxide in the flame. The main advantage of this technique is high degree of freedom from interference from its environment i.e. the small traces of one element can be accurately determined in the presence of high concentration of other elements (165). This method is also independent of flame temperature since atoms usually used in this method are in ground state.

1.6.9: X-ray Fluorescence Spectroscopy

Some of the elements e.g. Ti, Si, V, Mo etc in the zeolite which can not be determined quantitatively by the atomic absorption spectroscopy can be determined quantitatively by using X-ray fluorescence technique. To determine the exact quantity of the given element in the zeolite, the intensity of the signal for the standard sample prepared for comparison with it should be closely matched. The percentage error in the intensity should not be greater than ± 5% of the standard samples used for comparison.

1.7: SCOPE OF THE PRESENT WORK

Comprehensive information presented above reveals two important aspects in the development of titanium containing ultra stable zeolite type-Y (Ti-USY);

i) The reported method of the preparation of USY zeolite by controlled hydrothermal dealumination, then aluminum extraction and healing the structure through Si insertion can be adopted for the preparation of Ti-USY also and

ii) Among all the methods developed for preparation of Ti-USY, the one using ammonium titanyl oxalate seems to be the best. Where as the method seems to be simple, the resulting product contains many types titanium species like Ti^{4+} in the framework, TiO^{+} cations in exchangeable positions, TiO_2 nano particles in the micropores and TiO_2 clusters in the system. Despite several related studies, the nature of such species is not

completely understood as yet. Where as some reports on catalytic activity for oxidation of large molecules like cyclohexane using H_2O_2 are available, similar studies on acid catalyzed hydrocarbon conversions over Ti-USY are very rare. Therefore the present study was under taken with the following objectives.

a) To prepare very high silica Ti-USY and Fe-USY zeolite catalysts,
b) To characterize them using XRD, SEM, TG/DTA, UV/VIS, FTIR, ESR and MAS NMR spectroscopic methods,
c) To determine catalytic activity for some oxidation and acidic reactions like phenol oxidation, cyclohexanol dehydration and benzoylation of toluene and
d) To correlate the nature of surface active sites and catalytic activity of Ti-USY zeolites.

The zeolite Faujasite type- Y is low silica, large 3D pore zeolite, which is, not found in nature but can be easily synthesized hydrothermally in laboratory and industry. The structure of this zeolite is shown in the fig-1.1. The unit cell of Y is cubic with a large dimension of nearly 25 Å and contains 192 (Si, Al) O_4 tetrahedra, has remarkably stable and rigid framework structure with largest void space, which amounts to be nearly 40 % by volume of the dehydrated crystal. The crystallographic parameters of zeolite type-Y are presented in the table 1.7.

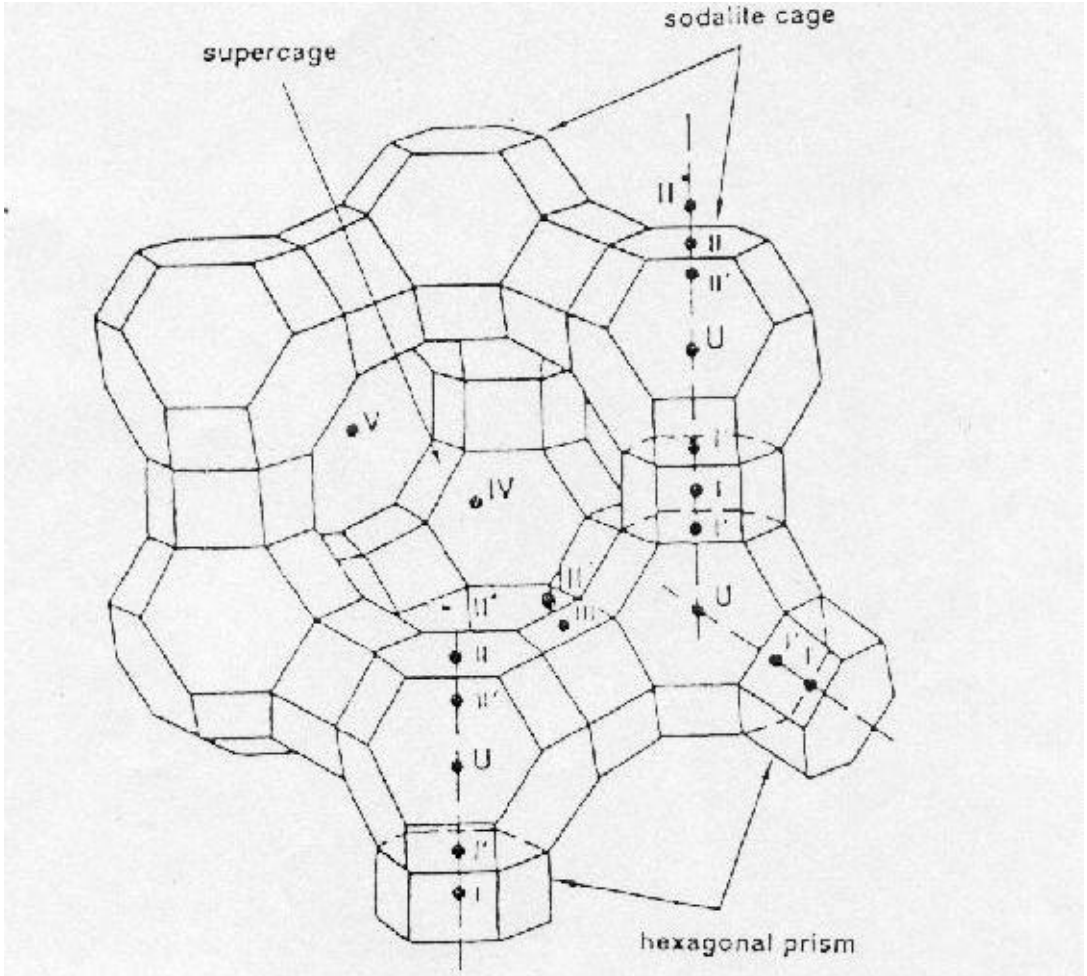

Fig.1.1: Morphology of Zeolite Faujasite type-Y showing Super cages, Sodalite cages, Hexagonal prisms and Cation exchange sites namely I, I', II, II', III, III', IV and V.

Table-1.7: Crystallographic parameters of Zeolite Faujasite type-Y

Structure group:	4
Chemical composition	$Na_2O.AL_2O_3.4.8SiO_2.8.9\ H_2O$
Typical oxide formula	$Na_{56}\ [(AlO_2)_{56}\ (SiO_2)_{136}].\ 250\ H_2O$
Variation in composition	Na : A l = 0.7 - 1.1; Si : Al =1.5 - 3.0
	Crystallographic data
Symmetry	Cubic, Density: 1.92 g/cc
Space group	Fd3m, Unit cell volume: 14901 to 15347 $Å^3$
Unit cell constant	A=24.85-24.61 Å
Structural properties.	
Framework	Truncated octahedra, â -cages linked tetrahedrally through D6-R's. Contains eight cavities~13 Å in diameter in each unit cell. Frame work density: 1.25-1.29g/cc
(Secondary building unit) SBU	6-6R -, Void volume: 0. 48cc/cc
Free Apertures	12-Ring, 7.4 Å; 6-ring, 2.2 Å
Dehydrated Free Apertures:	~7.4 Å

CHAPTER 2

2.0: EXPERIMENTAL

2.1: Reagents used in this study

For this study, pure sample of Na-Y was procured from Union Carbide Corporation, USA (Linde, SK-40). All other chemicals used are listed in the table 2.1.

2.2: Preparation of NH_4-Y:

10g of Na-Y zeolite powder was added to 200 ml of 2N NH_4NO_3 solution taken in a round bottom flask. This mixture was heated at 100°C with stirring for 12 h. The sample was then filtered, washed with hot deionised water till free from nitrate ion and dried at 100°C for 16h. The above procedure was repeated three times to obtain NH_4-Y with more than 80% of ion exchange.

2.3 : Preparation of Ti-USY, Fe-USY and Fe-Ti-USY

2.3.1:Preparation of low silica Ti -USY from NH_4-Y and $K_2TiO(C_2O_4)_2.2H_2O$ in single step (SSTP) method

Series of samples identified as SSTP-X-Y (where SSTP stands for single step method of preparation, X for temperature of preparation and Y for mol fraction of potassium titanyl oxalate per mol of Al used) was prepared by treating 5g of NH_4-Y in 200ml distilled water with appropriate quantity of potassium titanyl oxalate solution at required temperature as indicated in the table 2.2. The titanyl solution was added drop wise during 18 hours at the required temperature while stirring the solution constantly.

All the above samples were then filtered ,washed with hot deionised water till free from nitrate ions and then dried in oven at 100°C for 16 hr.

2.3.2:Preparation of high silica and very high silica USY by hydrothermal dealumination of NH_4 -Y

In the multiple step method of preparation of Ti-USY, the first step is the preparation of high and very high silica USY zeolites. In this method, NH_4-Y zeolite must be dealuminated in a controlled way by treating the sample in steam at increasing severity of hydrothermal condition with intermediate NH_4^+ ion exchange. These conditions have to be standardized before introducing Ti in the system. In order to standardize this condition, a series of hydrothermal dealumination experiments were

Table 2.1 : **Specification of the Chemicals used**

S.No	Name of the Chemical	Chemical Formula	Purity %
1.	Potassium Titanyl Oxalate BDH Chemicals Ltd, Poole England	$K_2TiO(C_2O_4)_2.2H_2O$	98.5%
2.	Ammonium nitrate, GR Merk India Ltd, Mumbai	NH_4NO_3	99%
3.	Tetraisopropylorthotitanate Merk India Ltd, Mumbai	$Ti[OCH(CH_3)_2]_4$	97%
4.	Isopropyl alcohol S. D. Fine, India Ltd, Mumbai	$(CH_3)_2CHOH$	99%
5.	Ferric ammonium oxalate S. D. Fine, India Ltd, Mumbai	$(NH_4)_3Fe(C_2O_4)_3.3H_2O$	99%
6.	Titanium (IV) butoxide ALDRICH, USA.	$Ti[O(CH_2)_3CH_3]_4$	99%
7.	Nitric Acid, (A.R) S. D. Fine, India Ltd, Mumbai	HNO_3	69-72%

Table 2.2: Preparation of low silica Ti-USY by single step (SSTP) method

S. No	Name of the sample	Mol fraction of $K_2TiO(C_2O_4)_2.2H_2O$	Temperature of reaction
1	SSTP-25-0.055	0.055	25°C
2	SSTP-25-0.11	0.11	25°C
3	SSTP-25-0.165	0.165	25°C
4	SSTP-25-0.22	0.22	25°C
5	SSTP-25-0.33	0.33	25°C
6	SSTP-25-0.44	0.44	25°C
7	SSTP-55-0.055	0.55	55°C
8	SSTP-55-0.22	0.22	55°C
9	SSTP-55-0.33	0.33	55°C

carried out. These samples are identified as A-B-C-MSTP where A, B, and C are the temperatures of repeated steam treatment and MSTP stands for multiple step method of preparation of USY. In a typical experiment, for the preparation of 550-MSTP, NH_4-Y zeolite was slowly heated in a tube furnace at a rate of 2^0C per minute up to 550^0C while passing steam continuously over the sample for 4 hours. After that, it was cooled in the atmosphere of steam to 200^0C, then in air to 30^0C.The sample was immediately put in to 300 ml of 1 molar NH_4NO_3 solution to convert it in to NH_4^+- form. The sample was then filtered, washed and dried at 100^0C. This sample was further steam treated at 700,850 and 925^0C successively with intermediate NH_4^+ exchange. Finally, the sample was washed thoroughly till free from nitrate ions and dried at 100^0C for 8 hrs. The details of the preparations are tabulated in the table-2.3.

2.3.2.1: Preparation of high silica Ti-USY from high silica USY (550-MSTP) sample by multiple step (MSTP) method

The high silica USY sample number-1 in the table 2.3 in previous part namely USY(550-MSTP) was treated with required amount of $K_2TiO(C_2O_4)_2$ solution at required temperature. Then, $K_2TiO(C_2O_4)_2$ solution was added drop wise during 18 hours at the required temperature while stirring the solution constantly. The solution was filtered, washed with hot deionised water till free from K^+ ions and then dried at 100^0C for 8 hours. These samples were further ion exchanged with NH_4NO_3 solution to remove K^+ ions from the sample. All samples were finally calcined in air at 450^0C for 6 hours to convert it in to protonic forms. These samples are identified as [550-MSTP-X-Y] where 550-MSTP stands for the USY sample used, X and Y stand for the reaction temperature and mol fraction of $K_2TiO(C_2O_4)_2$ solution used for reaction. The details of all these samples are also tabulated in the table-2.4.

2.3.2.2: Preparation of very high silica Ti-USY from very high silica USY (550-700-850-MSTP) sample by multiple step (MSTP) method

In another variation of the multiple step method of preparation, the high silica USY prepared as per the sample 3 in table–2.3 namely 550-700-850-MSTP was used to prepare Ti-USY. Similar procedure as described above was used for incorporating Ti. All

other conditions namely temperature of reaction and acid treatment were similar to those in the table-2.4. In addition to potassium titanyl oxalate [$K_2TiO(C_2O_4)_2$], two other Ti

Table 2.3: Preparation of USY by hydrothermal dealumination of NH_4 -Y

S.N	Name of the sample	Steaming temperature	Exchange with NH_4NO_3
1	550-MSTP	550ºC	Yes
2	550-700-MSTP	550ºC	Yes
		700ºC	Yes
3	550-700-850-MSTP	550ºC	Yes
		700ºC	Yes
		850ºC	Yes
4	550-700-850-925-MSTP	550ºC	Yes
		700ºC	Yes
		850ºC	Yes
		925ºC	Yes

Table 2.4: Preparation of high silica Ti-USY from high silica USY (550-MSTP) by multiple step (MSTP) method

S. N	Name of the sample	Mol fraction of $K_2TiO(C_2O_4)_2.2H_2O$	Temp. of reactn	NH_4NO_3 Treated	HNO_3 Treated
1	550-MSTP-25-0.11	0.11	25ºC	Yes	-
2	550-MSTP-25-0.22	0.22	25ºC	Yes	-
3	550-MSTP-25-0.33	0.33	25ºC	Yes	-
4	550-MSTP-25-0.44	0.44	25ºC	Yes	-
5	550-MSTP-55-0.11	0.11	55ºC	Yes	-
6	550-MSTP-55-0.33-HNO_3	0.33	55ºC	Yes	Yes
7	550-MSTP-200-0.44-HNO_3	0.44	200ºC	Yes	Yes

salts, namely Titanium (IV) butoxide $Ti[O(CH_2)_3CH_3]_4$) and Titanium isopropoxide $Ti[OCH(CH_3)_2]_4$ were also used. For the sake of comparison, a sample was also prepared without any Ti source but keeping rest of the treatment conditions identical. These samples are identified as [(Ti-Source)-MSTP-X-Y] where Ti-source stands for the source of Ti, namely Potassium titanyl oxalate (oxo), Titanium butoxide (Buto) or Titanium isopropoxide (Iso) and MSTP stands very high silica USY (550-700-850-MSTP), x for temperature of reaction and Y for mol fraction of Ti salt used in the reaction. The details of these samples are given in the table-2.5. These very high silica Ti-USY samples were modified further by acid treatment for ten times. This procedure removes maximum possible extra framework Al species in the sample.

2.3.2.3: Preparation of very high silica Fe-USY and Fe-Ti-USY from very high silica USY(550-700- 850-MSTP), $(NH_4)_3Fe(C_2O_4)_3.3H_2O$ and Ti salts

For incorporating Fe in the USY zeolite, we have adopted similar procedures, which lead to a very high silica USY zeolite. It is a variation of multiple step method of preparation. In this method, the very high silica USY was first prepared as per sample number 3 in the table-2.3. It was then reacted with Ammonium Iron (III) Oxalate $[NH_4)_3Fe(C_2O_4)_3.3\ H_2O]$ solution at 200^0C for 18 hours, filtered and washed. It was then treated with dilute HNO_3 at 100^0C for 4 hours, filtered, washed and dried. The whole cycle was repeated for 10 times to get the final sample. In order to incorporate Fe along with Ti in USY, one of the Ti salts among $K_2TiO(C_2O_4)_2.2H_2O$, $Ti[O(CH_2)_3CH_3]_4$ and $Ti[OCH(CH_3)_2]_4$ was also added in required quantities in the reaction mixture. The details of the samples are given in the table-2.6 below.

2.4: X-ray diffraction (XRD)

The samples after preparation were analyzed by X-ray powder diffraction for quantitative and qualitative phase identification by Rigaku (D MAX III VC) using a Ni-filter Cu K_α radiation (λ=1.5406Å) with graphite monochromator and Si as an internal standard. The most crystalline H-Y sample was assumed to be 100% crystalline and was used as reference sample to find out the crystallinity of other samples. The degree of crystallinity of the solid product was estimated from the XRD peak intensity using the following formula

Table. 2.5: Preparation of very high silica Ti-USY from very high silica USY (550-700-850-MSTP) sample by multiple step (MSTP) method

S.N	Name of the sample	HNO_3Exchg.	$K_2TiO(C_2O_4)_2$treatment	$Ti[O(CH_2)_3CH_3]_4$ Treatment	$Ti[OCH(CH_3)_2]_4$ Treatment	Temp.of treatment
1	Oxo-MSTP-200-0.33	0.01N	0.33M	-	-	200ºC
2	Buto-MSTP-200-0.33	0.01N		0.33M	-	200ºC
3	Iso-MSTP-200-0.33	0.01N	-		0.33 M	200^0 C
4	MSTP	0.01N	-	-	-	-
5	Oxo-MSTP-200-0.33-10	0.01N	0.33M	-	-	200ºC
6	Buto-MSTP-200-0.33-10	0.01N		0.33M		200ºC
7	Iso-MSTP-200-0.33-10	0.01N		-	0.33M	200ºC
8	MSTP-10	0.01N	-	-	-	-

Table- 2.6: Preparation of very high silica Fe-USY and Fe-Ti-USY from very high silica USY(550-700- 850-MSTP), $(NH_4)_3Fe(C_2O_4)_{3.}3H_2O$ and Ti salts

S.N	Name of the sample	HNO_3 Excge.	$K_2TiO(C_2O_4)_2$treatment	$Ti[O(CH_2)_3CH_3]_4$ Treatment	Ti $[OCH(CH_3)_2]_4$ Treatment	$(NH_4)_3Fe(C_2O_4)_3$	Reaction temp
1	Fe-USY	0.01N				0.05M	200^0C
2	Oxo-Fe-Ti-USY	0.01N	0.33M			0.05M	200ºC
3	Buto-Fe-Ti-USY	0.01N		0.33M		0.05M	200ºC
4	Iso-Fe-Ti-USY	0.01N			0.33M	0.05M	200ºC

$$\% \text{ Crystallinity} = \frac{\text{Peak area of the intense peaks of the product}}{\text{Peak area of the intense peaks of standard}} \times 100$$

The silicon was used as internal standard. The peak positions at 2θ values of 28.44 and 47.32 degree of Si were used as the reference for correction of peak positions of the sample while calculating the d values and unit cell parameters. The unit cell constant, a, was calculated from the following known formula for the cubic system :

$$d_{h,k,l} = \frac{a}{(h^2 + k^2 + l^2)^{1/2}}$$

where h, k and l are the miller indices, d is the lattice distance and a is the unit cell constant.

2. 5: Determination of Chemical Composition

The chemical composition of the samples was analyzed by using both X-ray fluorescence spectroscopy (XRF) and atomic absorption spectroscopy (AAS) depending up on the nature of the sample.

2.5.1: Atomic Absorption Spectroscopy:

In order to estimate the quantity of Na, K, Al and Fe in the sample, the anhydrous weight of the sample was first determined by calcining it in air to 1000^0C for 8 hrs. Then it was treated with concentrated HF in presence of H_2SO_4 to remove all SiO_2 as H_2SiF_6 by mild heating. The remaining residue was calcined to 1000^0C to find out the residue left out as oxide. The difference in the anhydrous weight and the residue gives the amount of Si in the sample. Thereafter, the residue was dissolved in minimum amount of $HF+H_2SO_4$ in water and made up to standard volume. The concentration of this solution was adjusted to the concentration range required for AAS analysis using Varian-GTA-100 Spectrometer 220 Fast Sequential instrument. The conditions shown in the table-2.7 were used for the analysis.

Table 2.7: Conditions for AAS analysis

Element.	Wavelength, nm	Nature of Flame
Si	251.6	NO_2-Acetylene
Al	309.3	NO_2-Acetylene
Ca	432.7	NO_2-Acetylene
K	589.0	Air-Acetylene
Na	766.5	Air-Acetylene

2.5.2: X-ray Fluorescence Spectroscopy:

Wavelength dispersive X-ray fluorescence spectrometer (Rigaku 3070-E) with rhodium target energized at 50 KV and 40 ma was used for the experiment. For XRF measurements, borate fusion technique was used to prepare glassy beads of reference standards and of samples. A calibration curve was made using standards for the analysis of Si and Al. For all analysis, Kα lines were selected and pulses were collected for 40 sec. Then background correction was applied before getting the results.

The sample beads were prepared by fusing the sample in a platinum crucible with appropriate amount of sample, potassium bromide and lithium tetra borate flux by heating to 1200 ^{0}C. For accurate quantitative analysis, glass beads of standard compositions were made and calibration curve was obtained before analysis of the sample. The composition of the sample with respect to SiO_2/Al_2O_3, SiO_2/TiO_2 and SiO_2/Fe_2O_3 ratio was calculated.

2.6 : Thermo-gravimetric analysis (TG/DTG/DTA)

The thermo-gravimetric analysis was carried out using SETARAM TG-DTA 92 instrument. The experiments were carried in air atmosphere by passing air at the rate of 30ml/min and the heating rate was 10^0/min.

2. 7: Scanning Electron Microscopy

. The system used was JEOL-JSM-5200 instrument. The samples were scanned for high resolution using SEM/EDX Philips XL30 high-resolution unit. The pictures were taken in different magnification with respect to the sample nature. The magnifications are given along with the micrograms. The samples were sputtered with gold to prevent

surface charging and to protect from thermal damage from electron beam. In all the analysis, samples were kept on the sample holder as a layer of uniform thickness of about 0.1mm.

2 .8: Fourier Transform Infrared Spectroscopy

The potassium bromide (KBr) pallet technique was used to record the FTIR spectra in the region 1800-400cm^{-1}.For the preparation of KBr pallets, 300 mg of previously dried KBr was mixed thoroughly with 0.5 mg of the sample and pressed in to pellets of 13 mm diameter with a pressure of 7 tons/$inch^2$.The spectrum was recorded using NICOLET 60 SXB spectrometer with resolution of 2 cm^{-1} and averaging over 250 scans.

For the nature of the surface hydroxyl groups and the nature of acidity, thin wafers of the samples weighing nearly 5-6mg/cm^2 were made by pressing a thin layer of the sample at a pressure of 7 ton/$inch^2$. The wafer was placed on the sample holder. It was then placed inside the heating compartment of the transmittance cell shown in the fig 2.1. The cell was connected to a high vacuum system. The sample was evacuated to 10^{-6} Torr at 400°C for 3h and then cooled to 100°C before recording the spectrum of the pure sample. Then the sample was allowed to adsorb pyridine at an equilibrium pressure of 20 mm of Hg for 30 min. The loosely adsorbed and free vapor of pyridine was removed by evacuating the cell for 1h. Then the spectrum was recorded. Thereafter, the sample was further heated to 200, 300 and 400^0C successively for 1 h at each temperature before recording the spectrum again. The spectrum was recorded with 2 cm^{-1} resolution after averaging over 500 scans.

2.9: Electron Spin Resonance (ESR) Spectroscopy

The ESR spectra of calcined Fe-USY samples were recorded on a Bruker EMX spectrometer operating at X-band frequency and 100 KHz field modulations. The samples were taken in specially designed quartz tubes (4.5 mm outer diameter) having a provision for evacuation and adsorption of gases. Microwave frequency was calibrated using a frequency counter fitted in the microwave bridge (Bruker ER 041 XG-D) and the magnetic field was calibrated by (ER) 35M NMR) gauss meter.

2.10: UV-VIS Diffuse Reflectance Spectroscopy

The UV-VIS diffuse reflectance spectra of the samples were obtained using a Shimadzu (model UB-2101 PC) spectrometer using barium sulphate as the reference sample.

2.11: Solid State Magic Angle Spinning NMR Spectroscopy

Broker model MSL-300 and DRX-500 FT-NMR spectrometer was used for our experiments depending on consideration such as the spinning speed and the sample volume. The experiments were performed as per the procedures described in detail in Chapter-IV.

2.12: Catalytic Properties

2.12.1: Liquid Phase Reaction

Phenol oxidation and benzoylation of toluene reactions were carried out in liquid phase in a batch reactor as shown in fig-2.2. Dilute H_2O_2 in phenol oxidation and benzoyl chloride in benzoylation of toluene were respectively added to the reactor vessel by using a syringe pump with a constant feed rate.. The water was used as solvent in this reaction. The products of both the reactions were analysed by GC (HP 5880A) equipped with a capillary column (50m X0.25mm, crossed- linked methyl- silicon gum).

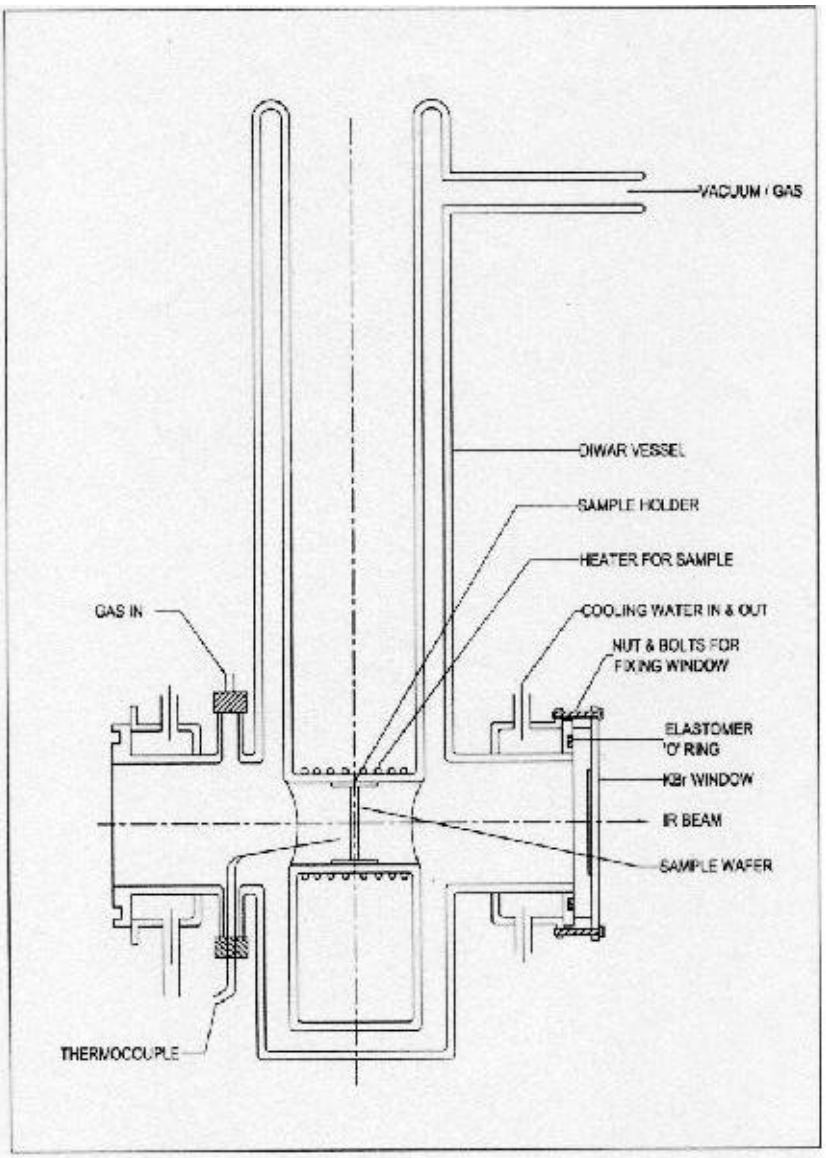

Fig.2.1: FT-IR Transmittance Cell for self supporting wafers of solid samples

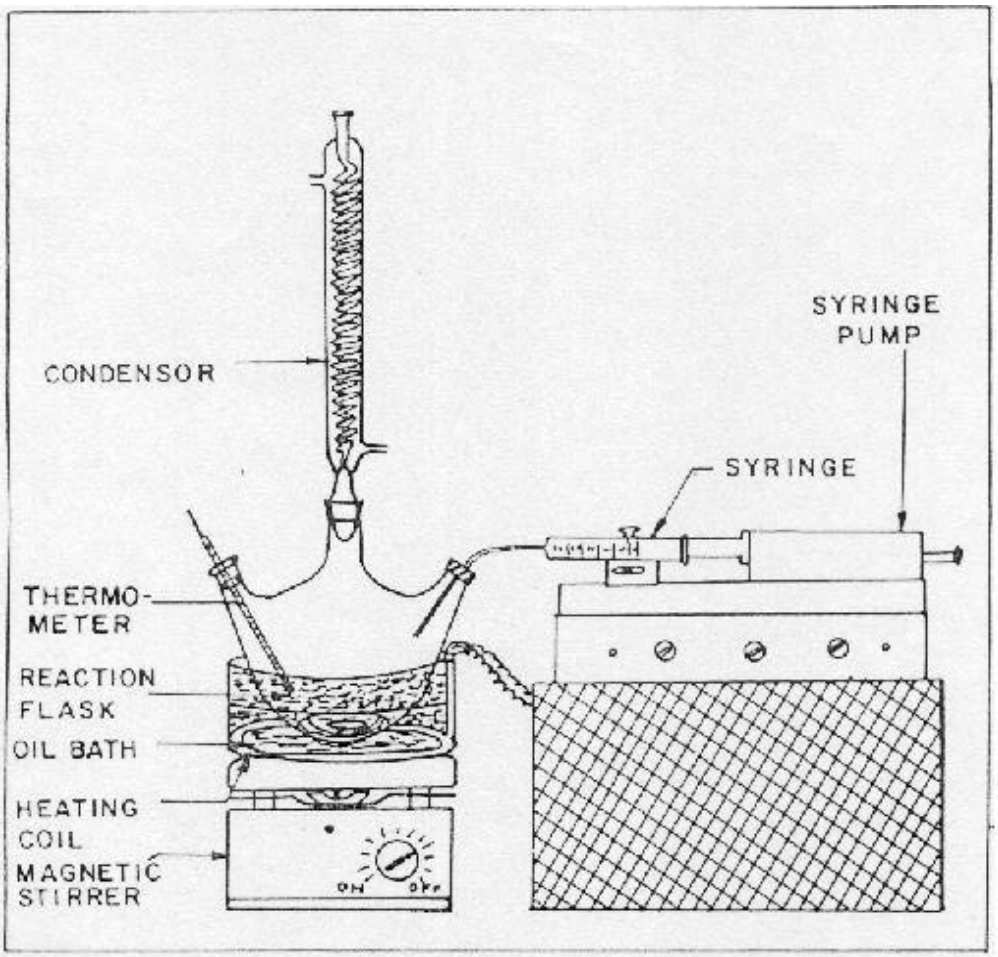

Fig.2.2 : Schematic diagram of liquid phase batch reactor.

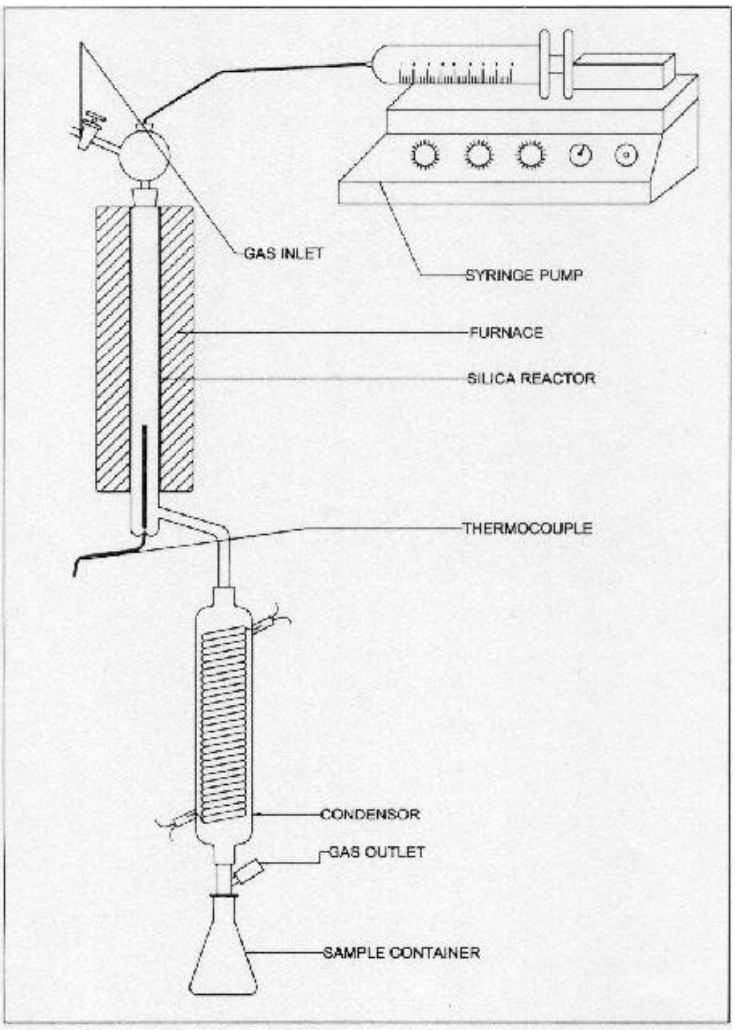

Fig.2.3 : Fixed bed reactor set up for gas phase reactions in atmospheric pressure

2.12.2: Gas phase reactions

Dehydration of cyclohexanol and methylation of O-toluidine reactions were carried out in a gas phase in a continuous down flow fixed bed silica tube reactor as shown in the fig-2.3.. The catalyst was activated at 500^0C prior to the reaction. The feed was passed in the reactor with required rate by using a syringe pump (Sage Instruments, USA). The reactions were carried out in the range of temperatures 200-350 ^{0}C and 200-450 ^{0}C for dehydration of cyclohexanol and methylation of O-toluidine respectively. The products were analysed by GC (HP 5880A) and GC (5889A) using mega bore column with a FID detector.

CHAPTER 3

3: PHYSICO CHEMICAL CHARACTERIZATION OF USY,Ti-USY, Fe-USY and Fe-Ti-USY

3.1: Low silica Ti-USY from NH_4-Y and $K_2TiO(C_2O_4)_2$ in single step (SSTP) method

3.1.1: Preparation of the sample

The carefully controlled steaming of ammonium exchanged zeolite-Y by slowly heating to high temperature followed by mild acid leaching forms highly crystalline USY zeolite. The structural rearrangement in the zeolite framework also occurs during this treatment. The SiO_4 tetrahedra fill up the framework vacancies created by dealumination. If the cation, which can be isomorphously substituted in the zeolite, is introduced in such a system, that cation will also enter in to the vacancies created by removal of Al. So far, three post synthesis Ti incorporation methods have been reported; (i) reaction with $TiCl_4$ vapor (92-98), (ii) reaction with ammonium hexaflurotitanate solution (98,99) and (iii) reaction with ammonium titanyl oxalate solution (100). Such methods seem to be analogous to the dealumination through isomorphous substitution of Si in Al-zeolites described in the literature. Of all the methods of Ti incorporation, the one using ammonium titanyl oxalate seems to be interesting because, Ti is not only claimed to be incorporated in the lattice but also ion exchanged as TiO^{2+} species in the zeolite.

All oxysalts of titanium such as $TiO(NO_3)_2$ and $TiOSO_4.xH_2SO_4$ hydrolyze in H_2O forming colloidal suspension. Owing to high acidity of the solution and the formation of large colloidal TiO_2 particles, these salts are not suitable for Ti incorporation. Where as potassium titanium oxalate, $K_2TiO(C_2O_4)_2$ is completely soluble in water and does not hydrolyze at the acidic pH value of 4-5 of the suspension of NH_4-Y zeolite in $K_2TiO(C_2O_4)_2$ solution in water. The nature of Ti species in this solution is reported to be monomer (TiO^{2+}) or dimer $(Ti_2O_3)^{2+}$ forms (166). K_2 [$TiO(C_2O_4)_2$] salt hydrolyses in the solution forming titanyl oxalate [$TiO(C_2O_4)$] and $K_2(C_2O_4)$. $TiO(C_2O_4)$ is soluble in water (167). So the ionic equilibrium is established in the solution which can be represented as K_2 [$TiO(C_2O_4)_2$] $TiO^{2+}\ldots 2(C_2O_4)^{-} + K_2^{2+}\ldots C_2O_4^{2-}$. Under the pH condition of about 3.5 of the suspension of NH_4-Y zeolite in the solution of K_2 [$TiO(C_2O_4)_2$ in water, K^+ ions will exchange for the NH_4^+ ions in the zeolite and oxalate $(C_2O_4)^{2-}$ ions will react with AlO^{5-} tetrahedra in the zeolite forming soluble aluminum

oxalate and thus dealuminate the framework. In addition, some of the complex titanyl oxalate ion remains adsorbed on the surface. The mechanism of the dealumination can be depicted as shown in the scheme 3-1

The chemical analysis of the samples was done by combination of AAS, XRF and MAS NMR techniques and the results are given in the table-3.1.

Table 3.1: Chemical composition of low silica Ti- USY prepared by single step (SSTP) method using $K_2TiO(C_2O_4)_2$ solution

S No.	Name of sample						$mSiO_2/mAl_2O_3$	mSi/mTi
		Na	K	Ti	Al	Si		
1	NH_4-Y	5.62	-	-	28.37	66.02	4.66	-
2	SSTP-25-0.11	4.3	5.02	0.85	24.811	65.21	5.26	130.31
3	SSTP-25-0.165	3.91	7.35	1.64	22.76	64.38	5.66	46.25
4	SSTP-25-0.22	3.6	9.78	2.43	20.24	63.95	5.23	38.45
5	SSTP-25-0.33	3.12	10.53	3.2	19.72	63.43	6.32	31.31
6	SSTP-25-0.44	2.34	12.98	2.46	19.43	62.84	6.47	34.01
7	SSTP-55-0.33	0.36	0.46	4.27	18.42	76.48	8.30	17.91
8	SSTP-200-0.44	0.21	0.32	4.56	16.48	78.43	9.52	17.20

As the amount of $K_2TiO(C_2O_4)_2$ used is increased from 0.055 to 0.44 mol fraction of Al (sample 2-6), (i) Increasing amount of NH_4^+ cations in the zeolite is exchanged by K^+ ion, (ii) AlO^{5-} tetrahedra in the framework are leached out creating silanol nests as shown in the scheme, and (iii) TiO_4^{4+} tetrahedra are introduced in the defects in the frame work removing the silanol nests and healing the framework. In addition, FTIR studies indicate the presence of oxalate species in strongly adsorbed state on the surface of the sample. The titanyl oxalate species is very complex, the structure of which is not fully understood as yet. These species may electronically interact with the Lewis acid sites as a ligand to remain on the surface. Such type of attachment is also hypothetically depicted in the scheme. Over all, Si/Al ratio in the framework increases from 4.95 to 5.30.These changes can be visualized in the scheme. The ratio SiO_2 / TiO_2 decreases from 130.0 to 34.0 as shown in the table which indicates that increasing amount of Ti is incorporated in the framework as the concentration of $K_2[TiO(C_2O_4)_2]$ increases. When the reaction was carried out at higher temperature of 55^0 C (samples 7-9), the amount of Ti incorporated in

the framework increases and the samples of higher dealumination (higher SiO_2 : Al_2O_3 ratio) and higher Ti incorporation in the framework (lower SiO_2 : TiO_2 ratio) are obtained. These samples were further characterized by other techniques as described in the following sections.

SCHEME-3.1

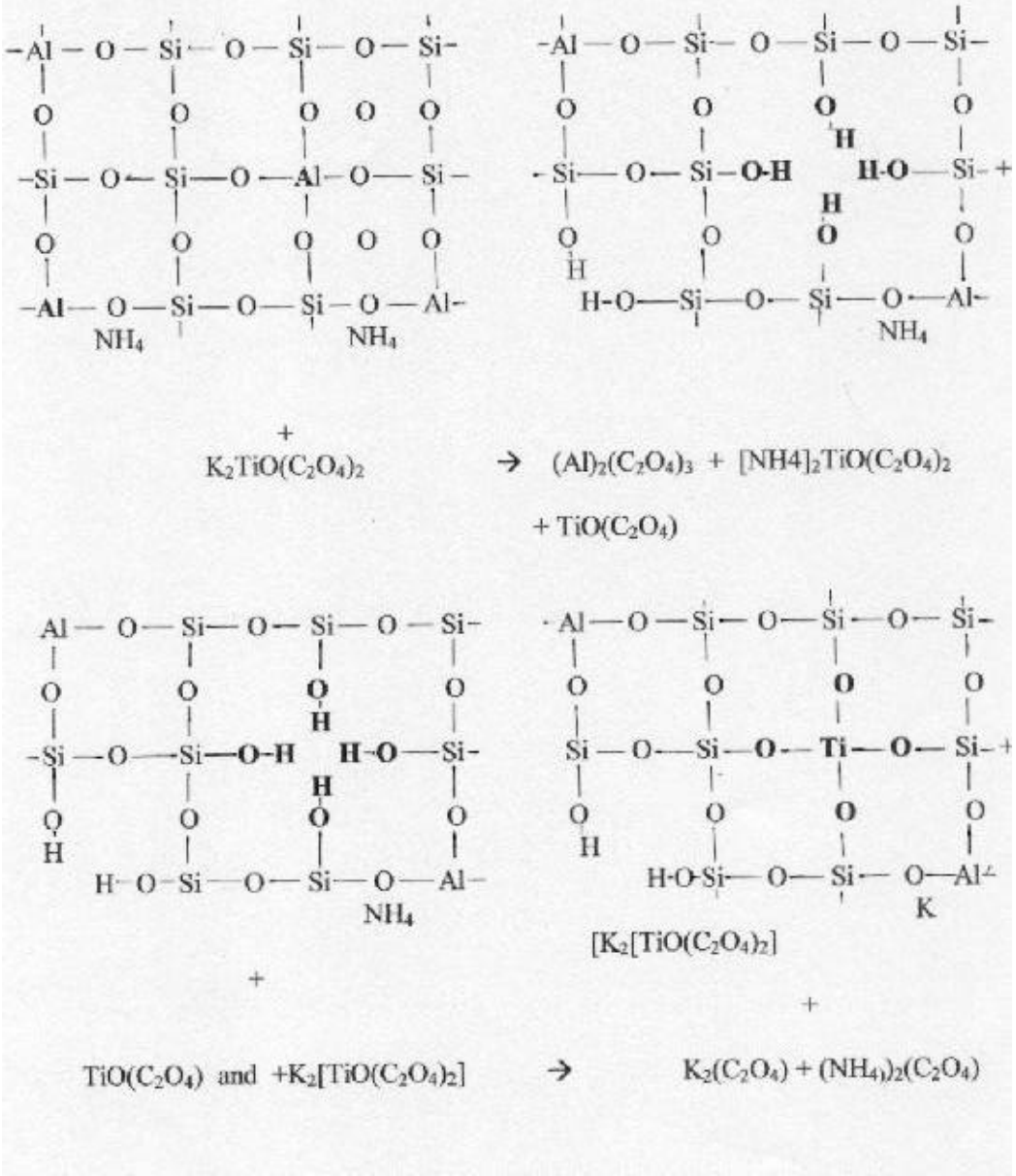

3.1.2: XRD Spectroscopy and Scanning Electron Microscopy :

In the fig-3.1, typical XRD patterns of these samples are shown. The d-values for all the hkl planes were corrected with respect to polycrystalline Si powder as internal reference and are given in the tables 3.2-3.7. The XRD patterns indicate that the samples retain good crystallinity in this reaction until Si:Ti ratio goes down to 31.3 but loose some crystallinity below this ratio. Inspection of the unit cell constant indicates a small decrease from 24.68 Å to 24.56 Å as the Ti amount increases. Despite considerable extent of dealumination occurs which reaches up to 40%, and which should have resulted in significant shrinkage of unit cell, the observed shrinkage is not proportional to dealumination, because simultanious Ti incorporation in the framework will expand the unit cell. This is attributed to the Al-O bond length of 1.75 Å, which is smaller than that of Ti-O (1.83Å) where as both of these are bigger than that of Si-O bond length (1.62 Å). The observed value is the result of these two combined effects. From the values of unit cell size, it seems that, the higher temperature of 55^0 C is favorable for Ti incorporation. The rate of aluminum extraction from NH_4-Y should not be much higher than the rate of insertion of Si or Ti in the defect sites. If the aluminum extraction is much faster as possibly occurs in the higher concentration of $K_2TiO(C_2O_4)_2$, then after certain degree of dealumination, the structure becomes very unstable and collapses (168).

In the fig-3.2, photo frames a-d, SEM photographs of these samples are presented. As the concentration of oxalate solution increases, the crystals seem to be agglomerated in to clusters of about 2-5 ìm. The figures also show that the crystallinity of the sample is maintained during these reactions.

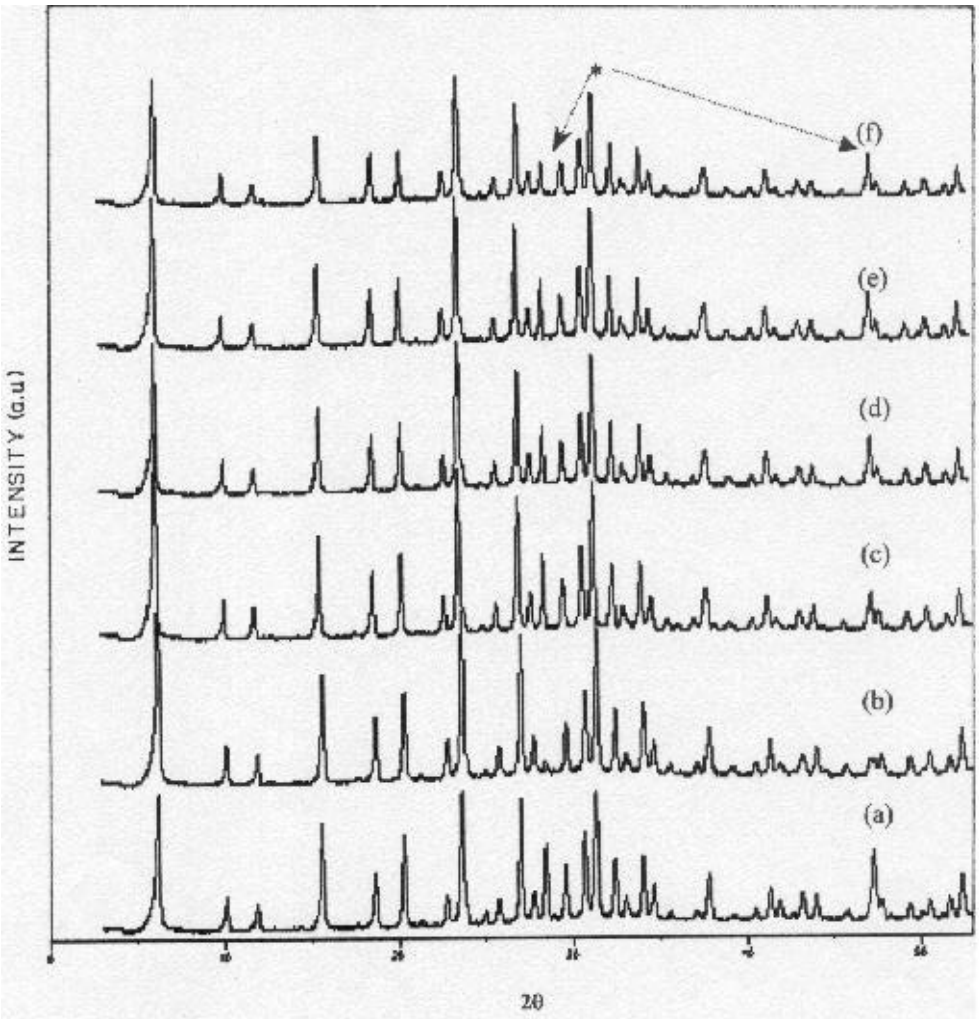

* Silicon Standard

Fig 3.1 XRD patterns of low silica Ti-USY samples

(a) NH_4-Y, (b) SSTP-25-0.165, (c) SSTP-25-0.11, (d) SSTP-25-0.22, (e) SSTP-25-0.33 and (f) SSTP-25-0.44

Table 3.2 : Unit cell parameters of Zeolite H-Y

h,k,l	d	x	a = d * x	(a*a*a)	Intensity	I/I0
1,1,1	14.31	1.7321	24.786	15227	1500	64
2,2,0	8.742	2.8284	24.726	15117	572	27
3,1,1	7.4367	3.3166	24.665	15005	836	38
3,3,1	5.6658	4.3589	24.697	15063	1617	71
4,4,0	4.3649	5.6569	24.692	15054	1436	62
5,3,3	3.7536	6.5574	24.614	14912	2326	100
6,4,2	3.2888	7.4833	24.611	14907	1984	87
6,6,0	2.9024	8.4853	24.628	14937	1032	44
10,6,2	2.0892	11.832	24.72	15105	578	27
		Mean				
value =			24.682	15036		

Table 3.3 : Unit cell parameters of Zeolite Na-Y

h,k,l	d	x	a = d * x	(a*a*a)	Intensity	I/I0
1,1,1	14.287	1.7321	24.745	15152	3240	83
2,2,0	8.759	2.8284	24.774	15205	770	20
3,1,1	7.4492	3.3166	24.706	15081	642	17
3,3,1	5.6718	4.3589	24.723	15111	2171	56
4,4,0	4.3602	5.6569	24.665	15005	1926	49
5,3,3	3.765	6.5574	24.689	15049	3270	84
6,4,2	3.2932	7.4833	24.644	14967	2661	68
6,6,0	2.9106	8.4853	24.697	15064	2027	52
10,6,2	2.0939	11.832	24.775	15208	851	22
8,8,6		12.806	24.713	15093		
		Mean value=	24.713	15093		

Table 3.4 : Unit cell parameters of Zeolite SSTP-25-0.11

h,k,l	d	x	a=d*x	a*a*a	Intensity	I/I0
1,1,1	14.226	1.7321	24.64	14960	4197	100
2,2,0	8.7264	2.8284	24.682	15036	950	23
3,1,1	7.4222	3.3166	24.617	14917	807	20
3,3,1	5.6571	4.3589	24.659	14994	2339	56
4,4,0	4.3646	5.6569	24.69	15051	2057	50
5,3,3	3.7432	6.5574	24.546	14789	3640	87
6,4,2	3.2945	7.4833	24.654	14985	3175	76
6,6,0	2.9068	8.4853	24.665	15005	2081	50
10,6,2	2.0561	11.832	24.328	14399	730	18
		Mean value =	24.609	14903		

Table 3.5 : : Unit cell parameters of Zeolite SSTP-25-0.165

h,k,l	d	x	a=d*x	a*a*a	Intensity	I/I0
1,1,1	14.017	1.7321	24.278	14310	4396	100
2,2,0	8.733	2.8284	24.701	15070	1013	24
3,1,1	7.443	3.3166	24.686	15043	826	19
3,3,1	5.6645	4.3589	24.691	15053	2308	53
4,4,0	4.3735	5.6569	24.74	15143	1948	45
5,3,3	3.7634	6.5574	24.678	15029	3645	83
6,4,2	3.296	7.4833	24.665	15005	3096	71
6,6,0	2.9097	8.4853	24.69	15050	2047	47
10,6,2	2.057	11.832	24.339	14418	810	19
		Mean value =	24.607	14901		

Table 3.6 : : Unit cell parameters of Zeolite SSTP-25-0.33

h,k,l	d	x	a=d*x	a*a*a	Intensity	I/I0
1,1,1	14.254	1.7321	24.689	15048	4396	100
2,2,0	8.7024	2.8284	24.614	14913	1013	24
3,1,1	7.4399	3.3166	24.675	15024	826	19
3,3,1	5.627	4.3589	24.528	14756	2308	53
4,4,0	4.3443	5.6569	24.575	14842	1948	45
5,3,3	3.7611	6.5574	24.663	15002	3645	83
6,4,2	3.283	7.4833	24.568	14828	3096	71
6,6,0	2.9051	8.4853	24.651	14979	2047	47
10,6,2	2.0564	11.832	24.332	14405	810	19
8,8,6	1.9032	12.806	24.373	14478	593	21
10,8,6	1.8442	12.961	23.904	13658	597	21
		Mean value=	24.506	14718		

Table 3.7 : : Unit cell parameters of Zeolite SSTP-25-0.4

h,k,l	d	x	a=d*x	a*a*a	Intensity	I/I0
1,1,1	14.3	1.7321	24.768	15195	2314	100
2,2,0	8.669	2.8284	24.52	14742	736	24
3,1,1	7.4586	3.3166	24.737	15138	649	19
3,3,1	5.6574	4.3589	24.66	14996	1539	53
4,4,0	4.3698	5.6569	24.719	15105	1239	45
5,3,3	3.7642	6.5574	24.684	15039	2885	83
6,4,2	3.2137	7.4833	24.049	13909	808	71
6,6,0	2.9009	8.4853	24.615	14914	1527	47
10,6,2	2.0564	11.832	24.332	14405	516	19
		Mean value =	24.565	14823		

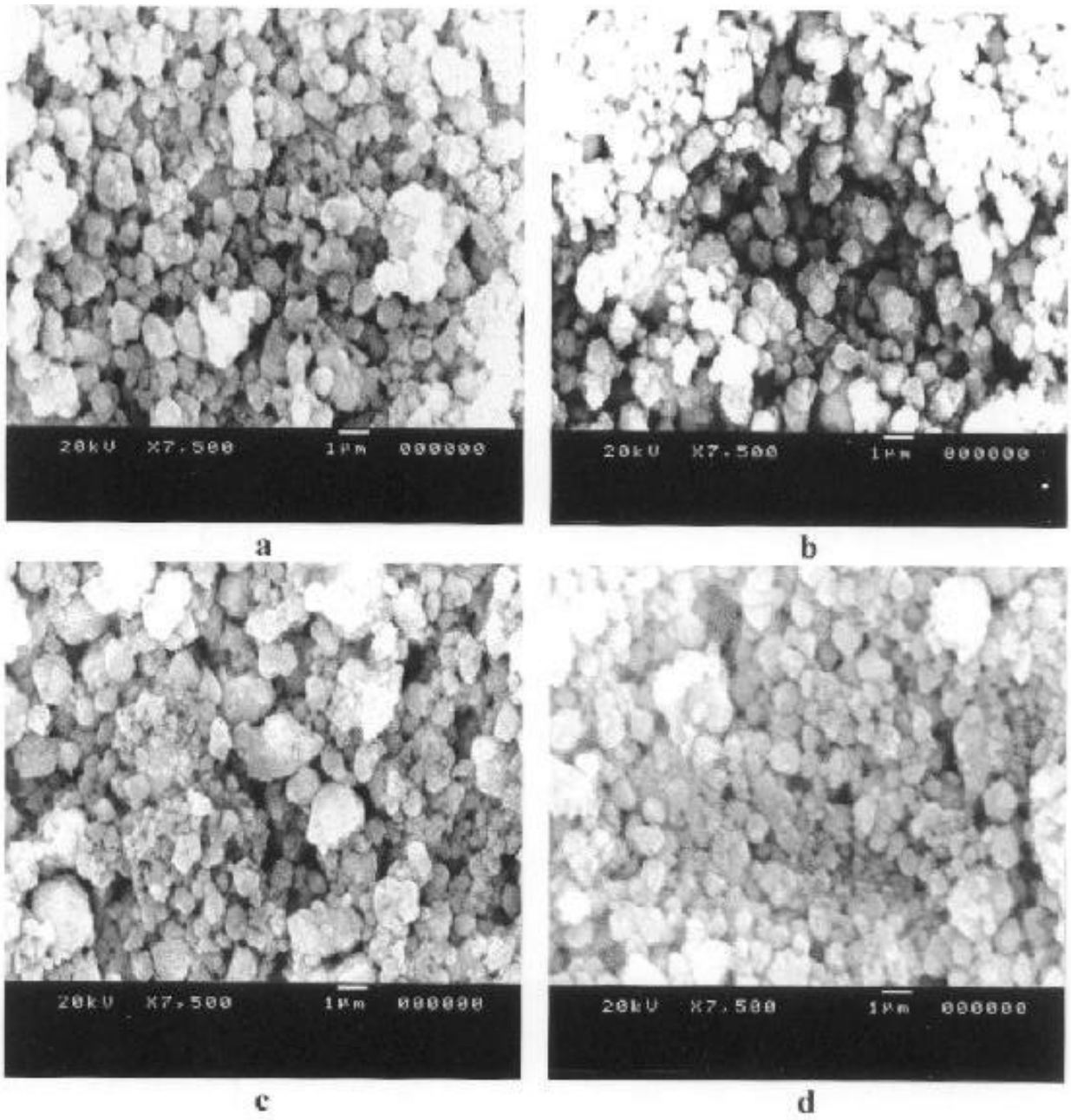

Fig 3.2: Scanning Electron Micrographs of low silica Ti-USY prepared from $K_2TiO(C_2O_4)_2$ solution (a) SSTP-25-0.165, (b) SSTP-25-0.22, (c) SSTP-25-0.33 and (d) SSTP-25-0.44

3.1.3: FTIR Spectroscopy:

FTIR spectra in the region of framework vibrations of Ti-USY samples prepared by treating NH_4-Y sample with different amount of $K_2TiO(C_2O_4)_2$ are presented in the fig-3.3. The spectrum of pure $K_2TiO(C_2O_4)_2$ is also included in the same figure for comparison..

In the table 3.8, the frequencies of vibrations are given and in the table 3.9, the general assignments for these vibrations are presented. The table 3.8 reveals no significant difference in the frequency values in these samples, excepting the appearance of new bands at 1709,1690 and 910cm^{-1}. The intensities of these bands are initially low, but go on increasing with the increase in the concentration of $K_2TiO(C_2O_4)_2$ used in the preparation. These bands are superimposing on some of the strong bands of H_2O, NH_4^+ and framework vibrations. Pure $K_2TiO(C_2O_4)_2$ shows characteristic bands at 1721,1690,1664 and 1390 cm^{-1} in this region. In comparison with this, the bands at 1709 and 1685 can be assigned to titanyl oxalate attached to the framework.

Table-3.9: Assignments of FTIR frequencies of framework vibrations in zeolite

Linkage type,	Frequency range, cm^{-1}
Internal tetrahedra	
Asymmetric stretch.	1250-950
Symmetric stretch.	720-650
T-O bend (T=Si,Al)	420-500
External linkages	
Double ring	650-500
Pore opening	300-420
Symmetric stretch	750- 820
Asymmetric stretch	1015- 1150

The low frequency shift in the bands of oxalate ion in the zeolite can be attributed to the interaction of oxalate group with the anionic framework and the hydroxyl groups on the zeolite (169). The band at 910 cm^{-1} may indicate the presence of Ti in the framework as has been mentioned by X. Liu et al (103). They have also observed a band at 908cm^{-1} for

Na^+ containing Ti-Y. It should be noted that in our samples also, K^+ cations are present in appreciable amount. Therefore the nature of FTIR spectra indicates that $[TiO(C_2O_4)_2]^{2-}$ ions are present as adsorbed species on the zeolite.

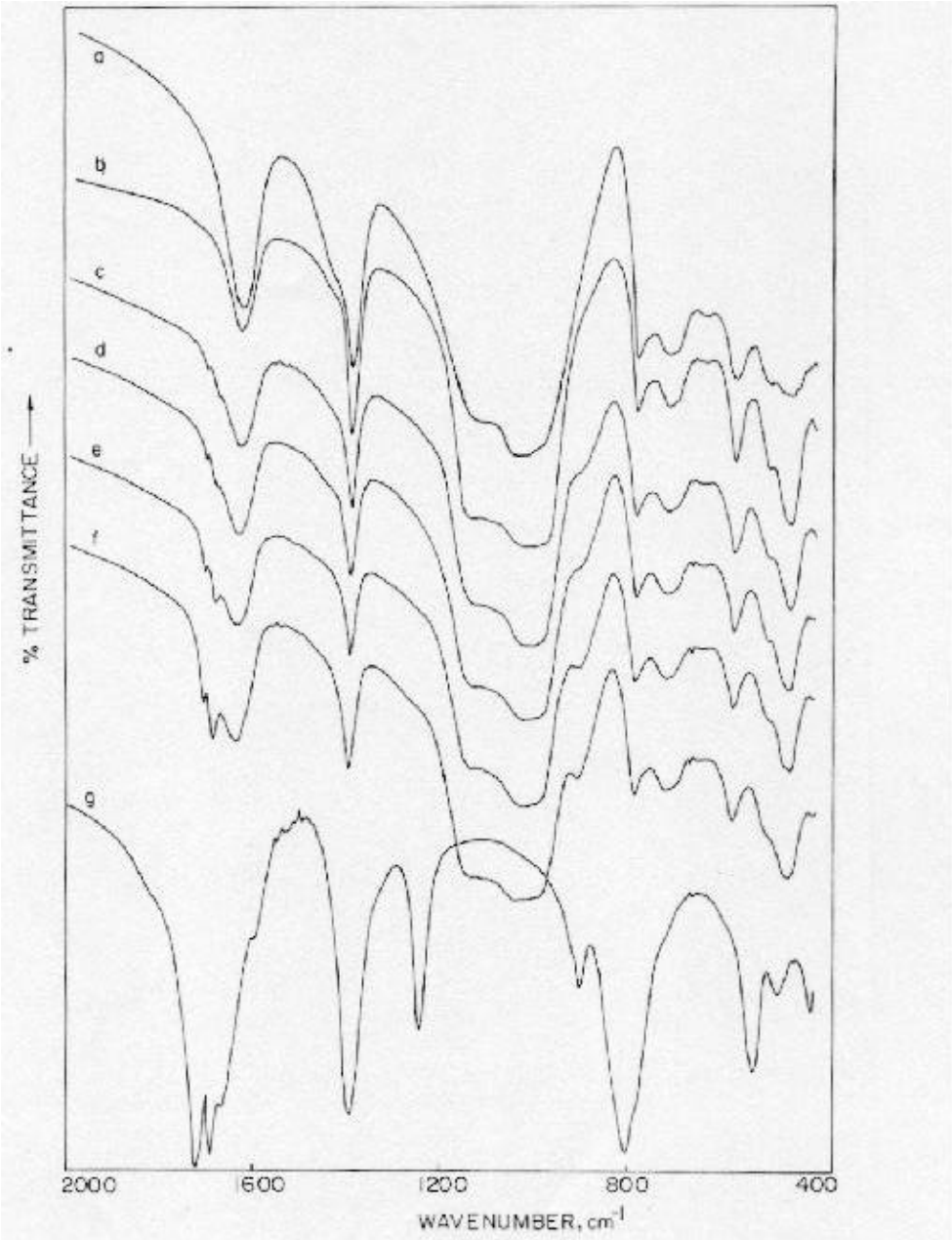

Fig.-3.3: FTIR spectra of low silica Ti-USY samples in the framework vibration region (a) SSTP-25-0.11, (b) SSTP-25-0.165, (c) SSTP-25-0.22, (d) SSTP-25-0.33, (e) SSTP-25-0.44 and (f) Potassium titanyl oxalate $[K_2TiO(C_2O_4)_2]$

Table-3.8: Frequency of framework vibrations of low silica Ti- USY prepared by Single step (SSTP) method using $K_2TiO(C_2O_4)_2$ solution

Sample.	Frequency, cm^{-1}												
SSTP-25-0.055	-	-	1636	1398	1137	1017	910	785	716	641	572	500	456
SSTP-25-0.11	-	-	1636	1399	1138	1017	910	785	719	640	572	500	456
SSTP-25-0.165	1709	1687	1637	1399	1142	1019	910	785	719	641	572		456
SSTP-25-0.22	1709	1690	1640	1399	1142	1019	910	785	719	638	572	500	456
SSTP-25-0.33	1709	1690	1640	1399	1142	1017	908	785	719	641	572	500	456
SSTP-25-0.44	1712	1690	1640	1398	1142	1017	908	785	719	641	572	497	456
$K_2TiO(C_2O_4)_2$	1721	1685	1664	1390	1242	-	-	801	-	-	525	478	406

3.1.4: UV / VIS Spectroscopy:

The fig 3.4 depicts the diffuse reflectance UV / VIS spectra of Ti-USY samples prepared with different amount of $K_2TiO(C_2O_4)_2$ solution. The spectra show increasing absorption in a wide span of frequency from 550 nm and peaking at around 220 nm. With in this range, three well-defined bands can be noticed at 215,230 and 290 nm and above that frequency; absorption continuously decreases which may have one or more number of broad and weak bands. The intensities of these bands are low for lower concentrations of $K_2TiO(C_2O_4)_2$ solutions, but go on increasing with the increase in the concentration of $K_2TiO(C_2O_4)_2$ solution used to prepare these samples. All samples contain features with respect to range of absorption and band intensities similar to those reported by J. Klaas et al and others for TiO_x species in dealuminated Y zeolite (170) and in TiO_x-SiO_2 samples (171-173), both prepared by $TiCl_4$ treatment. By following their interpretation, the insertion of TiO_x species by reaction of $K_2TiO(C_2O_4)_2$ solution in NH_4-Y zeolite can be considered to take place by (i) mono-functional, (ii) bi-functional and (iii) multifunctional manner as shown in the scheme-3.2. Following the previous literature, these species can be assigned to the bands at 290, 230 and 215 nm respectively arising by charge transfer from 2p orbitals of oxygen ligand to the 3d orbital of Ti cation. The absorption at higher frequencies in the spectra is assigned to quantum sized anatase particles. The frequencies of all the bands depend up on the kind of attachments (mono-functional, bi-functional or multifunctional). The mononuclear TiO_x species are forming via various kinds of attachments to different types of sites as indicated in the reaction scheme.

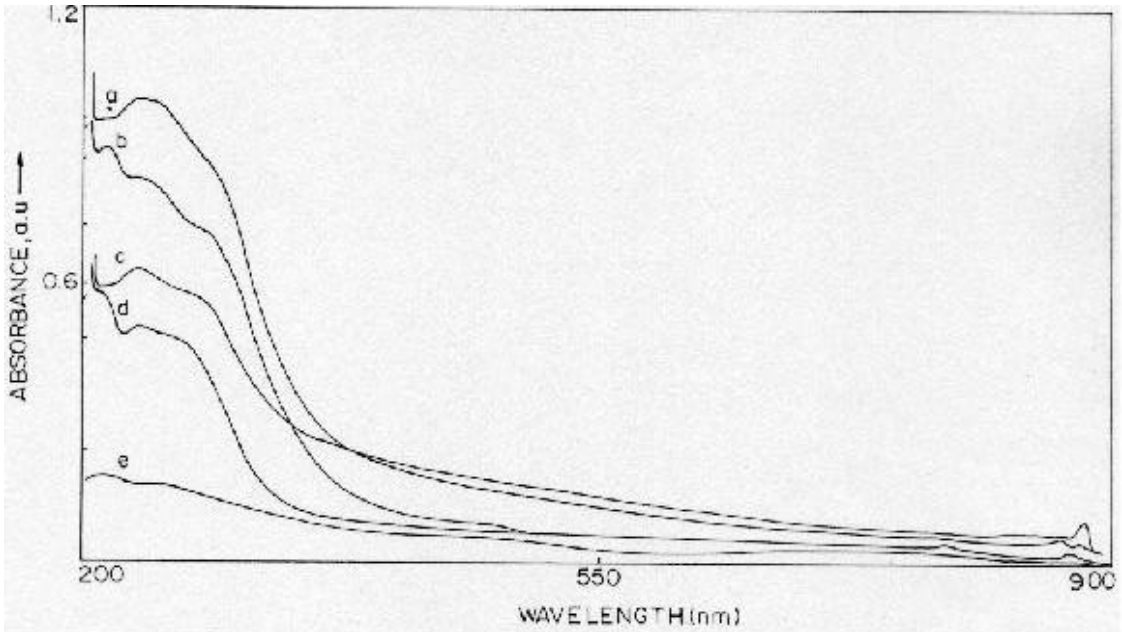

Fig.-3.4: Diffuse Reflectance UV-VIS Spectra of low silica Ti-USY samples (a) SSTP-25-0.44, (b) SSTP-25-0.33, (c) SSTP-25-0.22, (d) SSTP-25-0.165, and (e) SSTP-25-0.11

Scheme-3.2

$$\text{--Si - O -H} + K_2TiO(C_2O_4)_2 \rightarrow \text{--Si-O...H}\ [K_2TiO(C_2O_4)_2] \quad \text{(mono-functional)}$$

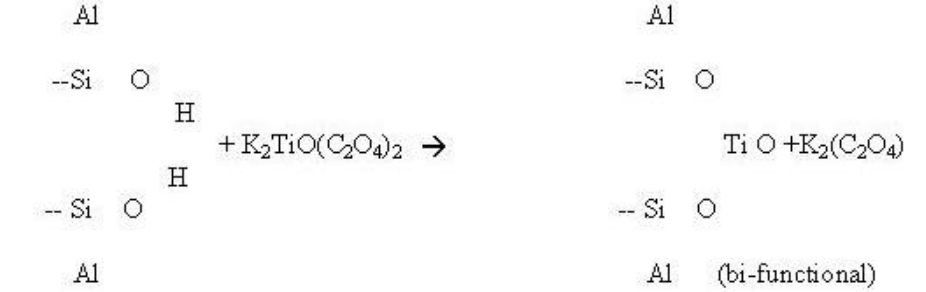

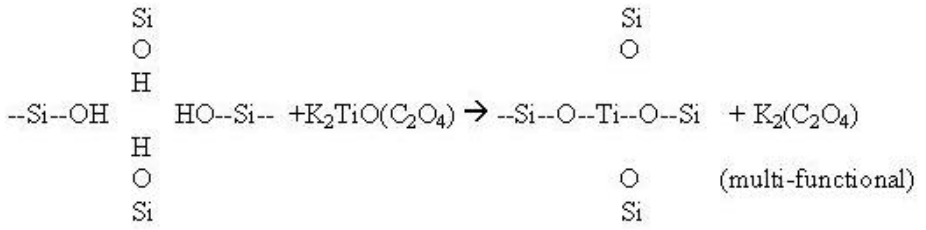

From these results, we are inclined to believe that Ti is coordinated to the zeolite structure in the tetrahedral vacancies (multifunctional), on the cation exchangeable sites with more than one point of attachment (bi-functional), and on the defect sites (tricoordinated Si) generated by dehydroxylation with a single point of attachment (mono-functional).

3.1.5: Thermo-gravimetric Analysis

The TG/DTG/DTA curves of Ti-USY samples prepared by single step method described above are presented in the fig-3.5-3.9 and compared with that of NH_4-Y sample .The loss in weight and the peak temperatures of endothermic and exothermic desorption/decomposition reactions are presented in the table-3.10.

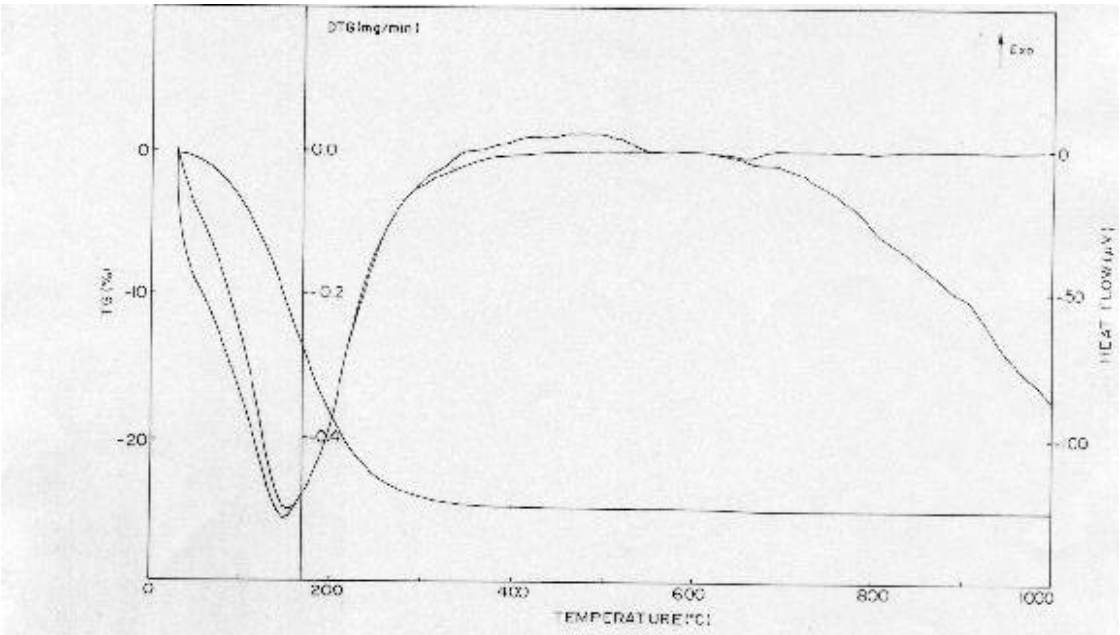

Fig -3.5: Thermograms of NH_4-Y zeolite

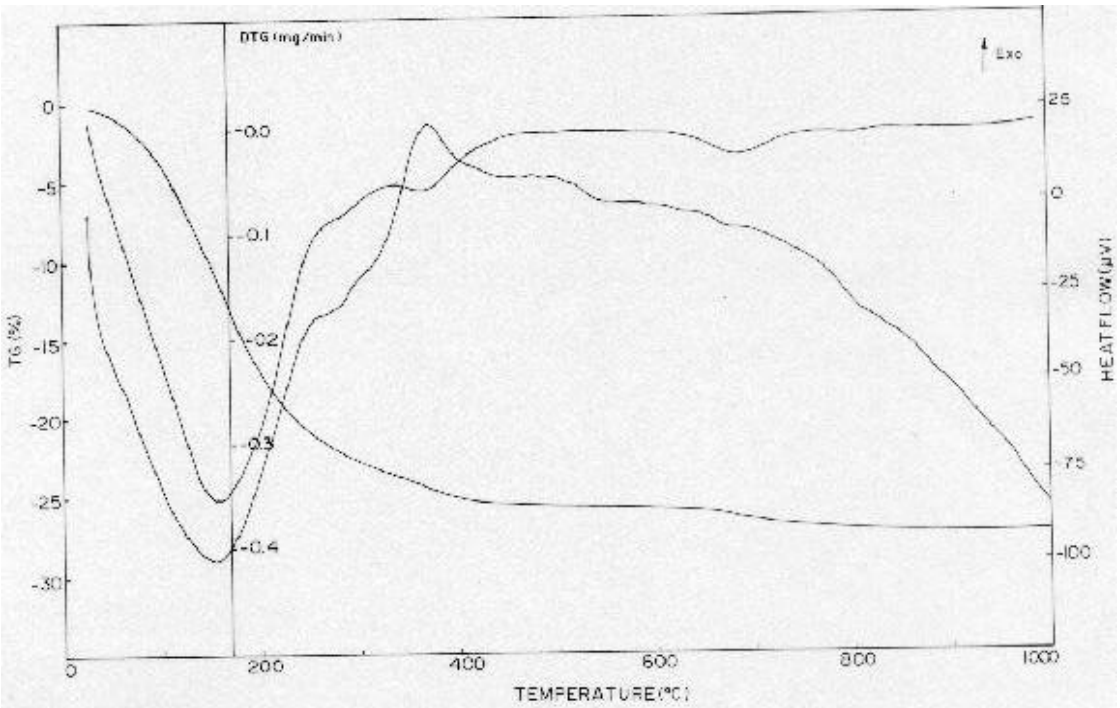

Fig.-3.6: Thermograms of low silica Ti-USY sample, SSTP-25-0.11

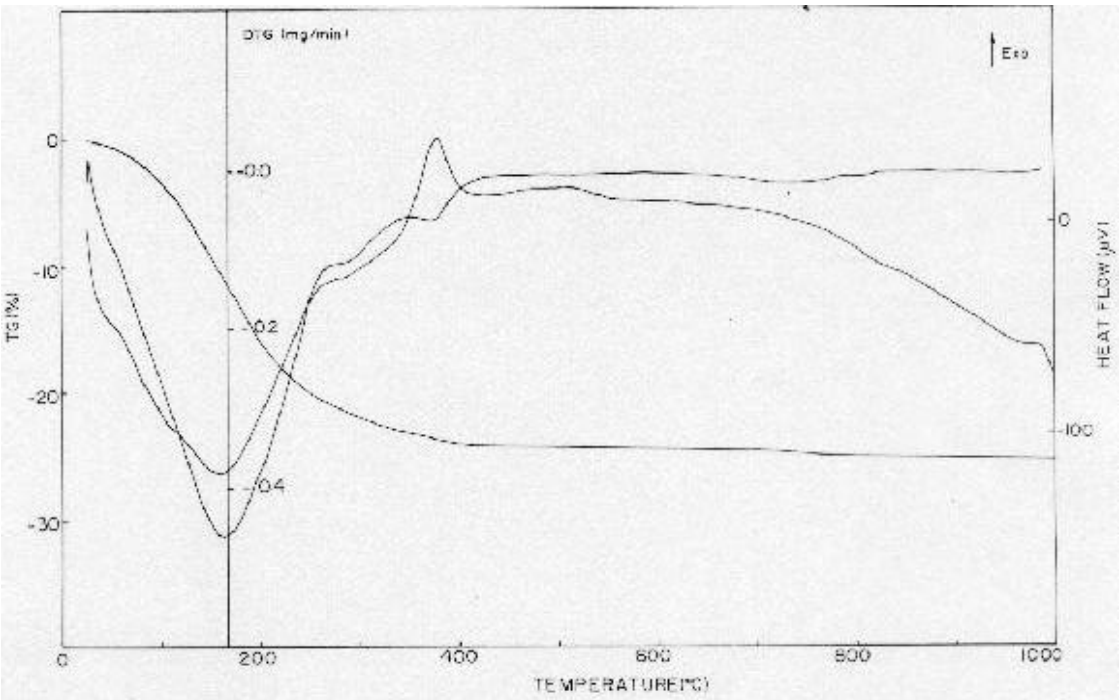

Fig.-3.7: Thermograms of low silica Ti-USY sample, SSTP-25-0.22

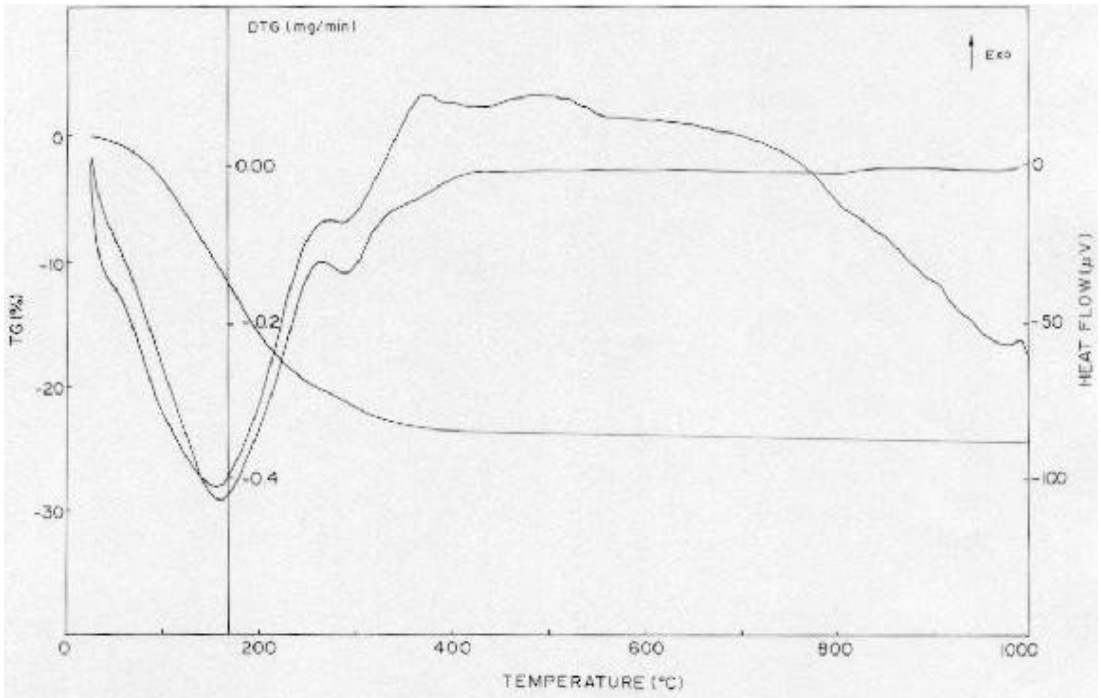

Fig -3.8: Thermograms of low silica Ti-USY sample, SSTP-25-0.33

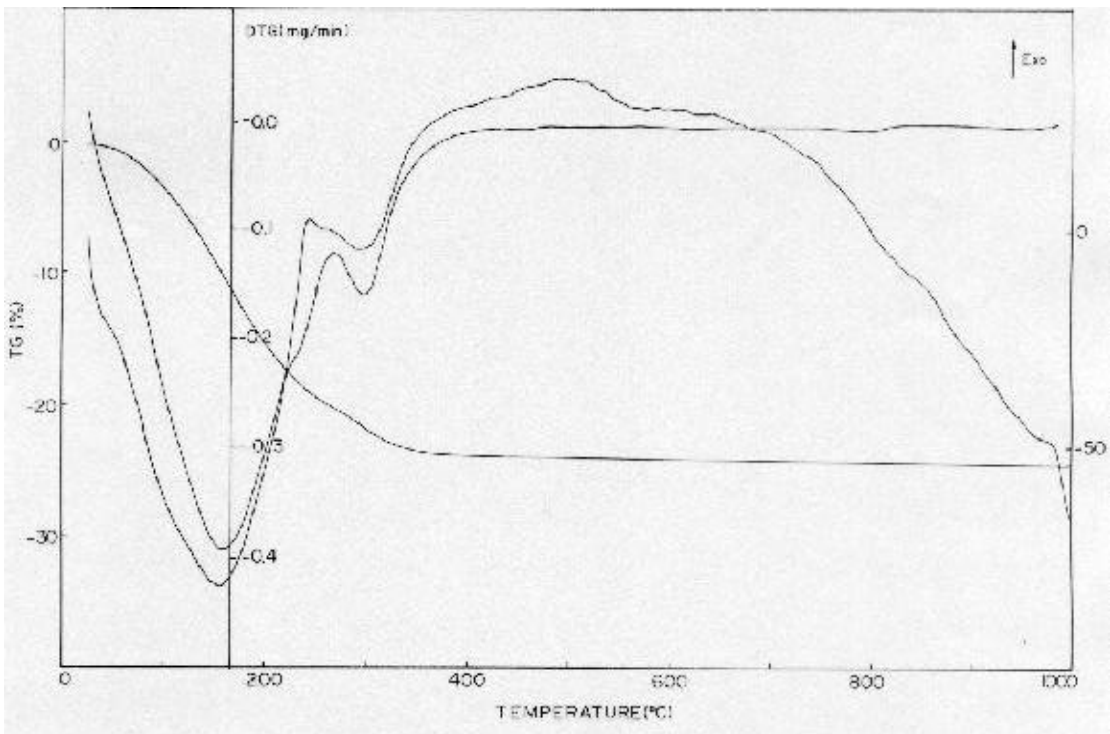

Fig.-3.9: Thermograms of low silica Ti-USY sample, SSTP-25-0.44

Table 3.10: TG/DTA data of low silica Ti-USY samples prepared by single step (SSTP) method using $K_2TiO(C_2O_4$ solution

Name of the sample	Peak Temp (^{0} C)	% Weight loss	Peak Temp. (^{0} C)	% Weight loss	Peak Temp. ^{0} C
NH_4Y	44(sh), 148	24.67	Broad	-	920
SSTP-25-0.11	45(sh), 151 287, 371	25.77	704	1.039	-
SSTP-25-0.22	45(h), 102(h) 157, 320, 380	24.1	710	-	987
SSTP-25-0.33	42(h), 95(h) 157,300,370	23.7	501 750	0.1	990
SSTP-25-0.44	42(sh), 96(sh) 156, 244, 302	24.0	501	-	980

Most of the weight loss of about 24% occurs below 500 ^{0} C in multiple steps for all samples. They are not so well separated. For NH_4-Y sample (fig-3.5), it occurs around 160^0 C with a low temperature shoulder around 75 ^{0} C which is attributed to the loss of water and NH_3 leading to the formation of H-Y zeolite. For all other samples (fig-3.6-3.9), a small endothermic peak around 300^0 C and an exothermic peak around 375 -500^0 C whose intensities increase with the amount of Ti incorporated are observed. These may be attributed to the decomposition of oxalate moiety in the zeolite, which is present in small amount in the sample. A small endothermic peak around 700^0 C, which becomes broader as the Ti concentration increases may be due to the decomposition of titanium hydroxide species originated from the decomposition of titanyl oxalate. A small exothermic peak is observed around 980^0 C, which is assigned to the exothermic structural collapse of the sample. A notable feature in these curves is that the exothermic peak due to structure collapse occurs at higher temperature as the Al content decreases and the Ti content increases in the sample.

3.2: High silica and very high silica Ti-USY by multiple step (MSTP) method

3.2.1: High silica and very high silica USY by hydrothermal dealumination of NH_4-Y

The success of the incorporation of Ti in high silica USY zeolite largely depends on the preparation of high silica USY itself. In order to obtain most suitable high silica

USY, hydrothermal dealumination of NH_4-Y was carried out under different conditions as described in the table 2.3 in Chapter-II .The samples were characterized by XRD, SEM and FTIR spectroscopic methods and they are presented in this part. In the fig-3.10, XRD patterns of NH_4-Y hydrothermally treated at increasing severity are presented. In the table 3.11, the values of unit cell constants (a values), unit cell volume (a^3 values) and the chemical composition of the framework determined by ^{29}Si MAS NMR are given.

Table 3.11: Chemical composition and unit cell constants of high silica and very high Silica USY by hydrothermal dealumination of NH_4-Y determined by combination of XRD, AAS, XRF and MAS NMR spectroscopy.

S. N	Name of sample	Unit cell const.	Unit cell vol.	Frame work, Si/Al	Unit cell Composition	%Deal minati on.
1	Na-Y	24.71	15093	2.4	$Na_{20}[(AlO_2)_{56}(SiO_2)_{136}]$	4 %
2	NH_4Y	24.68	15036	2.56	$Na_{20}[(AlO_2)_{54}(SiO_2)_{138}]$	10.4 %
3	550-MSTP	24.38	14493	8.75	$Na_2[(AlO_2)_{20}(SiO_2)_{172}]$	64 %
4	550-700-MSTP	24.34	14428	18.2	$Na_{1.49}[(AlO_2)_{10}(SiO_2)_{182}]$	82 %
5	550-700-850-MSTP	24.22	14202	26.3	$Na_{1.22}[(AlO_2)_7(SiO_2)_{185}]$	87.5 %
6	550-700-850-925-MSTP	24.15	14092	31.0	$Na_1[(AlO_2)_6(SiO_2)_{186}]$	89.3 %
7	550-700-850-MSTP-10	24.21	14183	52.06	$Na_{1.26}[(AlO_2)_{3.6}(SiO_2)_{188.4}]$	93%

The inspection of the XRD patterns reveals that the crystallinity of the sample is maintained in the hydrothermal treatment up to 850^0 C (sample 550-700-850-MSTP), and then it drops down in the sample treated further at 925^0 C. The unit cell constant which is the indication of dealumination was calculated to be 24.48, 24.35, 24.22 and 24.15 Å for these hydrothermally dealuminated samples. The unit cell constant drops to the extent of 1.9% from 24.68 Å for NH_4 –Y to 24.22 Å for severely dealuminated sample and the unit cell volume drops by 6.3% from 15036 $Å^3$ to 14092 $Å^3$, even then, the sample remains crystalline. The bulk Si/Al ratio increases marginally from 2.45 to 2.87 due to removal of some of the exchangeable extra aluminum species formed in the hydrothermal dealumination by intermediate ion exchange with NH_4NO_3 solution. Where as the framework Si/Al ratio determined by ^{29}Si MAS NMR increases very much from 2.56 to 26.3 for highly crystalline sample. The significant difference in the bulk and the framework Al is attributed to the presence of non-exchangeable Al species, but not

detectable "invisible Al" as per ^{29}Si and ^{27}Al MASNMR results described in the chapter-IV. The maximum framework dealumination is noted to be about 88%.

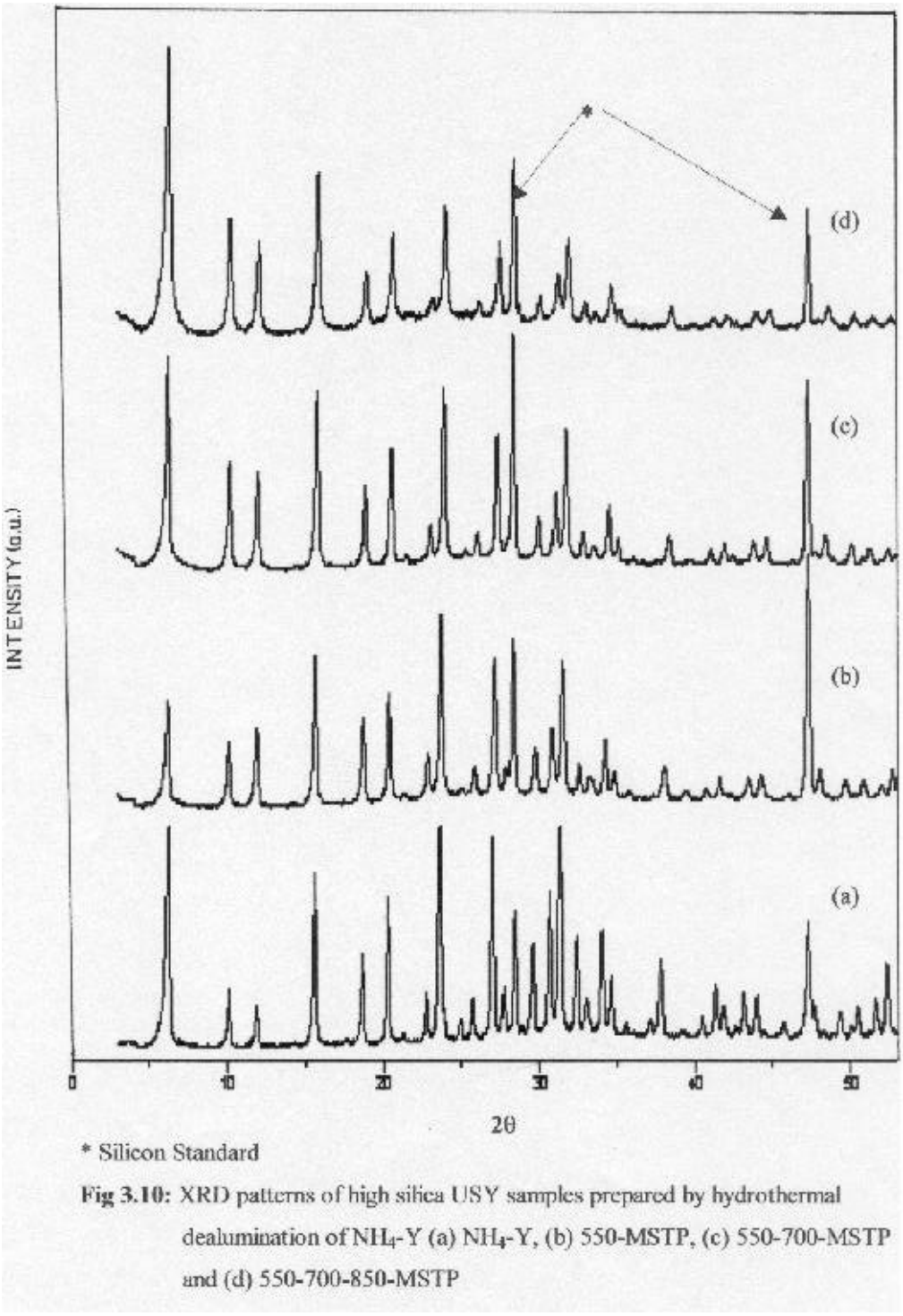

Fig 3.10: XRD patterns of high silica USY samples prepared by hydrothermal dealumination of NH_4-Y (a) NH_4-Y, (b) 550-MSTP, (c) 550-700-MSTP and (d) 550-700-850-MSTP

The hydrothermal dealumination of NH_4-Y zeolite generates USY with various types of surface active sites which can be represented as in the scheme 3.3.The decomposition of NH_4-Y at 550^0 C liberates NH_3 gas and generates Bronsted acid sites as shown in the reaction 1 and 2. Two molecules of Bronsted acid sites liberate a molecule of water and generate one Bronsted and one Lewis acid sites as shown in the reaction 3 and 4. The negatively charged framework reacts with a proton to completely remove one Al from the framework as shown in the reaction 5. Over all, a highly dealuminated surface of USY can be represented as shown in the equation (6) in the scheme. In summary, such a surface exposes variety of sites like

(1) Dealumination "nest" Bronsted sites perturbed by adsorbed legends like water,

(2) Dealumination "nest" silanol sites,

(3) Exchangeable proton sites,

(4) Al associated Bronsted sites,

(5) Lewis sites,

(6) Cationic Al sites, and

(7) Anionic Al sites.

With respect to Al species, the surface can be visualized as containing various kinds of Al species as given in the table 3.12.

The SEM photographs of these samples are presented in the fig 3.11. The crystallite size of NH_4-Y is around 0.5 to 1.5 ìm, which remains unchanged in the dealuminated samples as can be seen in the figure.

Scheme-3.3

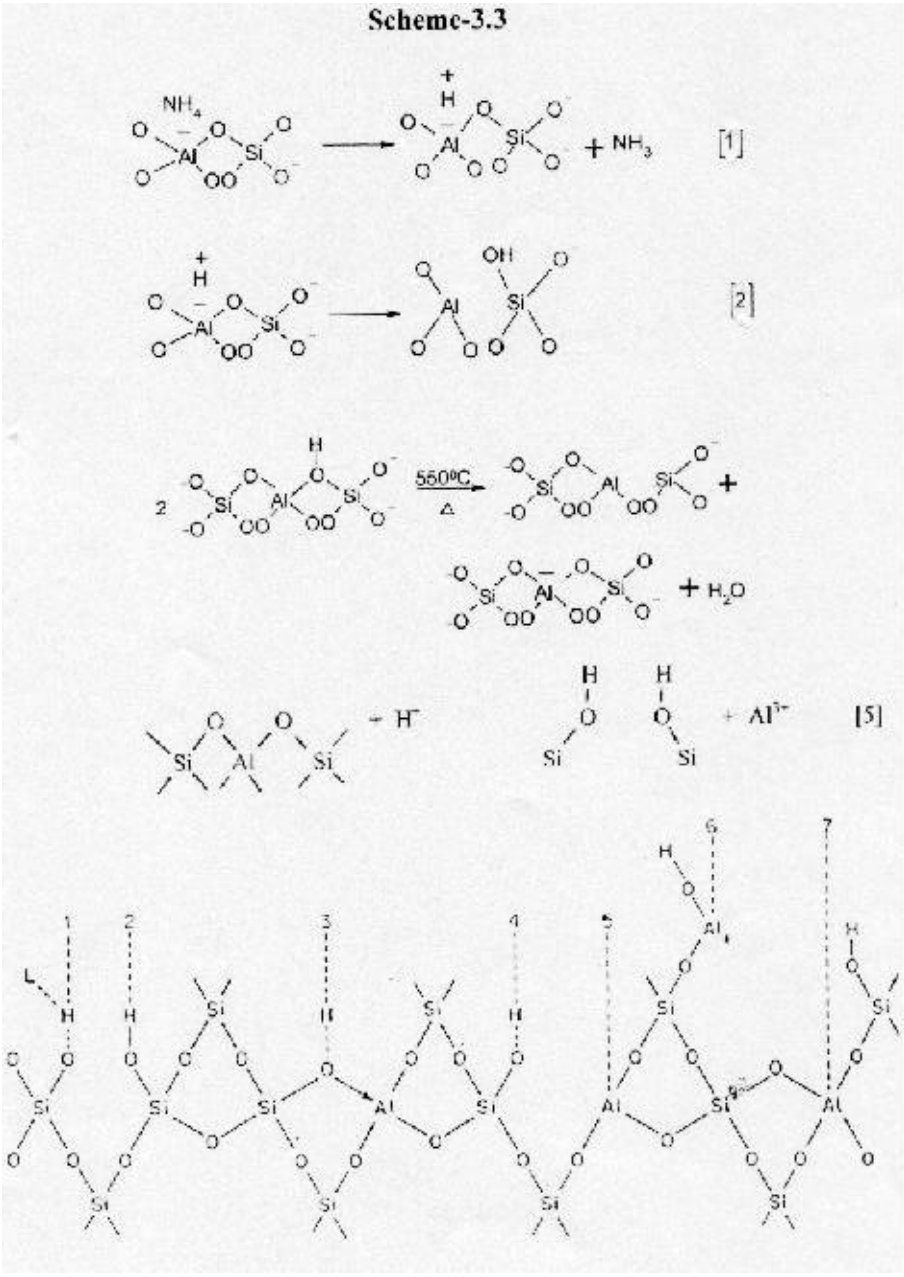

Table 3.12 : Types of Aluminum Species encountered in USY zeolites

Aluminum species in the zeolite framework (Al_F)	Extra framework Aluminum species (Al_{EF})
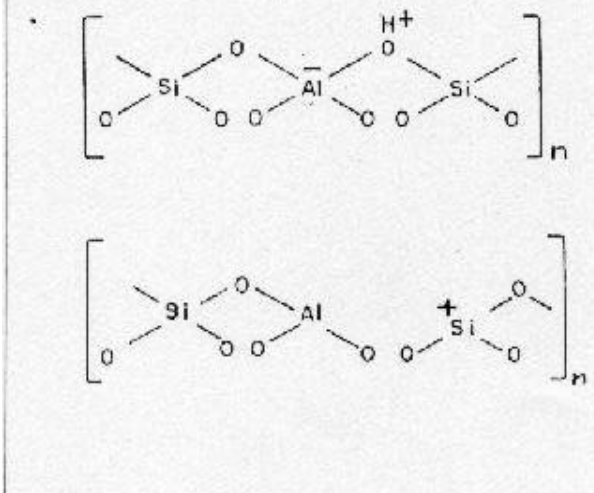	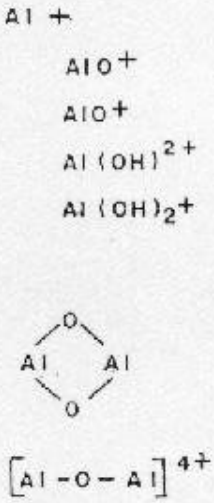

The fig 3.12 presents FTIR spectra of these samples in the framework vibration region. In the table 3.13, the frequency values of those vibrations are listed. All the characteristic fundamental vibrations of framework shift considerably to higher frequency as the dealumination increases. The bands at 1153,1013,786,711,574,507,and 460 cm^{-1} observed for NH_4-Y zeolite appears at 1208,1081,835,789,615,528 and 460 cm^{-1} respectively for the sample 550-700-850-MSTP. Under the conditions of hydrothermal dealumination, these samples not only retain the structural stability but have shown improvement in crystallinity as well, as evidenced by the development of sharper bands with higher intensity in the FTIR as well as in the XRD spectra. On the basis of these results, the samples 550-MSTP and 550-700-850-MSTP were selected for the incorporation of Ti to prepare high silica and very high silica Ti-USY respectively. From the properties described above, it can be inferred that these samples are highly crystalline USY samples of high silica and very high silica contents respectively. These two samples were used to prepare high silica Ti-USY and very high silica Ti-USY samples respectively as discussed below.

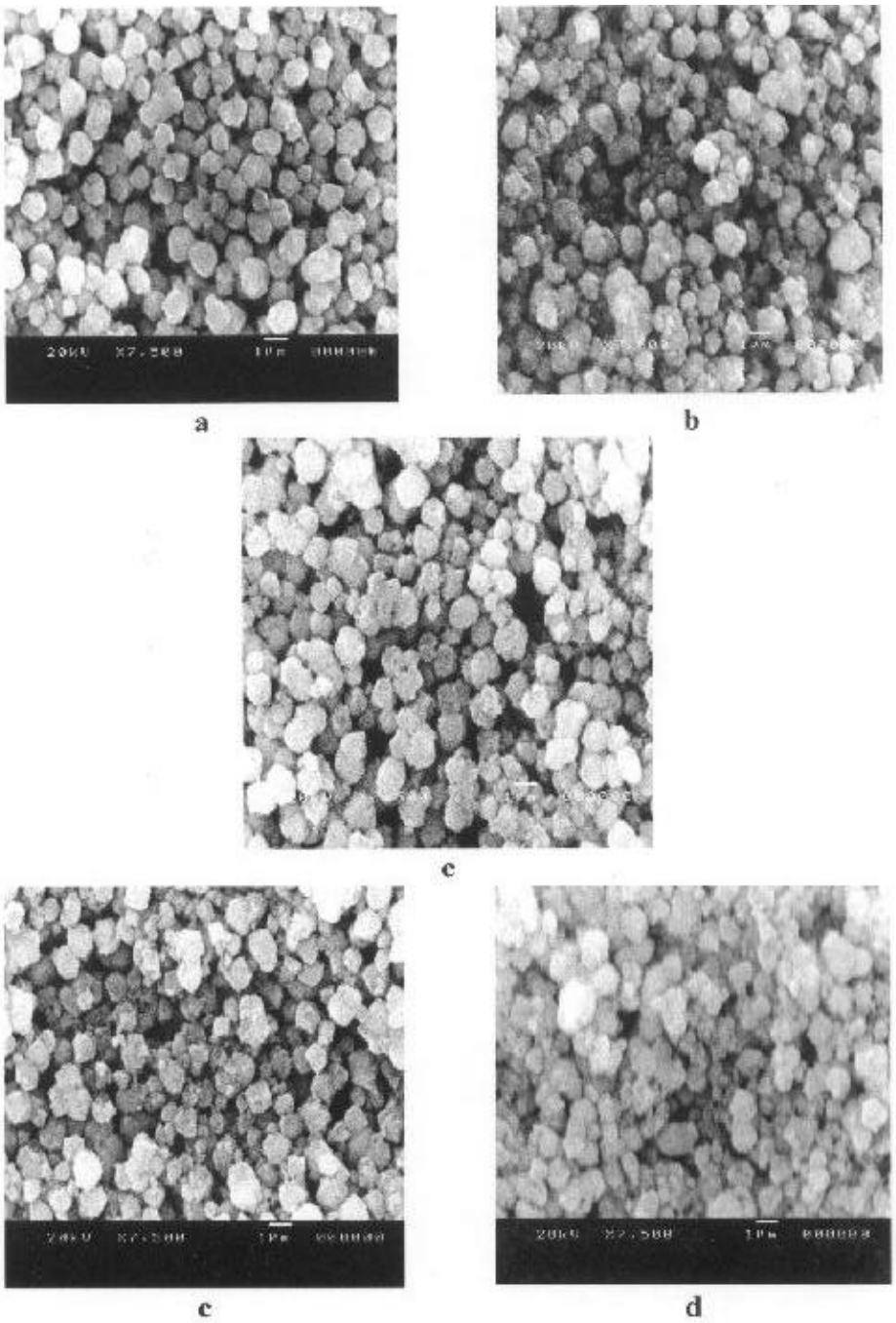

Fig 3.11: Scanning Electron Micrographs of USY samples prepared by hydrothermal dealumination of NH_4-Y (a) NH_4-Y, (b) 550-MSTP, (c) 550-700-MSTP, (d) 550-700-850-MSTP and (e) 550-700-850-925-MSTP

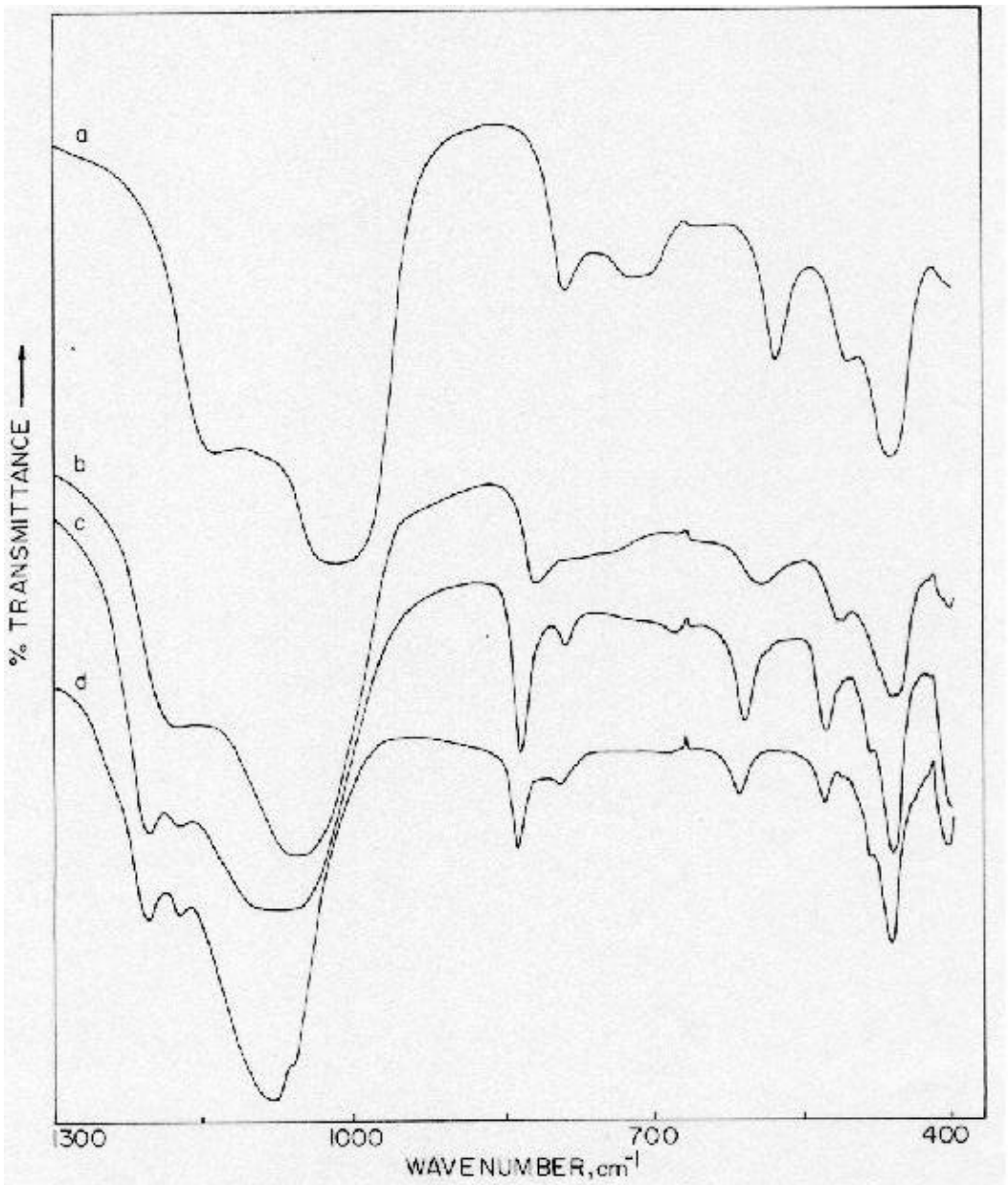

Fig.-3.12: FTIR spectra of USY samples prepared by hydrothermal dealumination in framework vibration region, (a) NH_4-Y, (b) 550- MSTP, (c) 550-00-MSTP, (d) 550-700-850-MSTP

Table 3.13: Frequencies of framework vibrations of high silica and very high Silica USY by hydrothermal dealumination of NH_4-Y.

Name of the sample	Frequency of vibration, cm^{-1}							
NH_4-Y	1153	-	1013	786	711	574	507	460
550-MSTP	1183	-	1053	817	789	592	513	460
550-700-MSTP	1208	1175	1071	831	789	607	527	460
550-700-850-MSTP	1208	1175	1081	835	789	615	528	460

3. 2. 2: High silica Ti-USY from high silica USY (550-MSTP) sample by multiple step (MSTP) method using $K_2TiO(C_2O_4)_2$ solution

In the multiple steps (MSTP) method of Ti incorporation, standard USY sample prepared by the hydrothermal treatment as described above (sample 3 in table3.11) was treated with $K_2TiO(C_2O_4)_2$. solution. The reaction was carried out at 25,55 and 200 ^{0} C with different concentration of $K_2TiO(C_2O_4)_2$ solution as described in the table 2.4 in chapter-II. The table 3.14 contains the chemical compositions of all the samples in this series. As the concentration of $K_2TiO(C_2O_4)_2$ increases from 0.11 to 0.44 mol fraction, the Na level in the sample decreases from 1.1 to 0.4 mol %, where as K level increases from 2.5 to 7.3 mol % and that of Ti increases from 0.51 to 2.31 mol %. Small amount of Al is reinserted in the framework from the extra lattice species as indicated by the Si/Al ratio, which drops from 2.6 to 3.15-mol %. As the temperature of the reaction increases from 25 to 200^0C, the concentration of exchangeable cations, Na and K decreases further, that of Al also decreases but that of Ti increases. The effect of HNO_3 is to assist in dealumination and reduce the concentration of Na and K cations to a very low level. From the results of chemical analysis, one important point should be noted that the concentration of Ti incorporated in the system reaches to a maximum level of about Si / Ti value of 30 irrespective of the temperature of reaction and concentration of $K_2TiO(C_2O_4)_2$.

Table 3.14: Chemical composition of high silica Ti-USY determined by combination of AAS and XRF spectroscopy, (mol %).

Sr. No.	Name of the sample	Na	K	Ti	Al	Si	mSi/mAl	Si / Ti
1	NH_4-Y	7.26	-	-	26.73	66.0	2.35	-
2	550-MSTP-25-0.11	1.1	2.5	0.58	26.6	67.1	2.6	121.5
3	550-MSTP-25-0.22	0.8	4.85	1.71	24.4	68.3	2.8	49.4
4	550-MSTP-25-0.33	0.5	5.35	2.02	23.2	68.4	2.95	32.6
5	550-MSTP-25-0.44	0.4	7.3	2.31	21.68	68.3	3.15	29.5
6	550-MSTP-55-0.11	0.2	6.5	0.62	22.10	70.6	3.2	116.7
7	550-MSTP-55-0.33-HNO_3	0.17	0.3	2.61	17.60	79.3	4.5	30.3
8	550-MSTP-200-0.44-HNO_3	0.1	0.18	2.83	15.6	81.2	5.2	28.8

In the fig-3.13, the XRD patterns of those samples are presented. The crystallinity of the samples remain almost unchanged and the crystalline forms of titanium oxide are not observed in the samples. The unit cell constant is found to be 24.49Å, which is higher than the value for parent USY zeolite, 24.38 Å. The starting USY sample contains NMR "invisible" Al species as described in the next part which is likely to be reinserted in the tetrahedral framework positions in the reaction medium. In addition, the incorporation of Ti will also contribute to the increase in the unit cell size. These points are further discussed while describing the results of FTIR data.

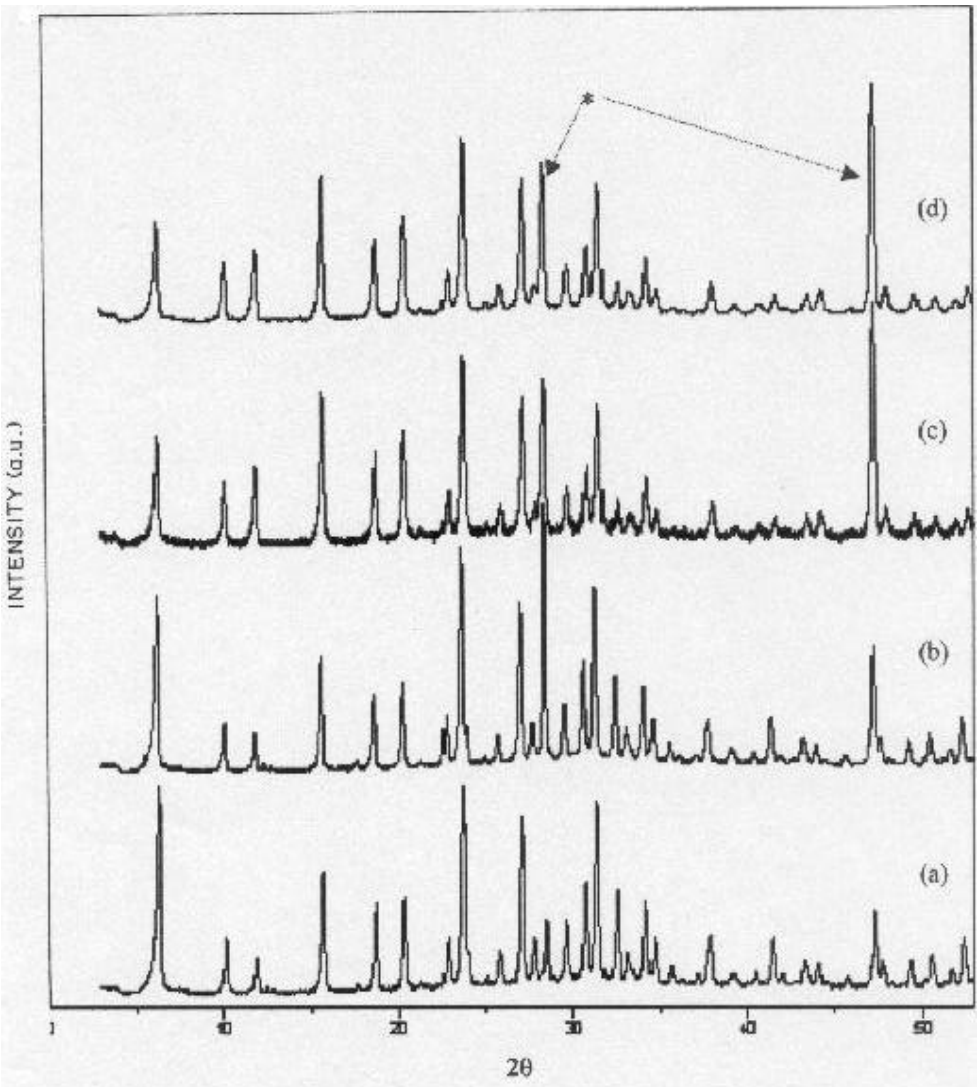

* Silicon Standard

Fig 3.13 XRD patterns of high silica Ti-USY prepared from $K_2TiO(C_2O_4)_2$ solution (a) 550-MSTP-25-0.11, (b) 550-MSTP-25-0.165, (c) 550-MSTP-25-0.22 and (d) 550-MSTP-25-0.33

The UV/VIS spectra of the above samples are given in the fig-3.14, which are similar in nature to those of low silica Ti-USY samples prepared in single step. Various kinds of surface species are available for reaction with $K_2TiO(C_2O_4)_2$ solution as depicted in the scheme 3.3 and table 3.12.The active sites for the reaction of TiO^+ species with the USY surface is supposedly mono-functional, bi-functional and multifunctional as described in the scheme 3.2 before.

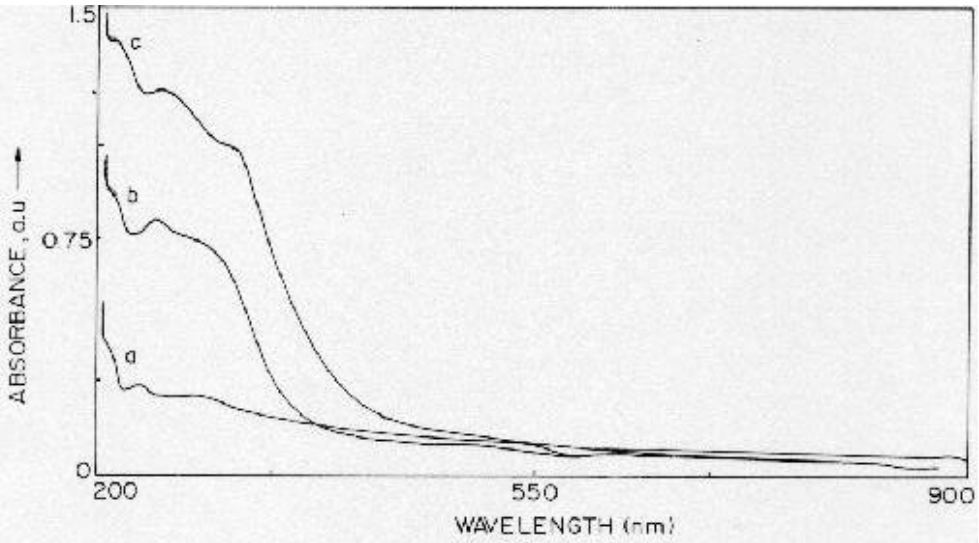

Fig.-3.14: Diffuse Reflectance UV-VIS Spectra of high silica Ti-USY samples, (a) 550-MSTP-25-0.11, (b) 550-MSTP-25-0.33, (c) 550-MSTP-25-0.44

It was described in the previous section, that $K_2TiO(C_2O_4)_2$ reacts with USY surface as monomeric mode and gives rise to the characteristic bands of these species in UV/VIS spectra at 290, 230 and 215 nm respectively. In the figure, the absence or less amount of quantum sized clusters of TiO_2 is indicated by the absence or very weak absorption in the region of high wavelength in the UV/VIS spectra. Similarly, the absence of extra lattice TiO_2 particles are also indicated in the XRD patterns, also described earlier.

The FTIR spectra in the region of framework vibrations are depicted in the fig-3.15 and the frequencies of different vibrational bands are tabulated in the table-3.15.The data for the starting USY zeolite (550-MSTP) is also given for the sake of comparison. In this result, two important points are to be considered (i) the presence of oxalate ions in the sample (ii) the shift in the characteristic band positions with respect to starting USY

sample .In the samples prepared with higher amount of $K_2TiO(C_2O_4)_2$, the bands due to oxalate species are clearly seen at 1718,1690 and 1390 cm^{-1}. These bands can be ascribed to oxalate species in comparison with those of pure $K_2TiO(C_2O_4)_2$ (fig 3.15,curve e). It is attributed to $[K_2TiO(C_2O_4)_2]$ adsorbed on the reactive sites of the zeolite as shown in the scheme 3.2 presented earlier. Remarkably, the band position of these oxalate ions are not shifted to low frequencies contrary to such a shift in the case of low silica Ti-USY prepared in single step method, also described earlier. It indicates that carbonyl groups in oxalate are less purturbed by the lesser anionic framework of high silica Ti-USY samples prepared in multiple step method compared to that of low silica Ti-USY prepared by single step method. Because of the same reason, we observe less amount of Na and K cations exchanged in the samples as can be seen by comparing the tables 3.1 and 3.11. Very significant shift in the frequencies are to be noted in the region of framework vibrations. All the bands of all the samples are shifted to low frequencies in comparison with the parent USY (550-MSTP) which indicates the substitution of heavier cations in the framework. Under the conditions of reaction, where in, soluble Al species can also be formed, the reinsertion of Al species, especially "MAS NMR invisible penta-coordinated Al "species can not be ruled out. Among the samples in this series, the bands are significantly shifted to high frequencies indicating the increasing dealumination as the concentration of $K_2TiO(C_2O_4)_2$ increases. In the region of asymmetric stretching vibrations around 1030 cm^{-1} to the low frequency side, the spectra show increasing absorption as the Ti content increases which develops in to a strong band around 980 cm^{-1}. A shoulder around 920 cm^{-1} also develops in all these samples. The band at 960 cm^{-1} has been reported to be related to Ti in the framework for various titanium zeolites (174-177). Therefore we can conclude that increasing amount of Ti is incorporated in the lattice of high silica Ti- USY zeolite with increasing concentration of Ti salt.

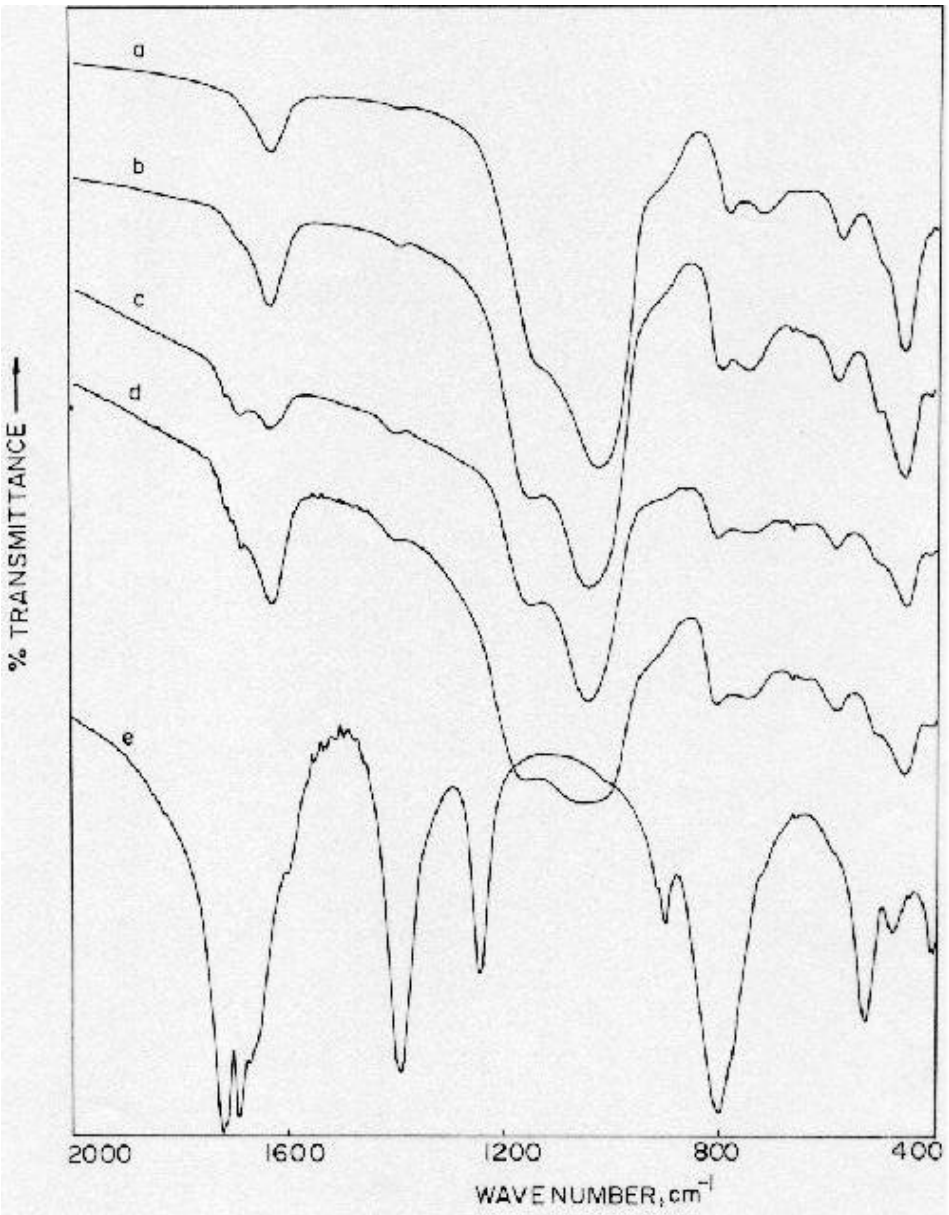

Fig.3.15: FTIR spectra of high silica Ti-USY samples in the framework region
(a) 550 MSTP- 25-0.11 (b) MSTP- 25-0.22, (c) 550 MSTP- 25-0.33
(d) 550 MSTP- 25-0.44, (e) Potassium titanyl oxalate [$K_2TiO(C_2O_4)_2$]

Table 3.15: FTIR frequencies of framework vibrations in high silica Ti-USY prepared by $K_2TiO(C_2O_4)_2$ solution

Name of the sample	Frequencies, cm^{-1}												
550-MSTP-25-0.11	456	506	572	641	719	785	910	1026	1142	1396	1637	-	-
550-MSTP-25-0.22	457	506	578	644	744	798	919	1043	1158	1396	1634	-	-
550-MSTP-25-0.33	456	506	581	647	741	804	919	1045	1151	1399	1634	1693	1718
550-MSTP-25-0.44	453	500	581	647	744	804	910	1048	1157	1399	1631	1690	1718

3.2.3 : Very high silica Ti-USY from very high silica USY (550-700-850-MSTP) sample by multiple step (MSTP) method using $K_2TiO(C_2O_4)_2.2H_2O$, $Ti[O(CH_2)_3CH_3]_4$ and $Ti[OCH(CH_3)_2]_4$

The benefits of using very high silica USY for incorporating Ti in the lattice rests in a very high density of "silanol nests", defect sites and very high stability in the acidic medium of reaction solution. The parent sample used in these preparations was very high silica USY, (550-700-850-MSTP), described in the previous section. Three different salts namely Potassium titanium oxalate, $[K_2TiO(C_2O_4)_2.2H_2O]$, Titanium butoxide $Ti[O(CH_2)_3CH_3]_4$ and Titanium isopropoxide, $Ti[OCH(CH_3)_2]_4$] were used for the reaction. The XRD patterns of the product samples are presented in the fig 3.16. In addition to the characteristic peaks of USY, the patterns show the presence of anatase form of TiO_2 in the sample as indicated by broad peaks around 2è values of 25.4, 38.0, and 48.55. In the table 3.16, unit cell constants as determined by XRD and the amount of framework (Al+Ti) as determined from the MASNMR method are presented. The unit cell constant remains almost the same, about 24.23 Å, in-spite of the framework composition increasing from 4 Al / U.C in the parent sample to 11 and 12(Al+Ti) / U.C for oxalate and butoxide treated samples respectively. In the sample prepared using isopropoxide, there is no change in the framework composition, which is only 5 (Al+Ti)/U.C. The increase in (Al+Ti) content of the framework but not the unit cell constant indicates that the lattice contraction due to Al removal (Al-O bond length = 1.75Å) is compensated by the insertion of heavier Ti cation having bond length Ti-O of 1.83 Å in the lattice. The data for samples prepared by reaction with Ti salts for 10 times with intermittent NH_4^+ exchange are also given in the table 3.15. These samples also do not show lattice expansion in spite of the increase in the frame work composition of (Al+Ti) / U.C to 14, 15 and 7.4 respectively.

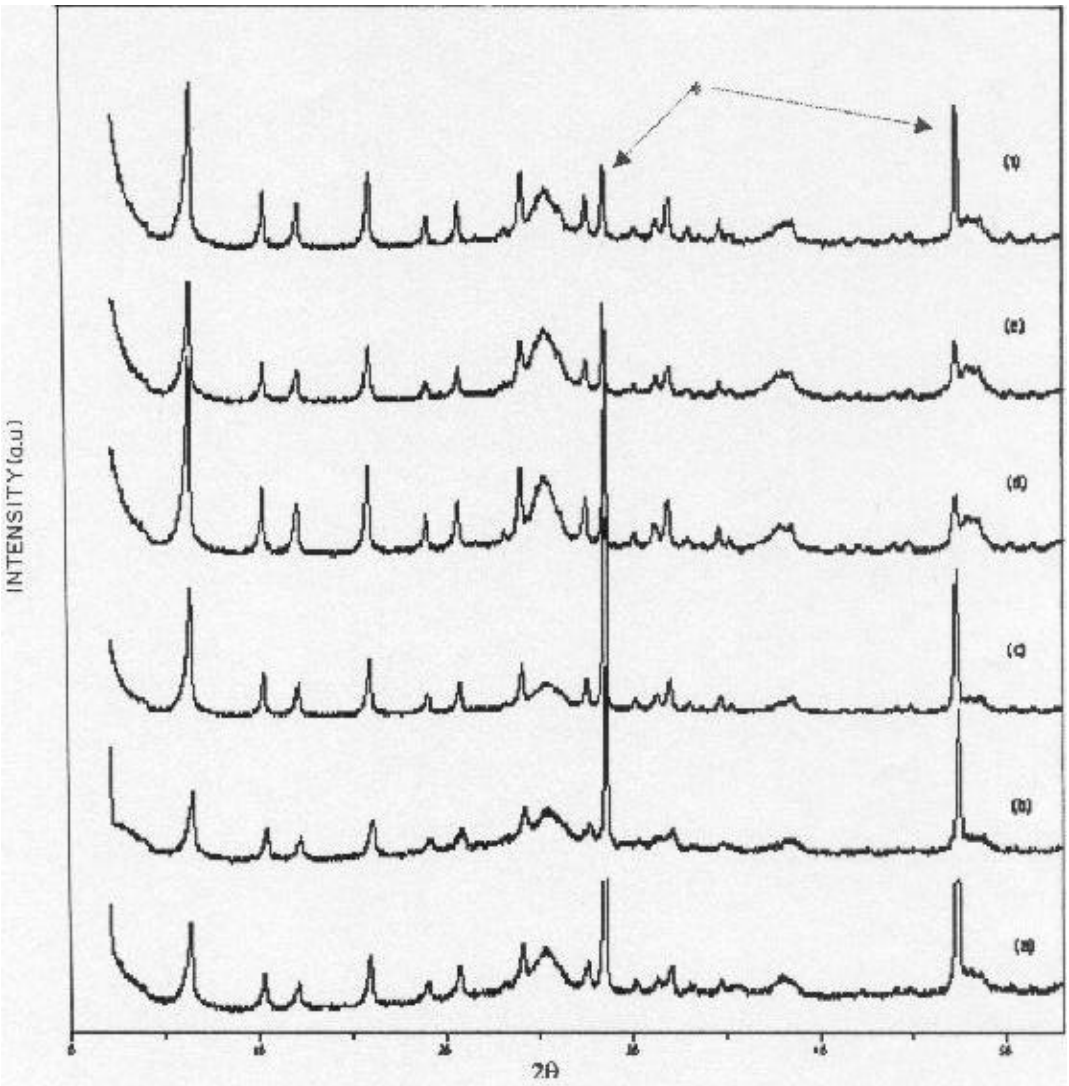

* Silicon Standard

Fig 3.16 : XRD-patterns of very high silica Ti-USY samples prepared using $K_2TiO(C_2O_4)_2$ (Oxa), $Ti[O(CH_2)_3CH_3]_4$ (Buto) and $Ti[OCH(CH_3)_2]_4$ (iso) and their acid treated products.

(a)Oxa-MSTP-200-0.33 (b) Buto-MSTP-200-0.33 (c) Iso-MSTP-200-0.33

(d) Oxa-MSTP-200-0.33 -10 (e) Buto-MSTP-200-0.33 –10 and

(f) Iso-MSTP-200-0.33-10

Table 3.16 : Chemical composition and unit cell properties of very high silica Ti-USY from very high silica USY (550-700-850-MSTP) sample by multiple step (MSTP) method using $K_2TiO(C_2O_4)_2.2H_2O$, $Ti[O(CH_2)_3CH_3]_4$ and $Ti[OCH(CH_3)_2]_4$

S.N	Name of the sample	Unit cell const.	FrameWork Si/Al+Ti	F Al/ Unit cell	Unit cell Composition	%Dealuminatn
1	Na-Y	24.71	2.4	56	$Na_{20}[(AlO_2)_{56}(SiO_2)_{136}]$	4
2	NH_4Y	24.68	2.56	54	$Na_{20}[(AlO_2)_{54}(SiO_2)_{138}]$	10
3	550-700-850-MSTP	24.21	26.29	4	$Na_{1.3}[(AlO_2)_7(SiO_2)_{185}]$	87.5
4	Oxa-MSTP-200-0.33	24.25	16.95	11 *		
5	Buto-MSTP-200-0.33	24.23	14.98	12 *		
6	Isop-MSTP-200-0.33	24.23	40.06	5 *		
7	Oxa-MSTP-200-0.33 -10	24.23	12.65	14 *		
8	Buto-MSTP-200-0.33 -10	24.3	12.0	15 *		
9	Isop-MSTP-200-0.33 -10	24.29	24.9	7.4*		
10	550-700-850-MSTP-10	24.20	52.06	4	$Na_{1.26}[(AlO_2)_4(SiO_2)_{188}$	93%

* framework (Al+Ti) / Unit Cell

In the fig 3.17, the UV/VIS spectra of these samples are presented. Similar to the samples of low silica Ti-USY described in earlier section, the spectra show four types of Ti species, mono-functional, bi-functional, multi-functional and TiO_2 of nano particle size. The schemes of these reactions are presented in the scheme 3.4 below.These species give bands around 215,230, 270 and 300-500 nm as can be seen in the figure. The significant difference should be noted in the spectra of samples having low and high concentrations of Ti as well as in the samples prepared by oxalate, butoxide and isopropoxide. The samples having high concentration of Ti shows higher amount of anatase nano particles compared to those having low amount of Ti for all three Ti salts. Among the three salts, butoxide gives samples with less amount of anatase phase, next comes the oxalate and isopropoxide gives maximum amount of anatase phase in the sample.The scheme for these reactions can be presented as below. From these observations, the butoxide seems to be the most efficient salt to incorporate Ti in the framework of USY.

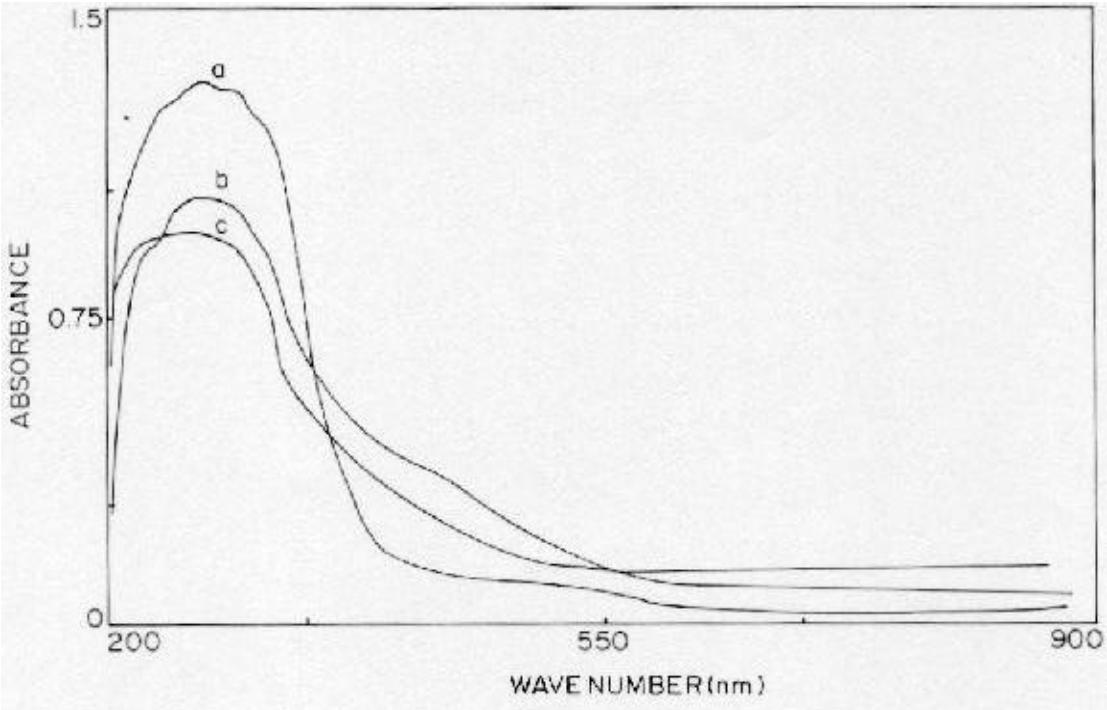

Fig.-3.17: Diffuse Reflectance UV-VIS Spectra of very high silica Ti-USY samples, (a) Buto-MSTP-200-0.33, (b) Iso-MSTP-200-0.33, (c) Oxo-MSTP-200-0.33

Scheme 3.4

1) For Titanium Butoxide :

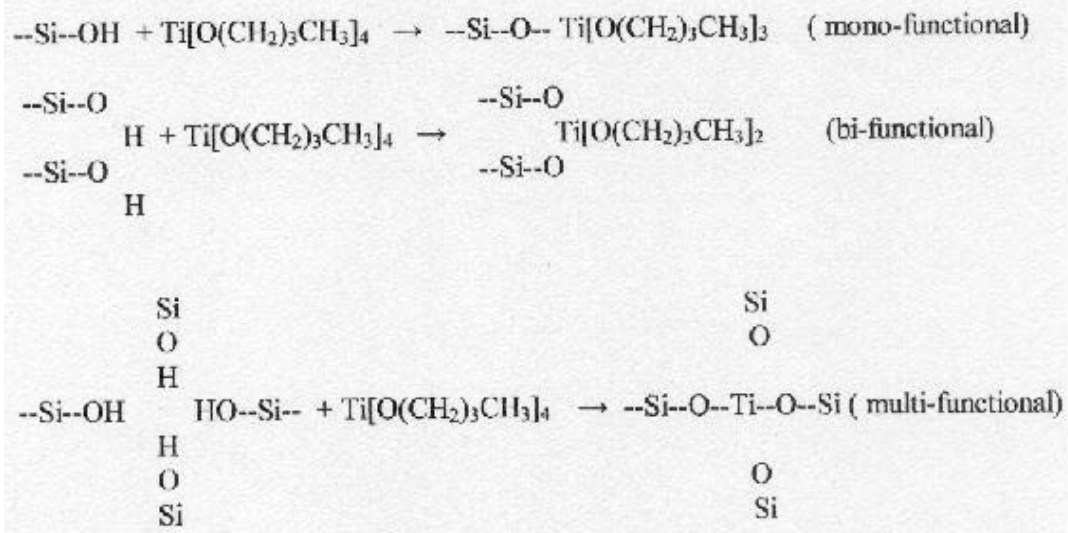

2) For Titanium Isopropoxide :

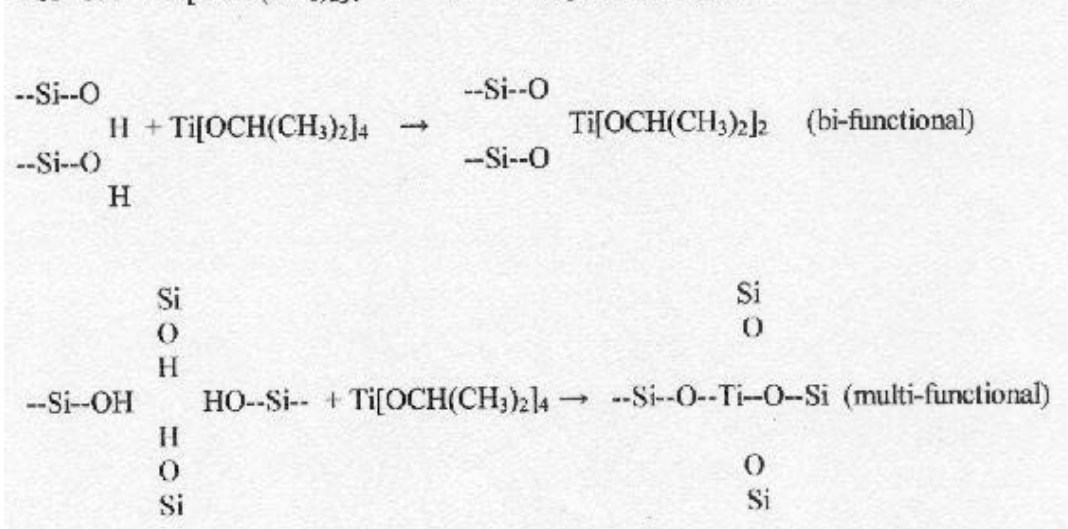

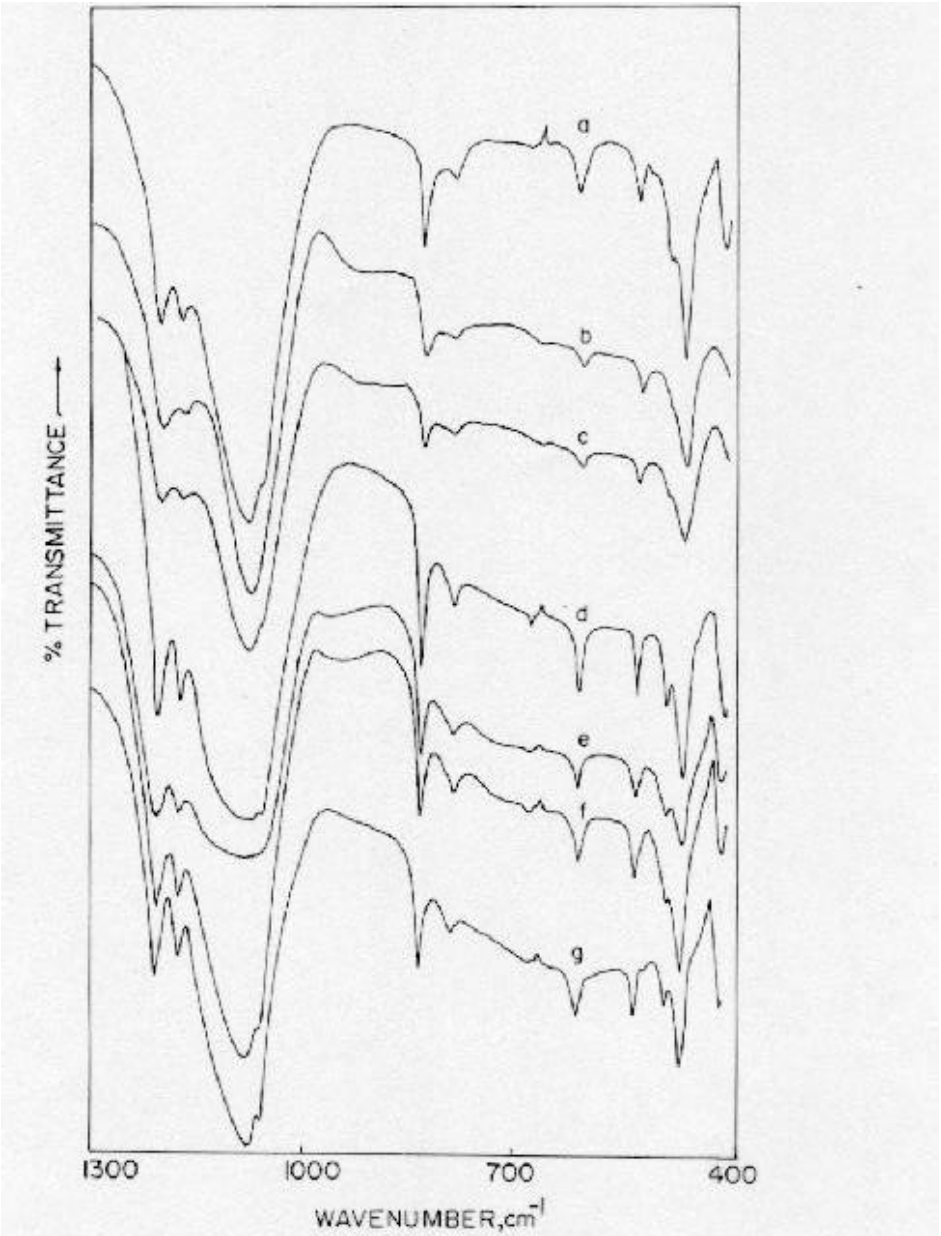

Fig.3.18: FTIR spectra of very high silica Ti-USY samples in the framework region, (a) NH_4-Y, (b) Oxa-MSTP-200-0.33, (c) Buto-MSTP-200-0.33, (d) Iso-MSTP-200-0.33, (e) Oxa-MSTP-200-0.33-10, (f) Buto -MSTP-200-0.33-10 and (g) Iso-MSTP-200-0.33-10

Table 3.17: FTIR frequencies of framework vibrations in very high silica Ti-USY prepared by $K_2TiO(C_2O_4)_2$(Oxa), $Ti[O(CH_2)_3CH_3]_4$ (Buto) and $Ti[OCH(CH_3)_2]_4$ (Iso) solutions and their acid treated samples

Name of the sample	Frequencies, cm^{-1}											
550-700-850-MSTP	460	483	527	613	682	791	835	-	1060	1080	1177	1207
Oxa-MSTP-200-0.33	458	483	527	606	668	787	831	947	1060	1076	1177	1201
Buto- MSTP-200-0.33	458	481	527	609	671	787	833	941	1057	1076	1175	1203
Iso- MSTP-200-0.33	458	483	528	611	681	789	835	-	1059	1078	1177	1210
Oxa-MSTP-200-0.33-10	460	484	529	611	680	789	835	960	1059	1078	1177	1208
Buto- MSTP-200-0.33-10	460	483	528	611	682	789	837	953	1060	1078	1177	1207
Iso- MSTP-200-0.33-10	458	482	528	611	680	787	835	928	1058	1076	1176	1208

SEM photographs of this series of very high silica Ti-USY samples are given in the fig 3.19. The photographs show that the morphology of the samples change noticeably depending up on the method of preparation. The crystallites agglomerate in the Ti-USY samples and in those samples where concentration of Ti is very high, some smaller particles, may be of TiO_2 agglomerates are noticeable. Over all, the samples look highly crystalline.

TG / DTA curves of high silica Ti-USY samples are presented in the fig 3.20-3.25. In the table-3.18, the loss in weight and the peak temperatures for different stages are given.

Table 3.18 : TG/DTA data of very high silica Ti-USY from very high silica USY(550-700-850-MSTP) sample by multiple step (MSTP) method using $K_2TiO(C_2O_4)_2.2H_2O$, $Ti[OCH(CH_3)_2]_4$ and $Ti[O(CH_2)_3CH_3]_4$

S.No	Name of the sample	Peak Temperature (° C)	Weight loss, %	Peak Temperature (° C)
1	Oxa-MSTP-200-0.33	32(sh), 91, 251	14.9	-
2	Iso-MSTP-200-0.33	40(sh), 80,225, 485	5.6	-
3	550-700-850-MSTP	42(sh), 84,333, 484	7.23	-
4	Oxa-MSTP-200-0.33-10	25, 88, 240, 338	4.41	701
5	Iso-MSTP-200-0.33-10	48(h), 93, 241, 330, 475	6.922	-
6	Buto-MSTP-200-0.33-10	44(h), 92,333, 477	5.127	-

DTA curves shows a very low temperature shoulder around 45^0C in all the samples and most of the weight loss due to occluded water occurs below 350 ^{0}C in all the samples. The temperature of this endothermic peak appears around 150^0 C for Na-Y and NH_4 –Y samples but for all Ti-USY, it occurs at much lower temperature. Even though micropore volume which is available for adsorption of water is much more, the loss in weight is very less for USY samples because of very high hydrophobicity of the sample. Presence of Ti in the framework or out side does not influence the adsorption of water positively, because Ti-USY is relatively hydrophobic. Some important differences occur in the nature of thermograms of these samples.Three stages of weight loss can be considered in all samples, only the first stage is very much clear and prominant. The

second stage which is very minor occurs around 300^0 C and the peak temperature can not be definitely pointed out. The third stage also can not be pointed out, which is continuous to the highest temperature of 1000^0C. The weight loss in this step is due to dehydroxylation of structural hydroxyl groups. Such structural hydroxyl groups are less on Na-Y and NH_4-Y but significant in all USY samples, because these zeolites have so many defect sites and silanol groups.

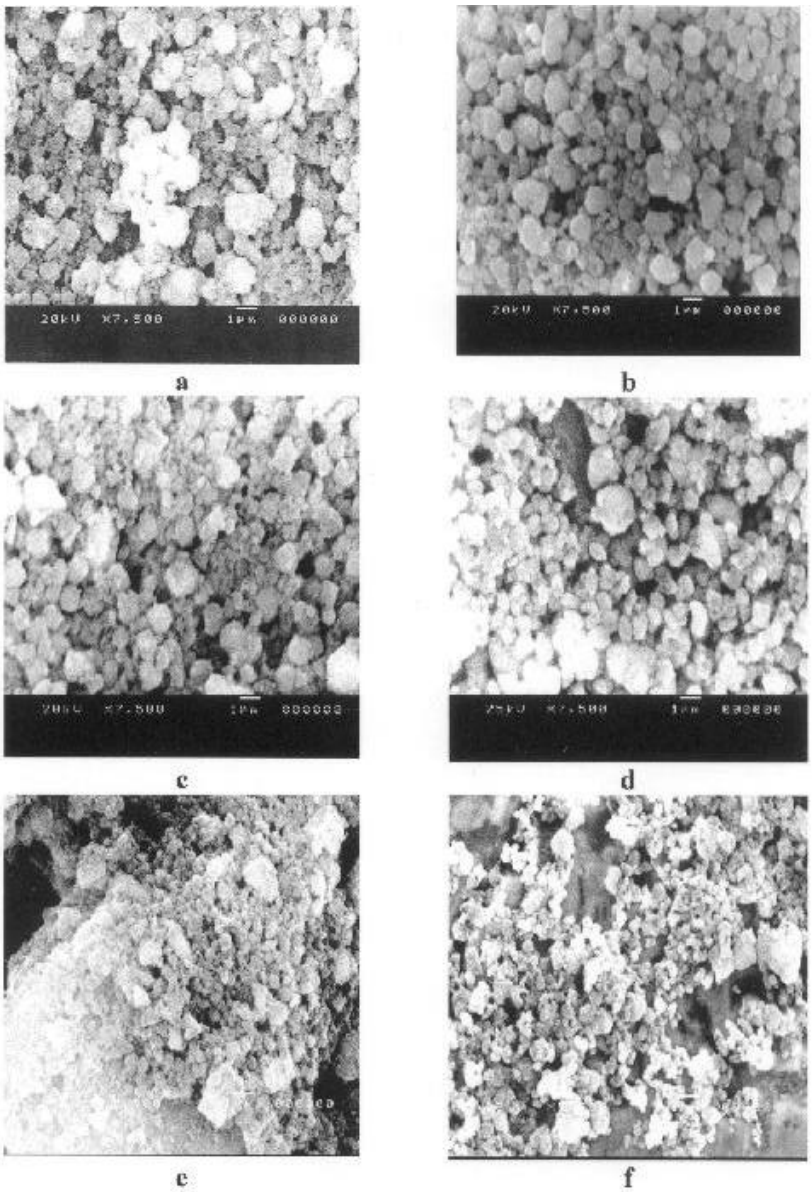

Fig 3.19 Scanning Electron Micrograph of very high silica Ti-USY
(a) Oxa-MSTP-200-0.33 (b) Buto- MSTP-200-0.33 (c) Iso- MSTP-200-0.33
(d) Oxa- MSTP-200-0.33-10 (e) Buto- MSTP-200-0.33-10
(f) Iso- MSTP-200-0.33-10

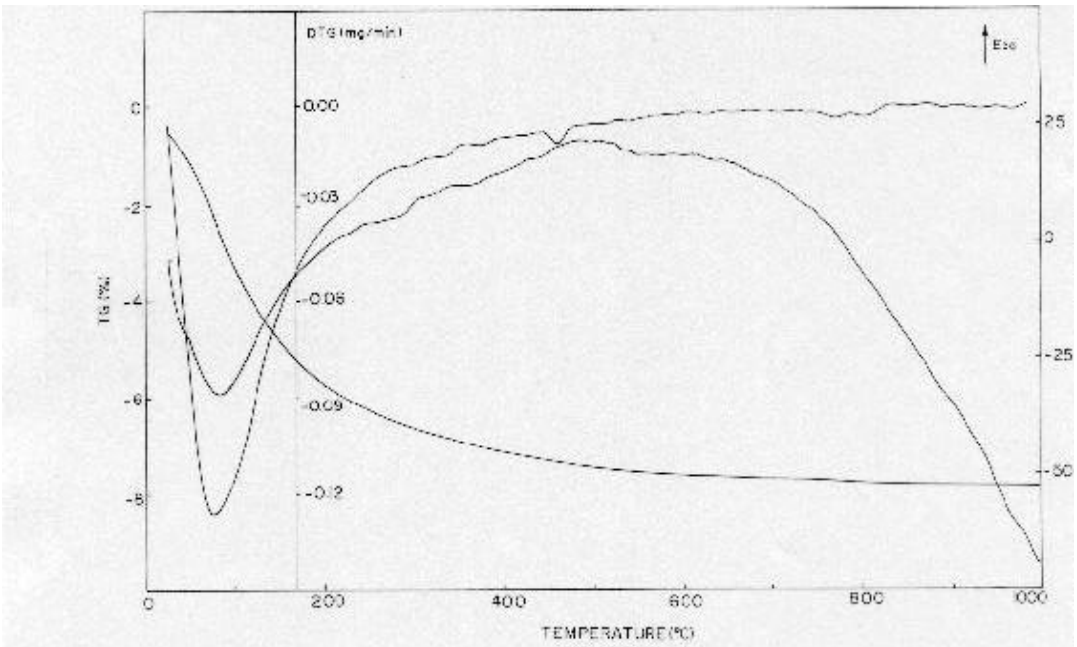

Fig.-3.20: Thermograms of very high silica Ti-USY sample, Oxa-MSTP-200-0.33

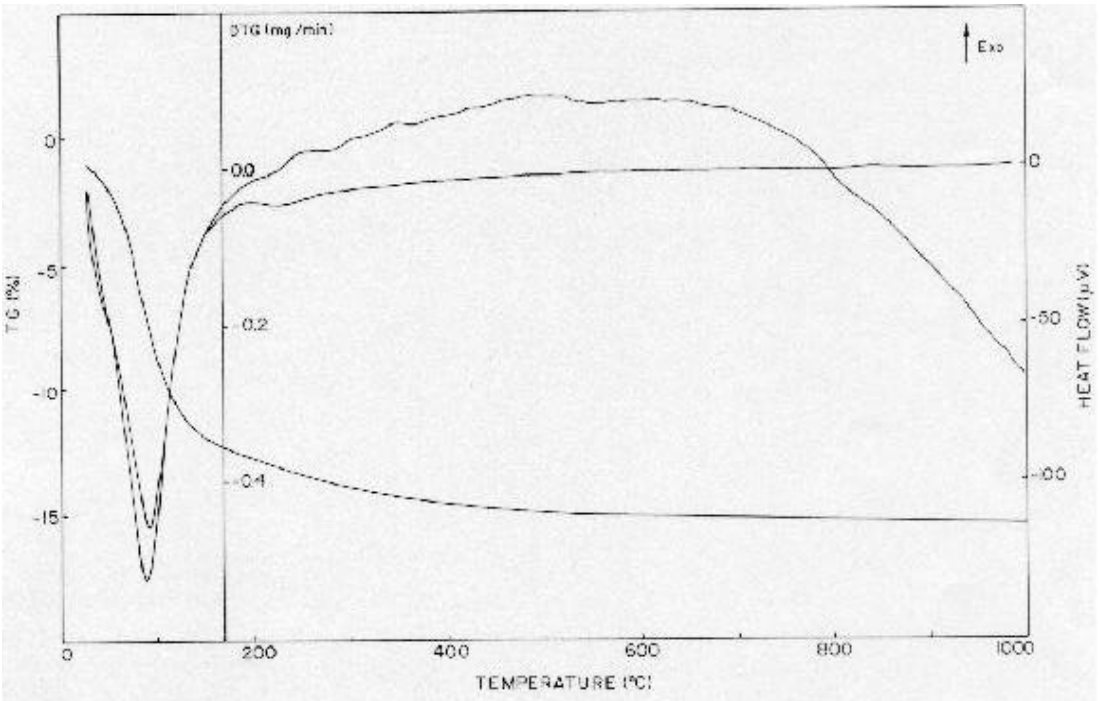

Fig.-3.21: Thermograms of very high silica Ti-USY sample, Iso-MSTP-200-0.33

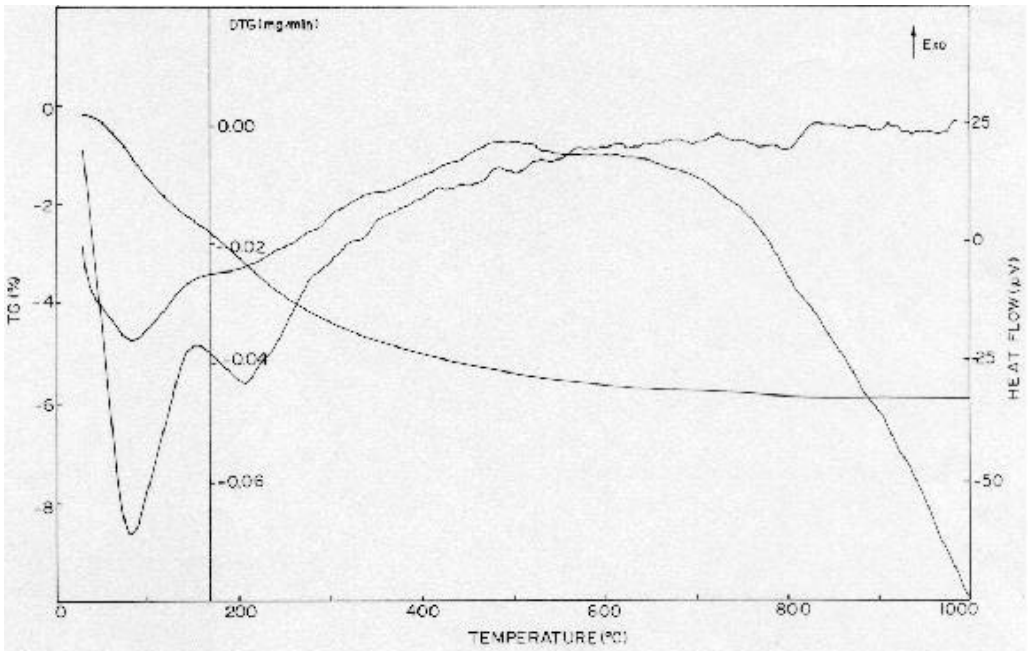

Fig.-3.22: Thermograms of very high silica USY sample, 550-700-850-MSTP

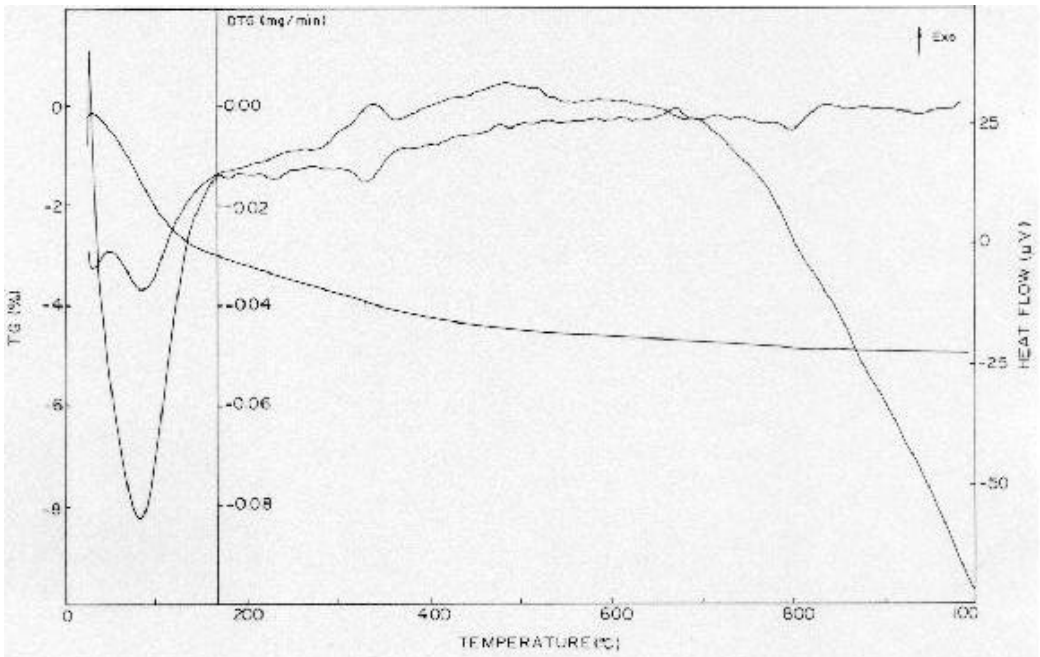

Fig.-3.23: Thermograms of very high silica Ti-USY sample, Oxa-MSTP-200-0.33-10

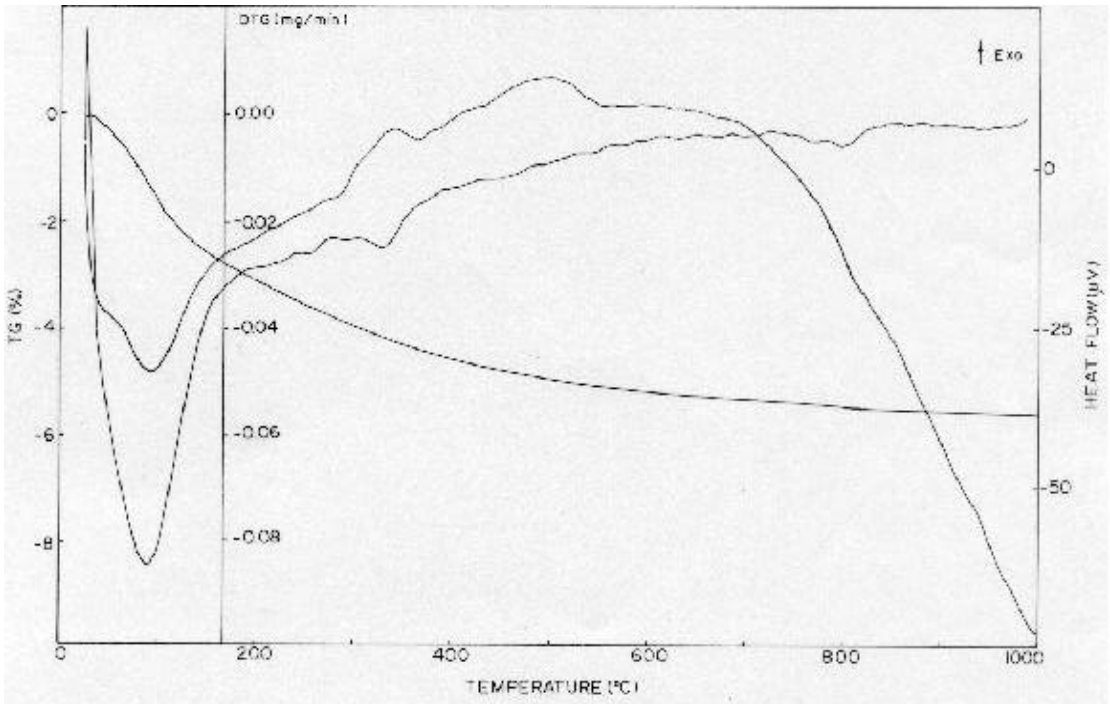

Fig.-3.24: Thermograms of very high silica Ti-USY sample, Iso-MSTP-200-0.33-10

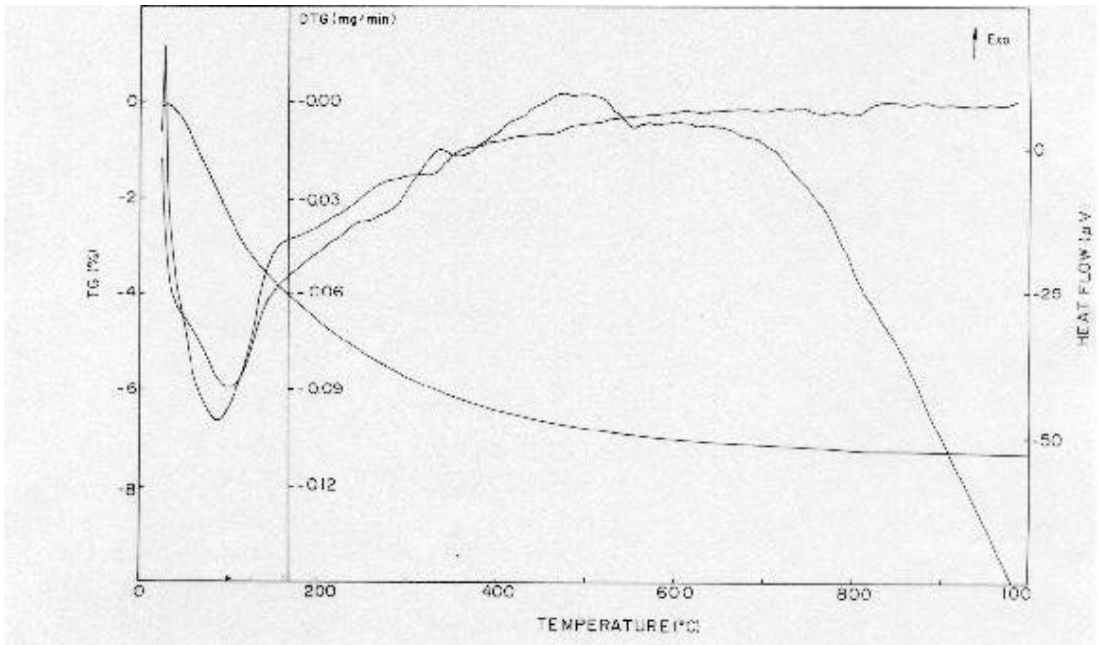

Fig.-3.25: Thermograms of very high silica Ti-USY sample, Buto-MSTP-200-0.33-10

3.2.4 : Very high silica Fe-USY and Fe-Ti-USY from very high silica USY (550-700- 850-MSTP) sample, $(NH_4)3Fe(C_2O_4)_3.3H_2O$ and $K_2TiO(C_2O_4)_2.2H_2O$

The parent material and the procedure for introducing Fe and Fe+Ti in USY was the same as for very high silica Ti-USY alone. The method of preparation was also the same as described earlier. In the fig-3.26, FTIR spectra of these samples in the framework vibration region are presented and the table 3.19 contains frequency values for all the bands. Most of the features of the spectra are same as those of very high silica Ti-USY samples, except a characteristic band at 1060 cm^{-1} in the region of asymmetric stretching vibration of M-O –M linkages. The asymmetric stretching vibration of Si-O-M linkage depends on the moment of inertia of this harmonic vibration. As the Fe-O bond length of 1.97 Å is longer than that of Si-O and Al-O which are 1.61 and 1.75 Å respectively, the moment of inertia of Si-O-Fe becomes more than that of Si-O-Si. Therefore the frequency of vibration of this mode shifts to low frequency for Fe containing samples. There are many examples of Fe containing zeolites other than USY in the literature where in, similar results have been reported(179-181). In addition to Fe in the framework, the presence of Ti can also be detected in the framework of Fe-Ti-USY samples from the characteristic band of Si-O-Ti linkages around 960 cm^{-1} in the FTIR spectra.

The fig 3.27 represents ESR spectra of Fe-Ti-USY zeolites. The spectra exhibit three characteristic signals of Fe. These three different signals correspond to three different g values of 2, 2.3 and 4.3 respectively as per the assignments published earlier (182-184). Among these species, the one giving a strong signal at g=4.3 corresponds to Fe^{3+} substituted in the framework (185,186). In general , Fe^{3+} species incorporated in the zeolite are usually located in, (a) the exchangeable sites of the zeolite framework i.e; at the cationic positions of the zeolite. (b) randomly oriented in hydroxy oxide form and (c) in the alumino-silicate framework.(185-188).

It is observed that the intensity of signal at g = 4.3 increases with the increase in the frame work location of Fe. The Fe^{3+}signal corresponding to g = 2 is assigned to the hexa-co ordinated complex located at the cationic sites of the hydrated USY zeolite (185). The signal at g = 2.3 is assigned to the randomly oriented Fe^{3+}ions with the characteristics of hydrated oxide species which does not belong to the framework

structure of the zeolite. The remaining three weak signals present in the spectra of some of the samples may be arising due to the traces of 3 different iron species occluded in the zeolite cavity. The spectra of these species may only be responsible for broadening ESR spectra of samples.

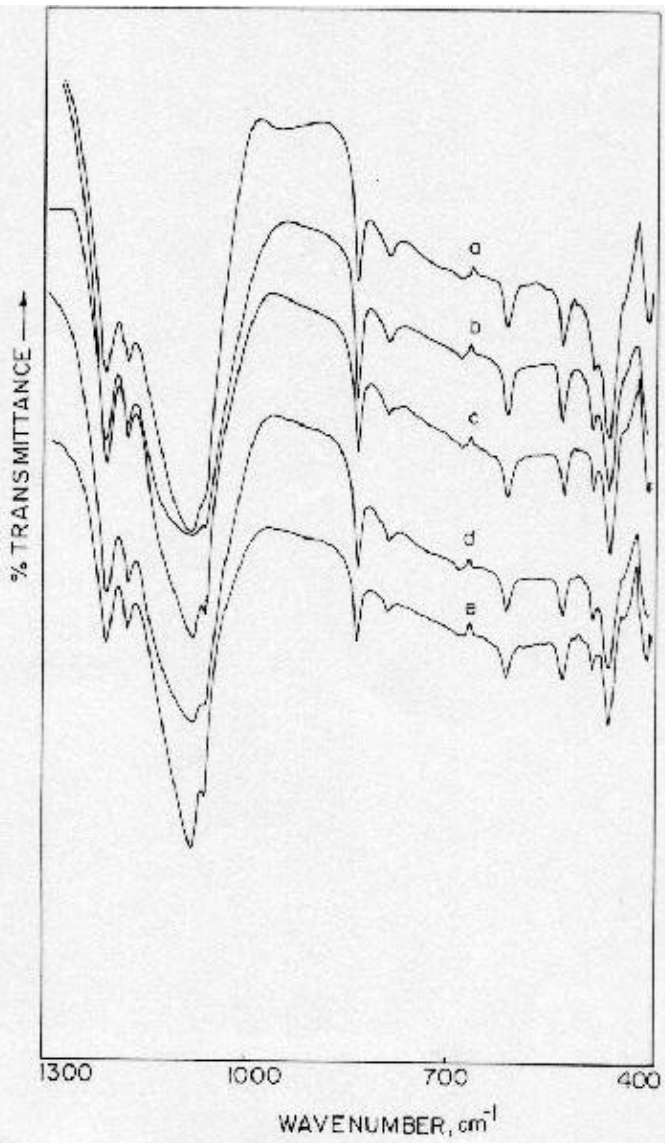

Fig.-3.26: FTIR spectra of very high silica Fe-USY and Fe-Ti-USY samples in the framework region, (a) Oxa-MSTP-200-0.33-10, (b) Iso-MSTP-200-0.33-10, (c) Iso-MSTP-200-0.33-10, (d) Buto-MSTP-200-0.33-10 and (e)Oxa -MSTP-200-0.33-10

Table 3.19 : FTIR frequencies of framework vibrations in very high silica Fe- USY and Fe- Ti-USY prepared by $(NH_4)_3Fe(C_2O_4)_3$ and $K_2TiO(C_2O_4)_2$(Oxa), $Ti[O(CH_2)_3CH_3]_4$ (Buto) and $Ti[OCH(CH_3)_2]_4$ (Iso) solutions and their acid treated samples

Name of the sample	Frequencies, cm^{-1}											
Fe-USY	460	483	528	611	681	789	832	960	1061	1078	1177	1210
Acid treated Fe- USY	458	484	528	611	682	789	835	-	1060	1078	1175	1206
Acid treated Fe-Ti-USY (Oxa)	456	483	531	611	680	789	833	925	1060	1076	1177	1206
Acid treated Fe-USY (Buto)	458	483	528	611	681	789	835	925	1060	1076	1177	1206
Acid treated Fe-Ti-USY (Iso)	460	484	528	611	680	787	835	935	1060	1078	1175	1206

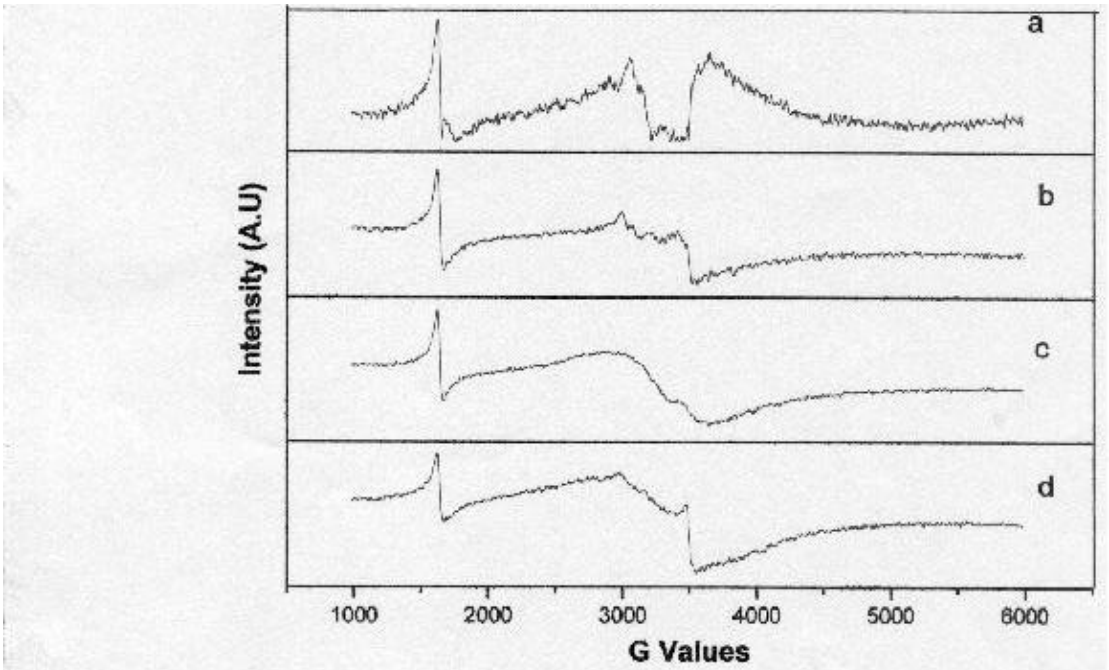

Fig.-3.27: ESR spectra of acid treated very high silica Fe-USY and Fe-Ti-USY samples prepared using $(NH_4)_3Fe(C_2O_4)_3$, and $K_2TiO(C_2O_4)_2$ (Oxa), $Ti[O(CH_2)_3CH_3]_4$ (Buto) and $Ti[OCH(CH_3)_2]_4$ (Iso) solutions (a) acid treated Fe-Ti-USY(Iso), (b) acid treated Fe-Ti-USY(Oxa), (c) acid treated Fe-USY and (d) acid treated Fe-Ti-USY (Buto)

3.3: Conclusions

(1) The incorporation of monomeric Ti species in the framework structure of ultra stable zeolite type-Y(Ti-USY) having a whole range of silica content (low, high and very high silica) is reported here for the first time.

(2) Structural properties like unit cell constant, framework Si / Al and Si / (Al+Ti) ratios of whole series of USY and Ti-USY were determined by XRD and Solid State MAS NMR spectroscopy and compared with the bulk composition to understand the ultra-stabilization process and Ti-incorporation.

(3) FTIR spectra of framework vibration in Ti-USY indicate the shift in the frequency to higher side due to dealumination and a new band around 930-960 cm^{-1} due to Ti-

O-Si linkages. The bands of oxalate species strongly interacting with the framework are also seen in the spectra of Ti-USY samples prepared from $K_2TiO(C_2O_4)_2$ solution.

(4) Diffuse reflectance UV-VIS spectra show bands at 215,230 and 290 nm characteristic of monomeric Ti species in the multi functional, bi-functional and mono-functional sites on the Ti-USY samples. The samples containing high amount of Ti show the presence of nano-sized particles of TiO_2 showing absorption higher up to 500 nm.

(5) From the results of SEM and TG/DTA, the ultra stability of the USY and Ti-USY samples are confirmed.

(6) ESR spectroscopy indicates that Fe is incorporated in the lattice of Fe-USY and Fe-Ti-USY samples.

(7) The physico-chemical characterization undoubtedly indicates that high amount of Ti is incorporated in the framework of Ti-USY zeolites having the whole range of silica, low, high and very high content.

CHAPTER 4

4 : SOLID STATE MASNMR STUDIES ON USY AND TI-USY ZEOLITES

4.1 :Introduction:

Our effort in this study has been to make USY materials by mild, severe and repeated and carefully controlled steaming with HNO_3 being used for acid leaching. Further to their ultrastabilization, tailored for the stability under catalytic steaming conditions, heteroatom substitution is a further step forward to enhance the catalytic activity while preserving thermal stability. We have prepared a series of USY by different steam temperature treatments of NH_4-Y zeolite (550°, 700°, 850° and 925°C). Also, we have tried to incorporate titanium into the USY framework structure using different Ti sources. Table 4.1 briefly summarises the USY materials prepared for the present NMR studies. The details of preparation and some of the properties have been already discussed in the chapter 2 and 3.

In the present study, we have used ^{27}Al and ^{29}Si MAS NMR, as well as ^{27}Al 3Q-MAS NMR, to study the structural characteristics in relation to the framework stability of the prepared USY materials. We also address the heteroatom substitution in USY by Ti (using different Ti sources) through ^{27}Al and ^{29}Si MAS NMR and also by ^{49}Ti NMR and compare the results with the Ti free USY.

4.1.1: ^{27}Al MAS NMR

In the study of zeolites by high-resolution solid state NMR, ^{27}Al is found to be a very useful technique to characterize the framework and non-framework environments. The ^{27}Al nucleus offers very high detection sensitivity due to its high natural abundance (100%). The only drawback with this nucleus is that it is a quadrupolar nucleus ($I > ½$) and hence it suffers from quadrupole interactions, which act as a perturbation on the Zeeman interactions (189). In the case of ^{27}Al, MAS NMR spectra are mainly concerned with the so-called “central transition” ($+1/2 \leftrightarrow -1/2$). The other transitions, called “satellite” transitions are seldom detected in zeolites, although they are invariably observed in ALPO- molecular sieve materials. When the theory of MAS NMR of ^{27}Al for the “central transition” is considered, it is found that the magic angle spinning is not able to remove the broadening introduced by second order quadrupole interactions (190). However, it is found that MAS NMR can be very effectively used to distinguish the

aluminum in framework and non-framework positions since they are well separated in the MAS spectrum due to a large difference in the chemical shift (40-50 ppm)(191).

Table4. 1: Materials used for solid-state MASNMR studies:

Starting material	Preparation Procedure	Identification of the product
Parent Na-Y	Commercial sample obtained fromUnion carbide Corporation, Linde Division, USA. (Linde, SK-40)	Na-Y
Na-Y	Ion exchanged thrice by 1.0 N NH_4NO_3 at 100° C for 4 h	Na,NH_4-Y
Na,NH_4-Y	Steam treated at 550° C for 4 h followed by ion exchange with 1.0 N NH_4NO_3 at 100°C for 4 h, and calcined at 450^0 C for 4 h.	550-MSTP (High silica USY)
550-MSTP	Steam treated at 700°C for 4 h followed by ion exchange with 1.0 N NH_4NO_3 at 100° C for 4 h, then calcined at 450^0 C for 4 h.	550-700-MSTP (Intermediate very high silica USY)
550-700-MSTP	Steam treated at 850°C for 4 hrs followed by ion exchange with 1.0 N NH_4NO_3 at 100° C for 4 h, then calcined at 450^0C for 4 h.	550-700-850-MSTP (very high silica USY)
550-700-850-MSTP	Steam treated at 925°Cfor 4 hrs followed by ion exchange with 1.0 N NH_4NO_3 at 100° C for 4 h, then calcined at 450^0 C for 4 h.	550-700-850-925-MSTP (very very high silica USY)
550-700-850-MSTP	Reacted with 0.33 mol fraction ofK Ti oxa-late at 200^0 C for 8 h, acid treated with 0.01 N HNO_3 solution at 100^0C for 4 h for 10 times and calcined at 450^0C for 4 h	Oxa-MSTP-200-0.33 (very high silica Ti-USY)
550-700-850-MSTP	Reacted with 0.33 mol fraction of Titanium butoxide at 200^0 C for 8 h, acid treated with 0.01 N HNO_3 solution at 100^0C for 4 h for 10 times and calcined at 450^0C for 4 h	Buto-MSTP-200-0.33 (very high silica Ti-USY)
550-700-850-MSTP	Reacted with 0.33 mol fraction of Ti (IV) isopropoxide at 200^0 C for 8 h, acid treated with 0.01 N HNO_3 solution at 100^0C for 4 h for 10 times and calcined at 450^0C for 4 h	Iso-MSTP-200-0.33 (very high silica Ti-USY)
550-700-850-MSTP	Acid treated with 0.01 N HNO_3 solution at 100^0C for 4 h for 10 times	MSTP-10

While conventional ^{27}Al MAS NMR can be used to distinguish tetrahedral and octahedral aluminum environments, it is not possible to get information about the nonequivalent aluminum sites within these coordination's (four, six). Moreover, the penta-coordinated aluminum is also "invisible" in MAS spectra. In order to characterize the aluminum environments fully, a new technique called "Multiple Quantum Magic Angle Spinning" (MQ-MAS) has been recently discovered (192 **)**. A brief introduction to this technique is given in the following section. In the present thesis, we have used both conventional ^{27}Al MAS as well as ^{27}Al MQ-MAS techniques to fully study USY and Ti-USY.

4.1.2 : ^{29}Si MAS NMR

MAS NMR technique is well suited to observe the ^{29}Si nucleus in molecular sieves since ^{29}Si is a spin ½ nucleus with an acceptable natural abundance of 4.7%(191). Due to the low natural abundance, the homonuclear Si-Si dipolar broadening is negligible and the only interaction that contributes to the ^{29}Si MAS spectrum is the isotropic chemical shifts. Further, since silicon in tetrahedral environments exhibits a slightly distorted T_d symmetry, the anisotropy of the ^{29}Si chemical shielding is rather small. This entails gathering high-resolution MAS spectra with practically no interference from spinning side bands.

In siliceous materials one observes only the signals of Q_4 [4Si] silicon in the zeolite framework (191). However, in aluminosilicates, the other silicon tetrahedral environments designated by Q_4[3Si,1Al], Q_4[2Si,2Al], Q_4[1Si,3Al] and Q_4[0Si,4Al] are distinctly observable since each aluminum substitution in the zeolite lattice shifts the ^{29}Si signal by approximately 5 ppm in the down field direction (191). The area under any given ^{29}Si resonance is directly proportional to the population of the structural unit to which the signal is assigned. When each distinct Q^4(nAl) environment is identified in the MAS spectrum, the corresponding site population is estimated by deconvolution and area measurement. It now becomes possible to compare the relative population of these sites with models involving different Si,Al ordering schemes. For a random Si, Al distribution obeying Loewentein's rule (2), the probabilities P_m for the occurrence of various Q^4

(mAl) configurations in a given material with Si/Al =R can be calculated using the binomial probability distribution, namely, (191).

$$P_m = \frac{4!}{m!(4-m)!} p^m (1-p)^{4-m} \qquad (1)$$

Where p = 1/R, p being the probability of occurrence of a Si-O-Al linkage. From the above equation one can derive the probabilities for the five different Q^4(mAl) configurations as

$$P_4 = p^4 \quad \text{for} \quad [Q^4(4Al)] \quad (m=4) \qquad (2)$$

$$P_3 = 4(1-p)p^3 \quad \text{for} \quad [Q^4(3Al)] \quad (m=3) \qquad (3)$$

$$P_2 = 6(1-p)^2 p^2 \quad \text{for} \quad [Q^4(2Al)] \quad (m=2) \qquad (4)$$

$$P_1 = 4(1-p)^3 p \quad \text{for} \quad [Q^4(1Al)] \quad (m=1) \qquad (5)$$

$$P_0 = (1-p)^4 \quad \text{for} \quad [Q^4(0Al)] \quad (m=0) \qquad (6)$$

Eq. (1) can be used to calculate the relative intensities for the whole range of Si/Al. When the calculated and experimentally measured signal intensities do not match, the Si,Al ordering scheme is definitely not random. However, when the calculated and measured intensities are similar, it is possible to construct a perfectly ordered model having the same relative intensities as a random model. (191)

4.1.3 : Quantitative Estimation of Framework Si/Al, [$(Si/Al)_{FW}$].

One of the merits of ^{29}Si MAS NMR of aluminosilicates is the quantitative determination of the framework Si/Al ratio. Conventional bulk chemical analysis methods yield only the overall Si/Al and do not give the value for $(Si/Al)_{FW}$. As noted earlier, every Al substitution causes the ^{29}Si signal to shift by approximately 5 ppm and allows us to estimate the population of various tetrahedral Q^4(nAl). It is important to note that Loewenstein's rule (2) precludes Al-O-Al linkages to be formed in zeolites. Therefore, every Al atom in a Q^4 (nAl). Unit is linked by bridging oxygen atoms to 4 Si atoms. This readily implies that every Si-O-Al linkage incorporates ¼ Al atoms and whole tetrahedral unit n/4 Al atoms. Since each ^{29}Si Q^4 (nAl).environment is shifted in the ^{29}Si MAS spectrum, the observed ^{29}Si signal intensity is directly proportional to the population of these respective T sites. The framework Si/Al is calculated using the formula (191).

$$\left(\frac{Si}{Al}\right)_{FW} = \sum_{n=0}^{4} I_{Si(nAl)} \Big/ \sum_{n=0}^{4} \frac{n}{4} I_{Si(nAl)} \qquad (7)$$

4.1.4 : ^{27}Al Multiple-Quantum MAS NMR (MQ-MAS NMR)

Multiple-Quantum Magic Angle Spinning (MQ-MAS) is a recently developed technique and has immense potential in material characterization, especially in various heteroatoms substituted zeolites. A general introduction to this technique and the application of MQ-MAS method in molecular sieve science is outlined below.

The removal of anisotropic broadenings, encountered in static samples, by MAS was discussed earlier. MAS is very rewarding when nuclei with spin quantum numbers ½ and 1 are concerned. However, MAS fails to give the isotropic spectrum for integer-half (n/2) quadrupolar nuclei. Since two thirds of the nuclei in the periodic table belong to this family, there has been a continuing effort to device an effective line narrowing method for (n/2) nuclei. Over the years, techniques such as Variable Angle Sample Spinning (VASS), Dynamic Angle Spinning (DAS) and Double Rotation (DOR) were introduced. The technical limitations imposed, especially by DAS and DOR, are removed in the case of MQ-MAS and a conventional MAS probe-head would suffice to perform the experiment. The basic principle behind the theory and practice of MQ-MAS is discussed below.

The interaction Hamiltonian for ^{27}Al is the quadrupolar Hamiltonian H_Q, which is a perturbation on the Zeeman Hamiltonian due to the main magnetic field H_Z. The Zeeman Hamiltonian is

$$H_z = -\gamma.\hbar.B_0 I_z$$

$$= -\omega_0 I_z \qquad \text{…….[8]}$$

and quadrupolar interaction, acting as a perturbation on Zeeman interaction is

$$H_Q = \nu_Q(\theta,\phi)[3I_z^2 - I(I+1)] \qquad \text{……..[9]}$$

For $\nu_0 >> \nu_Q$, the spread of quadrupolar frequencies is given by

$$\nu_Q(\theta,\phi) = \frac{e^2qQ/h}{2I(2I-1)} \frac{(3\cos^2\theta - 1 + \eta \sin^2\theta \cos 2\phi)}{2} \qquad \text{……..…[10]}$$

These frequencies are determined by the nuclear quadrupole coupling constant (e^2qQ/h), the asymmetry parameter (η) and the polar angle (θ, ϕ) defining the orientation of external magnetic field H_0 within the Principal Axis System (PAS) of the quadrupolar tensor. An important property of $H_Q = \nu_Q(\theta,\phi)[3I_z^2 - I(I+1)]$ is that $H_Q \propto I_z^2$ and cancels the presence of first order quadrupole effects on any $I_z = -m \leftrightarrow +m$ spin transition. This transition frequency is however broadened by second order effects, the broadening (Δ) being proportional to H_Q^2/H_Z. For experiments conducted under MAS, allowing for existence of isotropic chemical shift (ν_{cs}), and disregarding the effects of time dependent oscillating terms due to the motion of the rotor, the spin evolution for the symmetric $-m \leftrightarrow +m$ transition can be described by a multi rank expansion of its phase ϕ, (194).

$$\phi(m, \beta, t) = \nu_{cs}(2mt) + \nu_0^Q A_0(m)t + \nu_2^Q(\theta, \phi)A_2(m)P_2(\cos\beta)t + \nu_4^Q(\theta, \phi)A_4(m)P_4(\cos\beta)t \quad \ldots\ldots\ldots\ldots\ldots\ldots\ldots\ldots\ldots\ldots[11]$$

where,

$$A_0(m) = 2m[I(I+1) - 3m^2] \quad \ldots\ldots\ldots\ldots\ldots\ldots\ldots\ldots\ldots\ldots[12]$$

$$A_2(m) = 2m[8I(I+1) - 12m^2 - 3] \quad \ldots\ldots\ldots\ldots\ldots\ldots\ldots\ldots\ldots\ldots[13]$$

$$A_4(m) = 2m[18I(I+1) - 34m^2 - 5] \quad \ldots\ldots\ldots\ldots\ldots\ldots\ldots\ldots\ldots\ldots[14]$$

are zero-, second- and fourth- rank coefficients depending on the spin I and order m of the transition and

$$P_2(\cos\beta) = (3\cos^2\beta - 1)/2 \quad \ldots\ldots\ldots\ldots\ldots\ldots\ldots\ldots\ldots\ldots[15]$$

$$P_4(\cos\beta) = (35\cos^4\beta - 30\cos^2\beta + 1)/8 \quad \ldots\ldots\ldots\ldots\ldots\ldots\ldots\ldots\ldots\ldots[16]$$

are the second and fourth degree Legendré polynomials of $\cos\beta$, β being the angle between the spinning axis and H_0.

Eq. [11] contains the isotropic part (first two terms) and the anisotropic parts to first order (third term) and second order (fourth term). The angular dependent (θ, ϕ) frequencies of third and fourth terms of the Eq.[11] are responsible for the observed line broadening. Since spinning at one fixed axis cannot cancel the $P_2(\cos\beta)$ and

$P_4(\cos\beta)$ dependent anisotropies, simultaneously, as evidenced by the functional behavior of $P_2(\cos\beta)$ and $P_4(\cos\beta)$, a simultaneous fulfilment of second and fourth rank averaging condition is met by the DAS route for the geometrical part of the interactions

$$[P_2(\cos\beta_1)t_1, P_4(\cos\beta_1)t_1] + [P_2(\cos\beta_2)t_2, P_4(\cos\beta_2)t_2] = [0, 0]\text{…….[17]}$$

In an analogous manner, we may choose the spin dependent part of Eq. [11] to fulfill the following condition for second order averaging

$$[A_2(m_1)\,t1, A_4(m_1)\,t1] + [A_2(m_2)t_2, A_4(m_2)t_2] = [0, 0]. \quad \text{……..[18]}$$

The above condition can be met for any spinning angle. However, the choice of $\beta = 54.736^0$ ('magic angle') is preferred since broadening due to chemical shielding anisotropy and dipolar interaction can be removed at the 'magic angle'. For the signal detection, NMR selection rule restricts the implementation of Eq. [18] to $m_2 = -½ \leftrightarrow m_2 = +½$ transition, while m_1 can be chosen as 3, 5, 7, 9 as the case may be. The new experimental approach seeks to correlate the single quantum frequencies with the multiple quantum frequencies in such a way that isotropic spectrum may be constructed upon fulfillment of Eq. [18]. This is envisioned and realized through the two dimensional MQ-MAS experiment. For such an experiment, we can write for the phases in the evolution and detection dimensions as (194)

$$\phi_1 = \nu_1 t_1 = \pm [2m_1 \nu^{CS} + A_0(m_1)\,\nu_0{}^Q + A_4(m_1)P_4(\cos 54.736)\nu_4{}^Q(\theta, \phi)]t_1 \text{...[19]}$$

$$\phi_2 = \nu_2 t_2 = [\nu^{CS} + A_0(½)\,\nu_0{}^Q + A_4(½)\,P_4(\cos 54.736)\nu_4{}^Q(\theta, \phi)]t_2 \quad \text{…….[20]}$$

Where it may be noticed that the first order terms (A_2) are zero and do not appear due to $P_2(\cos\theta)$ dependence. Noting that $A_4(½)$ is always positive, the refocusing of the anisotropic terms can be achieved by properly choosing the sign in Eq. (19), knowing the magnitude and sign of $A_4(m_1)$. Positive sign is chosen when $A_4(m_1)$ is negative and negative sign is taken when the coefficient is positive. An isotropic echo is obtained when

$$t_2 = \frac{|A_4(m_1)|}{|A_4(½)|}t_1 = R(I, p)t_1 \quad \text{……[21]}$$

Based on the above theoretical considerations, a pulse sequence which correlates the triple quantum frequencies during the evolution period (t_1) with the single quantum

frequencies during the detection period (t_2) is used to conduct the MQ-MAS experiment. The figure 4.1 below shows the so-called *z*-filter pulse scheme for performing MQ-MAS experiments.

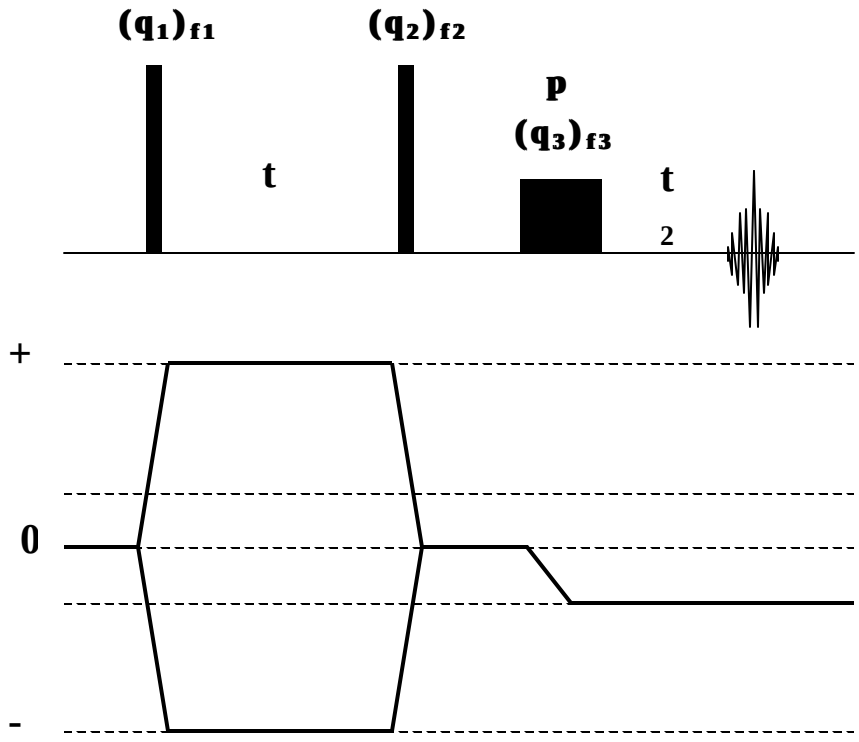

Fig.- 4.1:. The z-filter triple quantum MAS (3Q-MAS) pulse sequence used in the present studies for detecting the various nonequivalent aluminum sites in the USY and Ti-USY materials.

The diagram shows the coherence transfer pathways and the desired pathway is selected by proper phase cycling of the phases of the r.f pulses shown and the receiver which detects the signal. MQ-MAS experiments were performed using the above sequence on a Bruker DRX-500 FT-NMR spectrometer available at NCL

4.2 : Experimental procedure in Static, MAS and MQ-MAS NMR Spectroscopy:

All the NMR experiments were performed either on a Bruker MSL-300 or DRX-500 FT-NMR spectrometer depending on considerations such as the spinning speed and sample volume. ^{27}Al MAS and 3Q-MAS experiments were carried out on the DRX-500 at 130.29 MHz, while the ^{29}Si MAS experiments were carried out on the MSL-300 at 59.59 MHz. The high field operation was preferred for ^{27}Al in order to enhance the apparent resolution due to a reduction in the second order quadrupolar broadening and an increase

in chemical shift dispersion at the high magnetic field of 11.7 T. Considering the nutation behaviour (195) of a quadrupolar spin, the ^{27}Al r.f pulse length was chosen to be very short, namely, 0.6 - 1.0 μs. For ^{29}Si, a pulse of duration 2.5 μs (30^0 flip angle) and a recycle delay of 3 s were used. The sample was spun at 10.0 and 2.8 kHz for the ^{27}Al and ^{29}Si experiments, respectively. Chemical shifts were referenced with TMS (using TEOSi, -82.2 ppm with respect to TMS) for ^{29}Si and with $[Al(H_2O)_6]^{3+}$ for ^{27}Al. Typically 2000 and 6000 transients were accumulated for ^{27}Al and ^{29}Si experiments, respectively. Spectral deconvolutions were carried out using mixed Gaussian and Lorentzian line shapes using Bruker Win-NMR software on a PC.

For the ^{27}Al 3Q-MAS(196) experiments, a three pulse z-filter sequence due to Amoureux *et al*.(197) was used. Here, the z-filter modification enables the coherence transfer pathway ±3Q → 0 as an intermediate step, prior to the conversion step 0 → (-1Q), so that equal jumps are involved for the optimal selection of the mirror echo and anti-echo coherence transfer pathways, leading to a pure absorption mode 1Q → 3Q 2D spectrum to be obtained using the States method.(198). For the r.f field used (60 kHz), the first and second pulses were individually optimised to give maximum efficiencies for the ±3Q coherence creation and the ±3Q to 0Q conversion steps, respectively. The further conversion to SQC (-1Q) of the observed (-1/2, +1/2) central transition was achieved using a soft pulse 90^0 pulse of duration 9 μs. The phase cycling was designed to select only the desired pathway (0) → (±3) → (0) → (-1). Typically, the 2D accumulation involved 1024 (t_2) x 128 (t_1) values, using 960 scans for each of the t_1 steps 74.1 μs. A 2D Fourier Transformed followed by a shearing operation gave pure absorption mode 2D spectra in which the isotropic resonances are aligned parallel to the ω_{iso} axis.

Titanium NMR experiments were carried out using a broadband home-built static probe on the Bruker DRX-500 NMR spectrometer. The tuning and matching of the resonant circuit was achieved using a tapped parallel LC circuit.(199). Voltronics high voltage and high Q capacitors were used for the tuning and matching. The r.f was fed into the tuning circuit using a specially designed rigid co-axial line made of plumbing copper tubes with the ratio of the o.d of the inner conductor to the i.d of the outer conductor chosen to make a 50-ohm transmission line. The r.f coil was made out of 16 SWG and had an i.d of 10 mm and 12 number of turns. A padding of 100 pF was required to bring

the tuning frequency down to 28.184 MHz for ^{49}Ti. The circuit Q of the probe was found to be 160. In order to reduce the acousting ringing, the probe cover was made out of copper. A two-pulse spin echo sequence with a quadrature pulse phase cycle was used to obtain the spectrum. Chemical shifts were referenced to the ^{49}Ti resonance of external $TiCl_4$. Spectra were obtained with an echo delay of 100 μs, pulse repetition time of 150 ms, and approximately 300,000 scans. All measurements were carried out on static samples at room temperature. Since the gyro-magnetic ratio of the two magnetically active isotopes of titanium are very close to each other (to within 0.02%), both the ^{47}Ti and ^{49}Ti isotopes are observed in the same experiment.

4.3 : ^{27}Al MAS NMR results of Na-Y, NH_4-Y and USY Zeolites

The ^{27}Al MAS experiments were carried out on USY starting from Na.NH_4-Y. The spectra are presented in the Fig. 4.2. Only tetrahedral Al is detected in parent Na.NH_4-Y, in due evidence for the entire Al residing in the framework. Emergence of octahedral signal due to framework dealumination is noticed even at 550° C and, more importantly, the emergence of a new signal in the range 27.9 to 32.2 ppm, not seen in the parent Na-Y or NH_4-Y, is also noticed at 550° C. Consistent with other reports(200), this peak is assigned to penta co-ordinated Al species. The penta co-ordinated Al is usually not seen in MAS spectra at lower B_0 fields and is appropriately termed 'invisible' aluminum (200). Compared to 7.0 T field, our operation at 11.7 T is definitely rewarding since the second order quadrupolar broadening is reduced by a factor of 1.66, while the chemical shift dispersion is enhanced by the same factor, both contributing to the enhanced peak resolution for the revelation of five co-ordinate Al species. We observe that at mild steaming conditions at 550° C, not only considerable dealumination takes place, but the five co-ordinates Al is also created at the early stages of steaming. As seen in Fig. 4.2, further stepwise steaming treatment is seen to increase the peak intensity for the signal at 30.7 ppm at the expense of decreasing intensity for 53.9 ppm while the intensity of octahedral Al is affected to a much less degree (compare samples 550-700-MSTP and 550-700-850-MSTP). The process of dealumination leading to the final standard material 550-700-850-MSTP serves to redistribute the four co-ordinate framework Al environments into increasing five coordinate Al population. Beyond this, as for example at 925° C, framework collapse is imminent by the loss of Al^V signal and

the detection of a larger population of Al^{VI} exhibiting a larger broadening much ($\Delta\nu$ = 1700 Hz). Thus, ^{27}Al MAS results not only show that Al^{V} species are the stabilization species but additionally indicate that best ultra-stabilization is done by careful step-wise steaming down to 850° C and not beyond that. The three prominent signals in the case of standard material 550-700-850-MSTP, namely the tetrahedral (53.9 ppm), the penta coordinated (32.2 ppm) and the octahedral (4.6 ppm) environments, are further investigated by MQ-MAS technique to probe their structural inequivalence. This material forms the base material for further studies in this work.

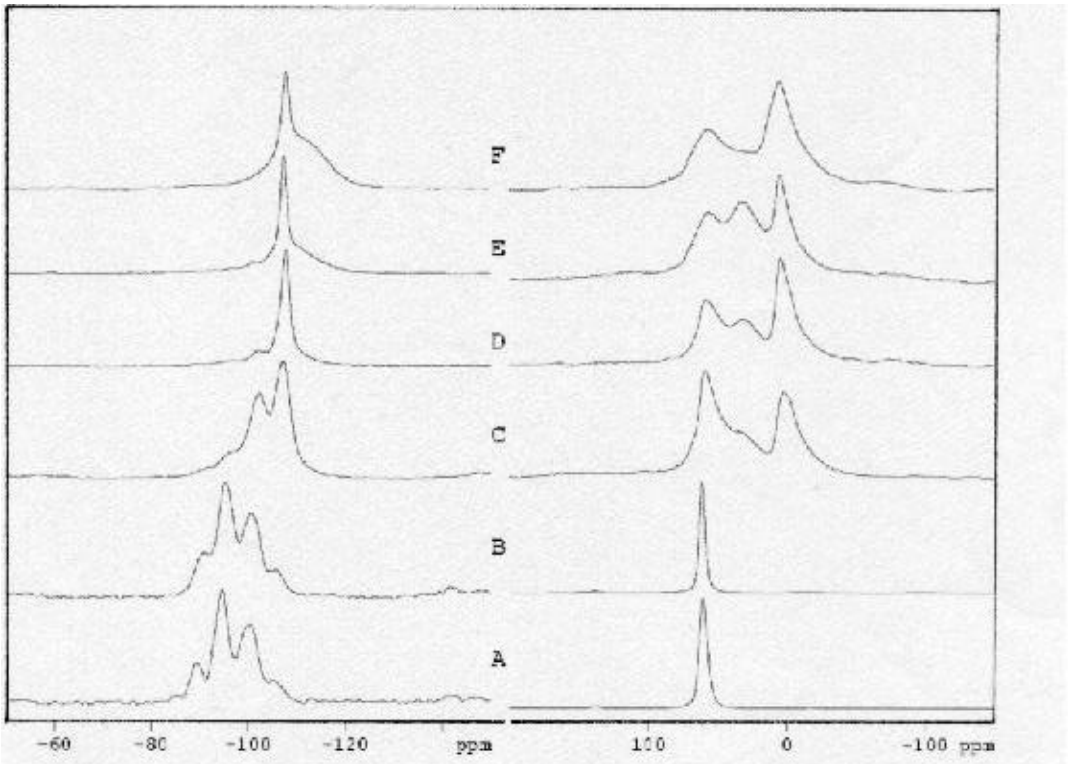

Fig.- 4.2 : ^{29}Si MAS (left) and ^{27}Al MAS (right) NMR spectra obtained from hydrothermally prepared USY samples (see Table 1).
(A) Na-Y (parent sample);
(B) Na,NH_4-Y (NH_4^+ ion exchanged Na-Y);
(C) 550-MSTP (NH_4-Y steamed at 550^0C);
(D) 550-700-MSTP (550-MSTP steamed at 700^0C);
(E) 550-700-850-MSTP (550-700-MSTP steamed at 850^0C) and
(F) 550-700-850-925-.MSTP(550-700-850-MSTP steamed at 925^0C)

4.4 : ^{29}Si MAS NMR results on Na-Y, NH_4-Y and USY samples

Both Na-Y and NH_4-Y give well-resolved ^{29}Si resonances as seen in Fig-4.2. Based on the observed chemical shifts positions, we identify Si(4Si, 0Al) [-105.0 ppm], Si(3Si, 1Al) [-100.6 ppm], Si(2Si, 2Al) [-94.7 ppm], Si(1Si, 3Al) [-89.4 ppm] and very barely detectable signal Si(0Si, 4Al) [-85.2 ppm] consistent with Na-Y and NH_4-Y chemical shift values for Si/Al = 2.48 (Linde-Y) (202,203). At 550° C, ^{29}Si MAS spectrum shows a dominant Si(3Si, 1Al) and Si(2Si, 2Al) resonances, whose integrated intensity is estimated by deconvolution for the determination of Si/Al, which is found to be 2.4. For the sample steamed at 700° C and 850° C, the Si(3Si, 1Al) and Si(2Si, 2Al) signals are very weak in intensity. Noticeably, we pick up a new signal in the region -110.0 to -111.2 ppm, whose intensity gradually increases from 550-700-MSTP sample to 550-700-850-MSTP sample. This observation is rationalized as follows. We take a recourse to the scheme 4.1 which is identical to the scheme 3.2 shown in chapter-III for Ti incorporation , where the mechanism of ultrastabilization proposed by Klinowski *et al*. (204,207) is sketched. During steaming, vacancies are created by the removal of framework aluminum, which now facilitate the insertion of silicon into the framework. The interstitial defects are partially removed by NH_4^+ ion exchange and then calcination as we have done in Oxa-MSTP-200-0.33, Buto-MSTP-200-0.33, Iso-MSTP-200-0.33 and using by acid treatment with 0.01 N HNO_3.in MSTP-10.When the reoccupation by silicon is complete and system is fully healed, the new Si-O-Si linkages that are formed can be thought of as belonging to the same ordered faujasite network. The SiO_4 tetrahedra for these new framework silicons will however be quite distorted compared to the SiO_4 tetrahedra of the fully ordered and undisturbed framework.This envisages that we ought to detect these environments quite distinctive of the main signal at -105.0 ppm since the geometrical distortion would reflect on the mean T-O-T angle at the central silicon and would cause an upfield resonance shift (205;206) for these new Q^4(4Si) environments. Our observation of the new resonance at -110.0 to -111.2 ppm is fully in agreement with this view and lends credence to the ultrastabilization mechanism proposed earlier by Klinowski *et al*. (204,207). We may thus ascribe this new resonance, at -110.0 to -111.2 ppm for the siliceous silicon Si(4Si, 0Al) which arises due to the

reoccupation of the vacancy created by framework Al removal by the scheme(203,204,207) given in the scheme 4.1.

Scheme-4.1

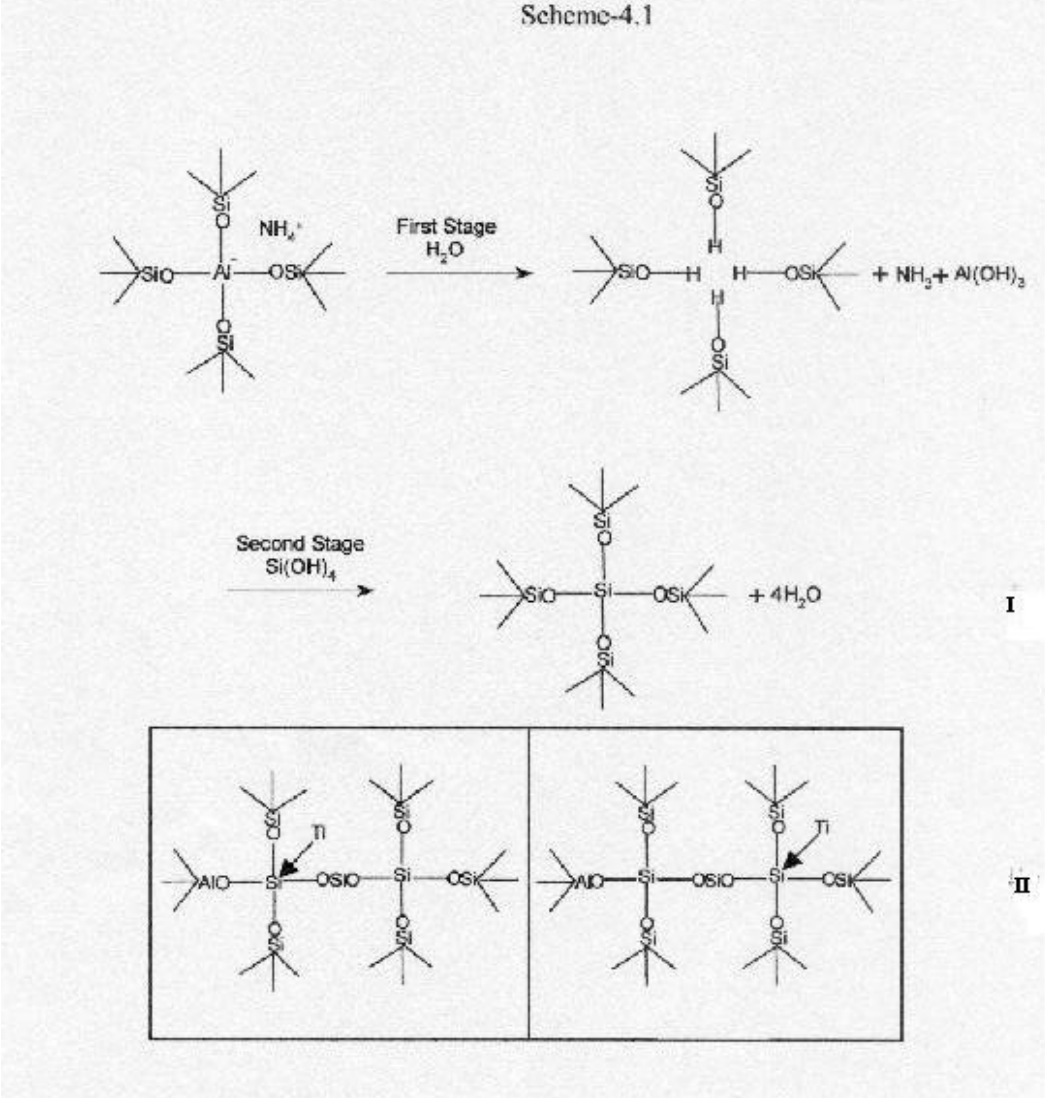

Further, in the 550-700-850-925-MSTP sample, the peak appearing in the range -110.6 to -111.2 ppm becomes more intense compared to original framework Si(4Si, 0Al) type silicon at -107.9 ppm. More importantly, the loss of Si(3Si, 1Al) and Si(2Si, 2Al) environments are noticed, thus suggesting the steaming treatment at 925° C has resulted in a partial collapse of the faujasite structure. The high field signal in the range -110.6 to -111.2 ppm is clearly seen in 700° and 850° steam treated samples. The intensity increases gradually with increasing steam temperature treatment. In 700° and 850° steam treated samples the Si(3Si, 1Al) environment is definitely present. ^{27}Al MAS NMR

spectra show that beyond 500 ^{0}C the dealumination confines the Al removed from the tetrahedral positions in the penta coordinated nonframework environment, as judged by the signal intensities for the Al^{IV}, Al^{V} and Al^{VI} species (see Fig..-4.2). The corresponding influence in the ^{29}Si spectrum is to reduce the intensity for the Q_4(3Si,1Al) peak with increasing steam treatment. The ^{29}Si MAS NMR results thus indicate that from the point of view of having a faujasite structure, steaming upto 850° C does ensure a standard USY base material. Such a material was chosen for Ti incorporation as discussed below.

4.5 : ^{29}Si and ^{27}Al MAS NMR results on Ti-USY samples

There has been a continuous effort in various laboratories to incorporate Ti in the framework of various zeolites (MFI, Beta, etc), including mesoporous materials (MCM-41 etc) for TiO_2 being catalyticaly and photo catalyticaly good oxidative catalyst material in its bulk form. There are numerous reports in the literature saying Ti substitution and characterization of various zeolites by XRD, MAS NMR, FT-IR, UV-VIS etc. Despite the numerous reports published in the literature, there seems to be a lack of unequivocal evidence for the isomorphic substitution of Ti in the lattice. In the case of zeolite Y there is only one very recent report by Wang Yang dong *et al* (208) on the preparation and characterization of Ti containing USY zeolites. However, ours is the first attempt to study Ti-USY using NMR technique. We have attempted in this work to isomorphically substitute Ti in USY, taking 550-700-850-MSTP sample as the standard base material.

For the Ti substitution, various Ti sources were used. These were 1) Potassium titanium oxalate K2[$TiO(C_2O_4)_2$], 2) Titanium butoxide ($Ti[O(CH_2)_3CH_3]_4$) and 3) Tetraisopropyl orthotitanate ($Ti[OCH(CH_3)_2]_4$.) Of these, first is water soluble while second and third are soluble in organic solvents.

^{27}Al MAS NMR spectrum of USY base material (550-700-850-MSTP) is compared with Ti-USY using different Ti sources in th fig.-4.3. A striking observation is that with K TiO oxalate (K_2 $TiO(C_2O_4)_2$) we observe the total absence of penta co-ordinated Al in the ^{27}Al MAS spectrum. The ^{27}Al MAS spectrum remains unaltered when the same level of treatment is given in the absence of a Ti source, whereas the choice of Ti source is seen to have an effect on the ^{27}Al MAS spectrum. For example with Ti butoxide ($Ti[O(CH_2)_3CH_3]_4$) and Tetraisopropyl orthotitanate ($Ti[OCH(CH_3)_2]_4$), the relative intensity of the penta co-ordinated Al is reduced at the expense of increasing intensity for

octahedral Al species. More strikingly, however we observe that Ti source containing alkali (K Ti oxalate) has a profound effect to eliminate altogether the penta co-ordinated Al species as verified in ^{27}Al MAS spectrum [Fig 4.3].

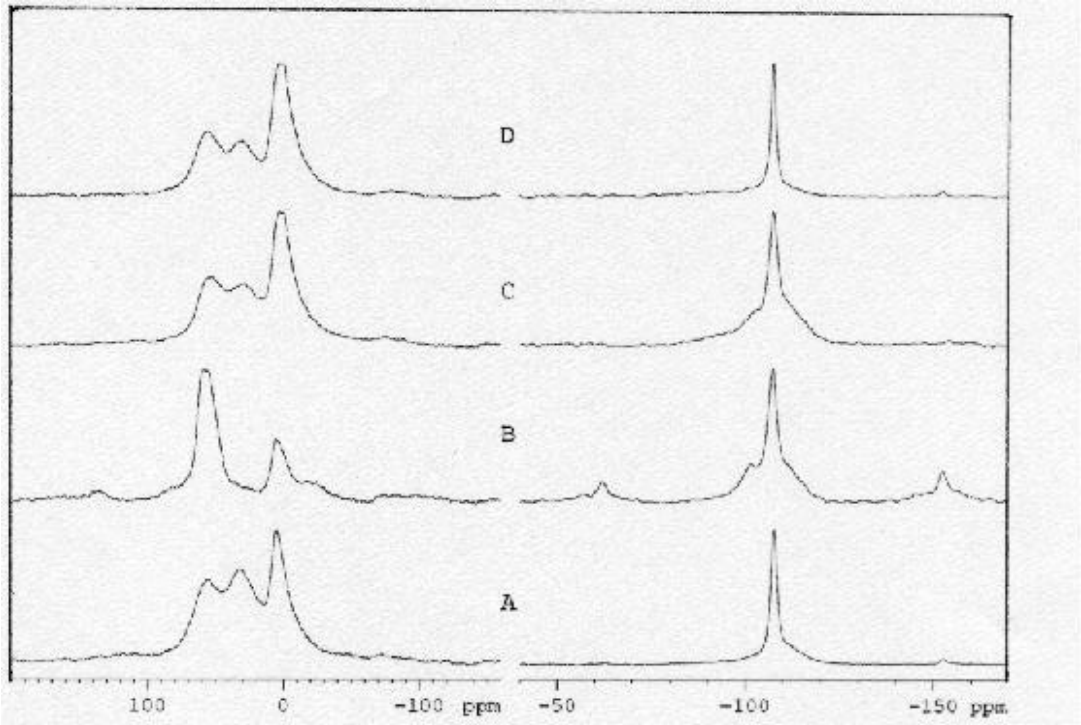

Fig.- 4.3 : ^{27}Al MAS (left) and ^{29}Si MAS (right) NMR spectra obtained in Ti-USY materials, prepared using various titanium sources.
(A) MSTP-10 (acid treated 550-700-850-MSTP sample, very high silica USY with no Ti source),
(B) Oxa-MSTP-200-0.33 (very high silica Ti-USY prepared using potassium titanium oxalate),
(C) Buto-MSTP-200.0.33 (very high silica Ti-USY prepared using titanium butoxide), and
(D)Iso-MSTP-200-0.33, very high silica Ti-USY prepared using titanium isopropoxide)

4.6 : Triple Quantum ^{27}Al MAS NMR of USY and Ti-USY

^{27}Al MAS NMR offers high detection sensitivity but suffers from inferior spectral resolution due to residual second order quadrupolar broadening of the observed ½ ↔ -½ spin transition which is not altogether eliminated at the magic angle. It is however feasible to detect Al environments belonging to different coordinations (four, five and

six). The main limitation with ^{27}Al MAS is the lack of fine resolution which precludes the identification of in-equivalent aluminum environments within any given coordination. The recently developed multiple quantum magic angle spinning (MQ-MAS) offers new opportunities in this direction. In this technique, the various orientation dependent frequencies of any symmetric multiple quantum (3Q, 5Q for ^{27}Al) transition are correlated with the corresponding second order quadrupole perturbed frequencies of the observed 'central transition' (½ ↔ -½) by a definite ratio R(I,p), where I is the spin quantum number of the nucleus and p the multiple quantum order. The anisotropic second order quarupolar broadenings can be eliminated in a 2-D experiment designed to provide a frequency correlation of the multiple quantum evolution (t_1) dimension with the single quantum detection (t_2) dimension. For the ^{27}Al 3Q- MAS experiment, the 3Q(-3/2 ↔ +3/2) to 1Q (-1/2 ↔ +1/2) correlation is established for R = 19/12. By knowing this definite ratio R, the 2-D data matrix is subjected to a shearing transformation, which aligns the isotropic axis parallel to the ω_1 axis. Isotropic spectra devoid of quadrupolar broadening are obtained by a sum projection of the sheared frequency domain 2-D spectra onto the ω_{iso} axis. As a further aid to quantification of the various isotropic aluminum resonances resolved by the MQ-MAS method, a graphical analysis of the 2-D contour plot can be readily carried out when the sheared frequency domain 2-D data are plotted after the isotropic shifts (ppm) are scaled by using an effective Larmor frequency
given by,

$$\omega_{iso} = (|R| - p)\,\omega_0 \left\{\delta_{cs} + 3/17\, C_Q^2\,(1+ \eta^2/3)\,[4I(I+1) - 3p^2]/\,[4I(2I-1)\,\omega_0]^2\right\} \rightarrow (22)$$

where, ω_{iso} = Larmor frequency in F_1 dimension

p = coherence order (3Q for aluminium)

ω_0 = Larmor frequency in F_2 dimension

I = spin number

η = asymmetry parameter

C_Q = quadrupolar coupling constant

|R| = the co-efficient

The 3Q-MAS experiments would additionally aid in mapping the Al site in-equivalence and distribution.

^{27}Al 3Q-MAS experiments are clearly superior since they lead to the detection of various Al environments in the structure under high-resolution conditions. In the study of USY and Ti-USY, the 3Q-MAS results on USY reveal the isotropic resonances for each co-ordination. The high field resonance at δ_{iso} = 1.1 to 9.1 ppm range is readily assigned to the non-framework Al^{VI} species. Considering the 62.0 to 72.8 ppm range for the occurrence of tetrahedral Al, it is rather straightforward to assign the two low field resonances to Al^{IV} species. The occurrence of the remaining isotropic signal at δ_{iso} = 38.1 to 42.5 ppm excludes these regions and confirms its assignment to the penta coordinated Al^{V} species. With the resolution of two distinct aluminum environments in the tetrahedral region, not provided by ^{27}Al MAS spectrum, a total of four different aluminum environments are detected in USY as shown in the fig-4.4.

Recently, Fyfe *et al.*(200) have carried out ^{27}Al 3Q-MAS experiment on USY at very high magnetic field of 18.8 T (800 MHz) and have identified two distinct tetrahedral, one pentagonal and one octahedral Al species in USY. Our ^{27}Al 3Q-MAS results on standard USY sample are consistent with these findings. Our results are also consistent with the recent study of non-framework sites of aluminium by Menezes *et al.*(209). The values of δ_{CS} and P_Q for the Al^{VI} and A^{IV} species find an overall agreement with the values reported by Fyfe *et al.*(200) and Menezes *et al.*(209). However, our P_Q value of 1.2 to 2.0 MHz for the second tetrahedral species is considerably smaller than the values 6.9 MHz reported in these works. Clearly, in our USY sample there is a clear absence of highly distorted Al^{IV} environments, implying thereby that our MSTP steam treatment has little influence on the stronger Al sites which could not be dealuminated. In the study of USY by Menezes,(209), they have used H_2SO_4 for acid leaching and this would invariably result in the formation of $Al_2(SO_4)_3$, not easily removed from the zeolite by washing. This would have led to the formation of amorphous Al^{IV} species, as attributed to in the study by Menezes,(209) et al, who inferred this by the shape of the contour which showed a distribution of P_Q values. In our study, the absence of this amorphous phase is clearly indicated by the 3Q-MAS data. This supports our view that an important aspect of ultra-stabilization is also to ensure that controlled heating and acid leaching by HNO_3 is mandatory if a crystalline USY, devoid of the amorphous phase, is to be obtained. Our 3Q-MAS results conclusively show that ultra-stabilization is not only accompanied by the

distribution of a part of the framework aluminum into the non-framework (due to dealumination) and 'invisible' (Al^V) positions, but additionally by the formation of new framework tetrahedral species. Results presented in Table-2 give the values of quadrupolar coupling constant (QCC) for each site for 550-700-850-MSTP and Buto-MSTP-200-0.33 samples.

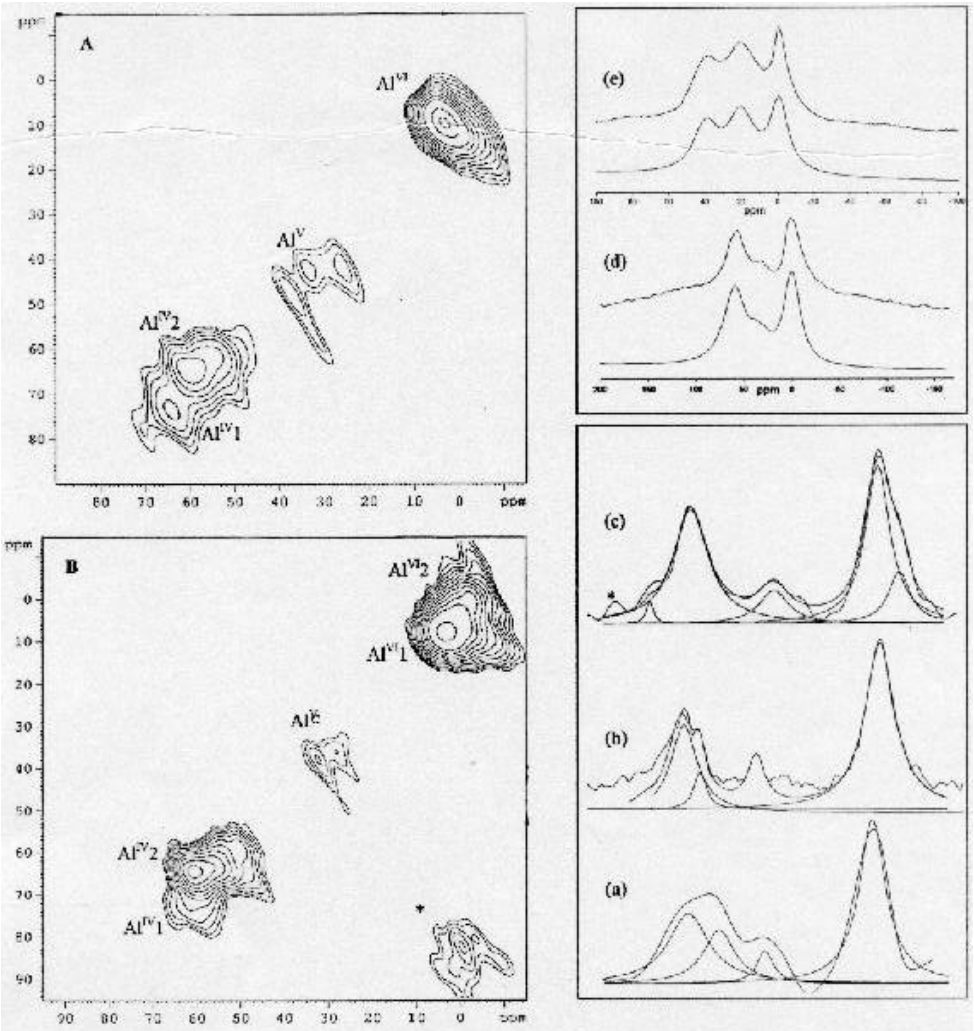

Fig.- 4.4 : ^{27}Al triple quantum magic angle spinning (3Q-MAS) spectra of (A)550-700-850-MSTP(very high silica USY with no Ti source) and (B)Buto-MSTP-200-0.33(very high silica Ti-USY prepared using titanium butoxide) showing the resolution of the tetra (Al^{IV}), penta (Al^V) and octahedral (Al^{VI}) aluminum environments. The corresponding isotropic spectra, obtained after a projection of the sheared 2-D data matrix on to the isotropic axis, are compared on the right of the contour plots, (a), (b) and (c). Also the simulations of ^{27}Al MAS spectra of (A) recorded on DRX-500 and MSL-300 are given in (d) and (e). The various Al environments are marked in the figure. The chemical shifts and the quadrupole coupling parameters, deduced from a graphical analysis of the 2-D contour data, are given in Table 2.

Table 2: Mapping the Al site in-equivalence and distribution. by ^{27}Al 3Q-MAS NMR for very high silica USY and Ti-USY samples

550-700-850 MSTP/Buto-MSTP-200-0.33	δ_{CS} in ppm	δ_{iso} in ppm	δ_{QIS} in ppm	C_Q in MHz
Tetrahedral I	69.8/64.4	72.8/66.0	2.8/1.6	2.6/2.0
Tetrahedral II	62.6/61.1	64.1/62.0	1.5/0.9	1.9/1.5
Pentagonal	37.0/33.9	42.5/38.1	5.48/4.3	3.6/3.2
Octahedral	7.3/6.0&0.01	9.1/7.8&1.1	1.9/1.8&1.1	2.1/2.0 &1.6

4.7 : Graphical Analysis

We have done graphical analysis of the data obtained after shearing using the program "xfshear" to obtain the QCC values. In this graphical analysis, the 2-D data is plotted after the 3Q-MAS dimension is appropriately scaled by the effective Larmor frequency (according to Eq. 22) while the MAS dimension has ppm scale in which 1 ppm = ω_0. The square 2D contour plot is constructed with the CS axis to lie along the slope of 1 and the QIS axis to lie along a slope of –10/17. Projection of the contours onto the F1 axis (isotropic axis) gives the isotropic shift values (δ_{iso}).

4.8 : Evidence for Framework Ti Substitution in USY (Ti-USY)

In the study of Ti substituted USY using different titanium sources, we gather a striking evidence for the incorporation of titanium in the USY framework. When we compare ^{27}Al MAS spectra of 550-700-850-MSTP sample and the same sample after further dealumination by acid treatment (MSTP-10 sample) wherein no titanium source is present, we find that the peak intensity of various Al resonances show no change in their relative intensities. This shows that additional thermal and acid treatment practically causes no disturbance of any aluminium environment (tetra, penta and octa).

However with titanium source titanium butoxide, which was found to be the good source, we do see an enhanced intensity of the octahedral Al in the Buto-MSTP-200-0.33 sample. From the ^{29}Si MAS NMR comparison of 550-700-850-MSTP, MSTP-10 (same sample after further dealumination by acid treatment) and Buto-MSTP-200-0.33 sample, which is presented in the fig.-4.5,we gather that the additional treatment used for Ti incorporation does not change the ^{29}Si MAS NMR spectra (comparing 550-700-850-

MSTP and Buto-MSTP-200-0.33 samples). However, a comparison of Buto-MSTP-200-0.33 and MSTP-10 samples shows that the Si(4Si, 0Al) peak intensity is considerably reduced and the signals in -101.38 ppm and -95.52 ppm occurs with enhanced signal intensity. This observation suggests that Ti substitution probably occurs at the siliceous Q^4(4Si) sites. This also would be in accordance with the Ti→Al avoidance which is possible only when Ti substitution takes place in Q^4(4Si) and not Q^4(3Si, 1Al) or Q^4(2Si, 2Al) sites(194,210).

Titanium incorporation in the lattice as evidenced by ^{29}Si and ^{49}Ti NMR is accompanied by partial dealumination in the USY lattice. We compare in fig-4.3, the ^{29}Si MAS spectra of the MSTP-10 (without titanium source) with the corresponding spectra taken from titanium containing USY (using different titanium sources). In 550-700-850-MSTP sample, where no titanium is present, the ^{29}Si resonances corresponding to -107.36 ppm and -101.01 ppm have been identified and assigned. The resonances belonging to Si(1Al) and Si(2Al) are detected with low signal intensity since for 550-700-850-MSTP sample, the Si/Al = 26.29. Since 550-700-850-MSTP is the standard material for titanium treatment, any titanium incorporation into the zeolite lattice would enhance the signal intensity in the region -101.01 ppm where silicon adjacent to titanium would appear. Inspection of spectra in Fig. 4.3 shows that pronounced signal intensity occurs in this region in Buto-MSTP-200-0.33 sample, which was prepared using titanium butoxide. A careful inspection of Fig. 4.3 in fact reveals that we may detect a set of resonances, not seen in 550-700-850-MSTP sample, at -101.38, -95.52 ppm and -90.0 ppm. Considering the enhanced signal intensity for these peaks over the spectral intensity in the same spectral range of 550-700-850-MSTP sample, we reckon that these new set of resonances must arise from silicon environments of type Q^4(Si,Ti). The revelation of these new environments arises when the framework Si/Ti ratio is rather small, as it has been observed in the titanosilicate structure of ETS-10 (Si/Ti = 5) (194,210). In 550-700-850-MSTP sample, Si/Ti ratio was found to be 1.99 by x-ray fluorescence spectroscopy. We believe that this is the first direct evidence from ^{29}Si MAS NMR about the presence of lattice titanium in Ti-USY.

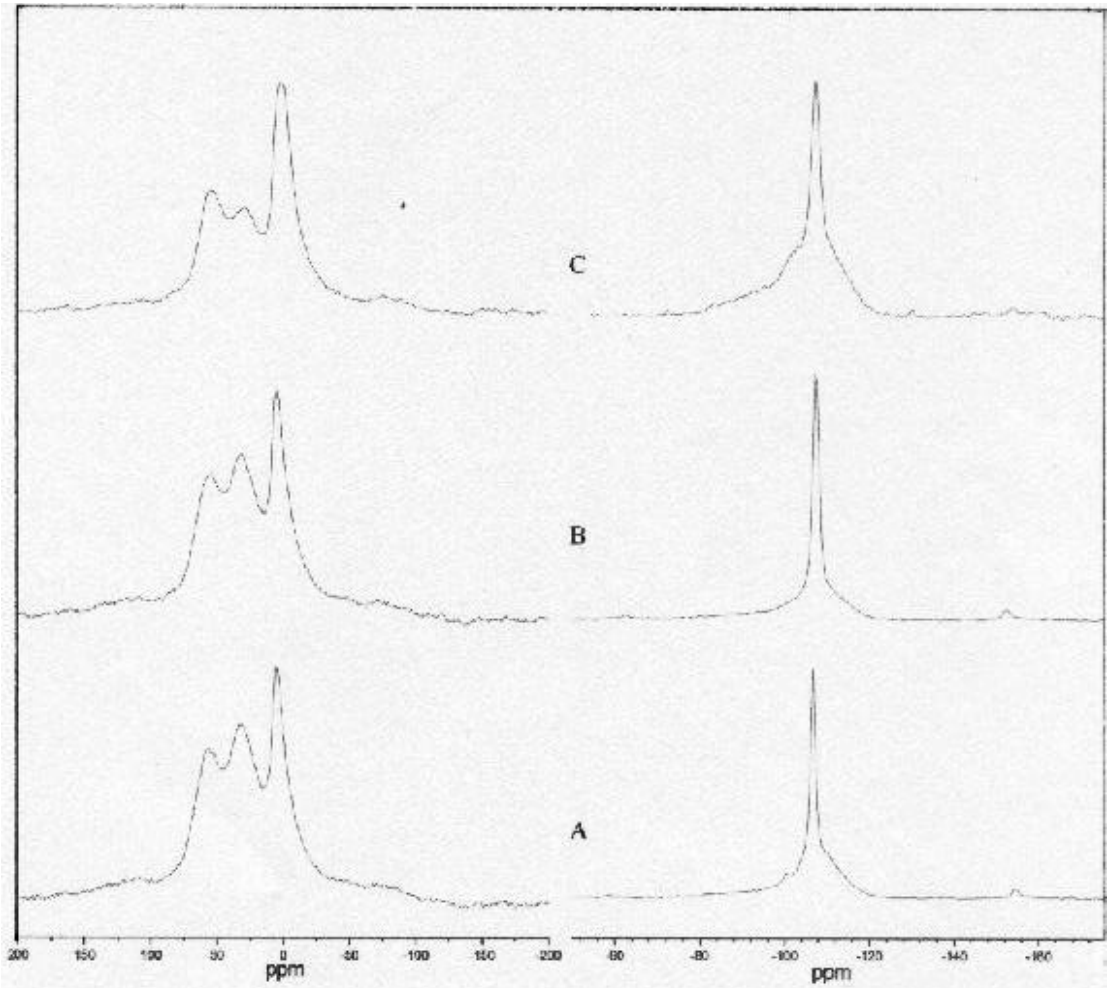

Fig.- 4.5 : ^{27}Al MAS (left) and ^{29}Si MAS (right) NMR spectra obtained in
(A) 550-700-850-MSTP(very high silica USY with out Ti),
(B) MSTP-10 (acid treated 550-700-850-MSTP sample)
(C) Buto-MSTP-200-0.33 (very high silica Ti-USY prepared using titanium butoxide)

As a further verification of Ti substitution in USY framework, we have taken a Ti substituted USY, Buto-MSTP-200-0.33 sample for the observation of the titanium NMR. Ti offers two magnetically active nuclei whose gyromagnetic ratios are close to each other to give a 2% increase in the Larmor frequency for the ^{49}Ti nucleus. Essentially one detects both ^{47}Ti and ^{49}Ti in the same experiment. They are quadrupolar belonging to n/2 family I = 5/2 for ^{47}Ti and I = 7/2 for ^{49}Ti so that in solid state experiments one could

invariably observe only the central transition (+1/2 ↔ -1/2) (211a) We note that the second order quadrupolar broadening of the central transition is dependent on $(e^2Qq/h^2)^2/\nu_0$ where e^2Qq/h is the quadrupolar coupling constant and ν_0 is the Larmor frequency. For operation at 11.7 T field, the frequency shifts due to the two isotopes amounts for 7 kHz, while spectral spread due to quadrupolar effects would largely depend on the strength of the quadrupolar interaction. Considering that the quadrupolar moments of ^{47}Ti and ^{49}Ti differ by a factor 0.04, the quadrupolar interaction would tantamount to a change of 1 MHz in quadrupolar coupling for ^{49}Ti, over ^{47}Ti for which we assume e^2Qq/h = 4 MHz. With these considerations, we have attempted the ^{47,49}Ti static experiments on Ti-USY and the spectrum is presented in the fig.-4.6.

The ^{47,49}Ti NMR spectrum of $TiCl_4$ liquid is shown in Fig. 4.6 (a). Two sharp signals are detected: ^{47}Ti (high field signal) and ^{49}Ti (low field signal). The separation between the two signals is 244.6 ppm. The spectrum of TiO_2 (rutile phase) is shown in Fig. 4.6 (b). This spectrum shows the quadrupole pattern for the observed +1/2 < -- > -1/2 "central transition" (e^2Qq/h = 7.5 MHz and η =0.2 for the quadrupolar interaction). ^{47,49}Ti NMR spectrum of very high silica Ti-USY (Buto-MSTP-200-0.33) is shown in Fig. 4.6 (c). Clearly, this spectrum is not identical to the spectrum of TiO_2, although part of TiO_2 spectrum appears in very high silica Ti-USY due to presence of some rutile TiO_2 phase in the sample. By subtracting the TiO_2 component from very high silica Ti-USY spectrum, we obtain the difference spectrum of Fig. 4.6 (d). This gives titanium signal due to titanium incorporated in the zeolite lattice. This signal is quite narrow (11 kHz width),showing that the electric field gradient is rather small. The observed titanium must correspond to octahedral titanium since tetrahedral titanium gives broad spectra. Coordination of Ti to 4 Si and OH groups can give such an octahedral geometry.

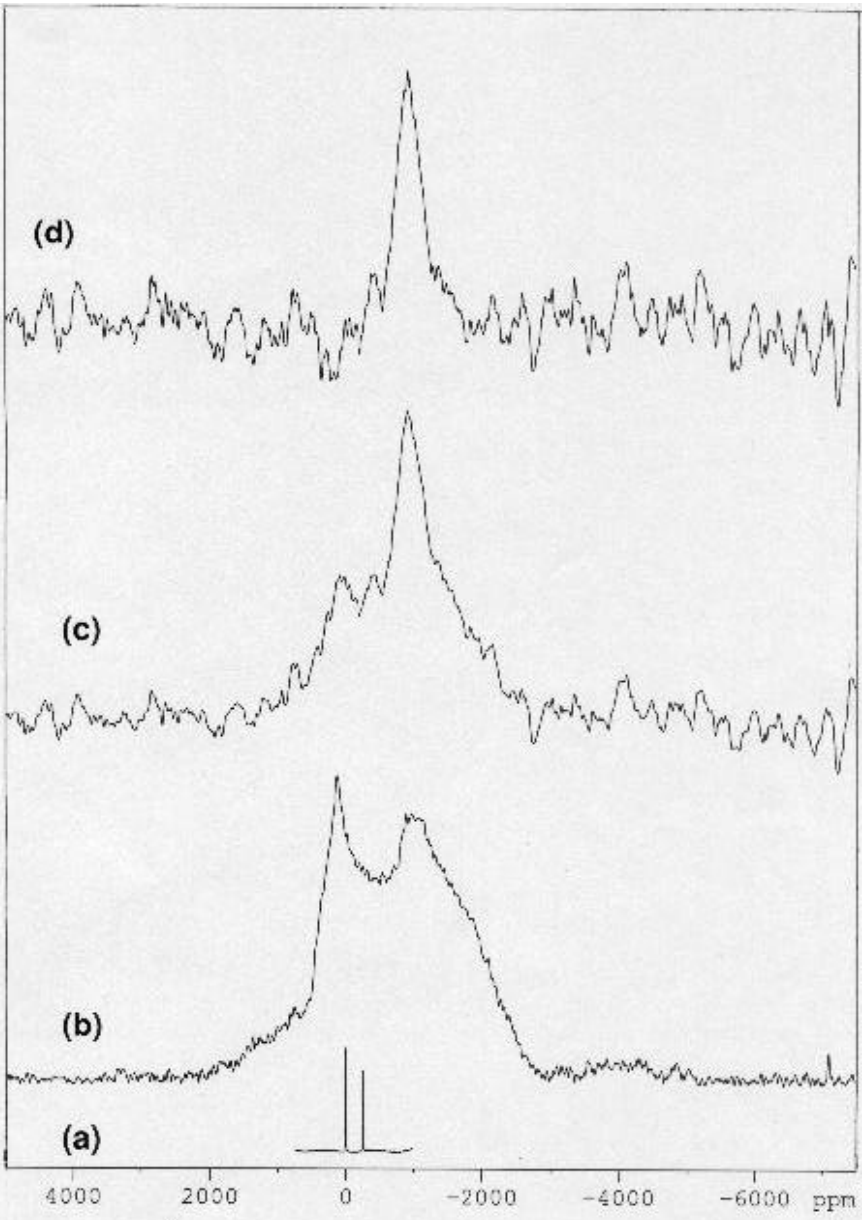

Fig. 4.6: Static titanium NMR spectra of (a) TiCl4; (b) TiO2 (rutile); (c) MSTP−200−0.33(Buto)and (d) difference spectrum.

4.9 : Conclusions

1) In the present study, we have used ^{27}Al and ^{29}Si MAS NMR, as well as ^{27}Al 3Q-MAS NMR, and ^{49}Ti NMR to understand the structural characteristics in relation to the framework stability and the hetero-atom substitution of Ti (using different Ti sources) in USY and compare the results with the Ti free USY.
2) ^{27}Al 3Q-MAS results not only show that (Al^{V}) species are not only the stabilization species, but conclusively show that ultra-stabilization is accompanied by the formation of a new tetrahedral species in additon to the distribution of a part of the original framework aluminum into the non-framework (due to dealumination) and 'invisible' (Al^{V}) positions.
3) Ti incorporation by reaction with $K_2TiO(C_2O_4)_2$ solution does not create (Al^{V}) species
4) In the ultrastabilization process, Si tetrahedra are reinserted in the "silanol nest" defect sites generating a new ^{27}Si resonance, at -110.0 to -111.2 ppm for the siliceous silicon Si (4Si, 0Al) which are different than parent Si sites and are highly distorted.
5) The Ti incorporation generates a new set of resonances at -101.38, -95.52, and -90.0 ppm. which we reckon that these new set of resonances must arise from silicon environments of type Q^4(Si,Ti). This observation suggests that Ti substitution probably occurs at the siliceous sites avoiding Al-O-Ti linkages as per Lowenstein"rule. We believe that this is the first direct evidence from ^{29}Si MAS NMR about the presence of lattice titanium in Ti-USY.
6) We have attempted $^{47,49}Ti$ MAS NMR using spin-echo technique for very high silica Ti-USY and pure TiO_2 (rutile). The difference spectrum gives titanium signal due to titanium incorporated in the zeolite lattice. The observed titanium must correspond to octahedral titanium since tetrahedral titanium gives broad spectra. Coordination of Ti to 4 Si and OH groups can give such an octahedral geometry.

CHAPTER 5

5: ACIDITY AND CATALYTIC ACTIVITY OF USY, Ti-USY AND FE-Ti-USY

5.1: INTRODUCTION :

The isomorphous substitution of Ti in to the 12-membered ring zeolites like Beta (212), Mordenite (213)..) Hexagonal Y type (214) Ferririte (215) and USY (170) have expanded the scope of oxidation properties to the realm of bigger aromatic ring compounds. Even then, published literature is limited to those applications where oxidation of organic compounds by hydrogen peroxide (H_2O_2) or tertiary Butyl hydroperoxide[$(CH_3)_3COOH$)] is reported. TiO_2 not only shows redox catalytic properties (216-218), but can form strongly acidic binary metal oxide catalysts such as TiO_2 / Al_2O_3 and TiO_2/SiO_2. They exhibit good catalytic activity for many acid catalyzed reactions like amination of phenol, isomerization of 1-butene, and cracking of n-heptane (178). Otherwise, to our knowledge, there are no reports on the acidic and their catalytic properties for hydrocarbon reactions of Ti-modified zeolites. In the only study of its kind known to us, Wang et al (178) have reported acidity and n-heptane cracking activity for Ti-USY of very low Si/Al ratio. In the present study, we have prepared series of Ti-USY samples of very high Si/Al ratio and determined the nature of the surface acidity by FTIR spectroscopy. The catalytic activity for oxidation of phenol by H_2O_2, cyclohexanol conversion, o-toluidine methylation and benzoylation of toluene were tested and correlated with the acidity. The table 5.1-5.3 contains the brief information on the samples used for alkylation of toluidine, deydration of cyclohexanol and benzoylation of toluene, and oxidation of phenol respectively.

5.2 : FTIR Spectroscopy

Amongst four different series of samples which have been studied in this work, we have chosen some samples considering the framework Si./Al ratio, amount of Ti incorporated and co-incorporation of Ti and Fe in USY. These samples are tabulated as per the reactions and are described below.

Table 5.1: Samples for Alkylation of O-toluidine

S.N	Name of the sample	NH_4-Y was steam treated at	Intermittant exchage with NH_4NO_3
1	H-Y, (dry calcined NH_4-Y)	550ºC (calcined in dry air)	Yes
2	550-MSTP (high silica USY)	550ºC	Yes
3	550-700-MSTP (high-very high silica USY)	550º	Yes
		700ºC	Yes
4	550-700-850-MSTP(very high silica USY)	550ºC	Yes
		700ºC	Yes
		850ºC	Yes
5	Oxo-MSTP-200-0.44 (very high silica Ti-USY)	Sample 4 was further treated at 200^0 C	With $K_2TiO(C_2O_4)_2$ solution of 0.44 mol fraction

Table 5.2 : Samples for Cyclohexanol Dehydration and Benzoylation of Toluene

S.N	Name of the sample	HNO_3 Exchange	$K_2TiO(C_2O_4)_2$ treatment	$(NH_4)_3Fe(C_2O_4)_3$ treatment	Temp.of reaction
1	Oxo-MSTP-200-0.33 (very high silica Ti-USY)	0.01 N	0.33 M		200^0C
2	Oxo-Fe-Ti-USY (very high silica Fe-Ti-USY)	0.01N	0.33M	0.05M	200ºC
3	MSTP-10(acid leached very high silica USY)	0.01N for 10 times			100^0C

Table 5.3 : Samples for Hydroxylation of Phenol by H_2O_2

S.No	Name of the sample	Mol fraction of $K_2TiO(C_2O_4)_2.2H_2O$	Temperature of reaction	NH_4NO_3 treatment	HNO_3 treatment
1	H-Y (dry calcined NH_4-Y)	-	550^0 C	Yes	-
2	550-MSTP-55-0.44-HNO_3 (acid leached very high silica Ti-USY)	0.44	55º C	Yes	Yes
3	550-MSTP-200-0.44 -HNO_3 (acid leached very high silica Ti-USY)	0.44	200º C	Yes	Yes

5.2.1 : FTIR Spectra of Very High Silica USY , Ti-USY and Fe-Ti-USY in Hydroxyl Stretching Region

In the table 5.1-5.3, the samples of USY, Ti-USY and Fe-Ti-USY prepared under different conditions are described which were used for reaction studies. The FTIR spectra in the region of hydroxyl group stretching of some of the typical samples used here are presented in the fig 5.1 and 5.2. The figures illustrate how the position and the concentration of surface hydroxyl groups change in the hydrothermal dealumination conditions of increasing severity. The H-Y zeolite(fig-5.1,a) shows characteristic bridging hydroxyl groups (Si-OH-Al) at 3640 (high frequency, HF) and 3550 cm^{-1} (low frequency, LF) and surface silanol (Si-OH) groups at 3744 cm^{-1} respectively. The HF band arises due to -OH groups situated in the super cages and the LF band arises due to -OH groups in the sodalite cages. The difference in the frequency value arises due to stronger hydrogen bonding of the -OH groups with the nearby anionic oxygen on the framework in the smaller sodalite cages. Steam treatment at 550^0 C broadens the over all sharpness of the bands. The intensity of silanol band at 3740 cm^{-1} increases and the formation of two new strong bands at 3704 and 3600 cm^{-1} are clearly seen (fig 5.1,b). The intensity of HF and LF bands at 3640 and 3550 cm^{-1} decreases and the bands become broader and appear only as shoulders. On increasing the steaming temperature(fig 5.1, c), the intensity of bands at 3744, and at 3600 cm^{-1} further increases and the bands at 3640 and 3550 cm^{-1} becomes obscure. In the spectrum of this sample after acid treatment (fig 5.1,d), the intensity of the silanol band at 3744 cm^{-1} decreases, the band at 3704 cm^{-1} remains unaffected and the bands at 3640 and 3550 cm^{-1} reappear. In addition, two new bands at 3676 and 3620 cm^{-1} appear. In the case of Ti-USY, the intensity of the bands at 3600, 3704 and 3675 cm^{-1} decreases and yet another band around 3725 cm^{-1} appears. Enhancement of acidity in USY is attributed to the formation of new types of Bronsted acid sites vaguely referred as "super acid sites" (219). Most recently, Cairon et al (220) have reported the creation of a high intensity new band at 3700 cm^{-1} in the steamed samples having some Na^+ ions and attributed this band to the presence of Na^+ cation and dehydroxylated sites in the zeolite. The acidity of this band was very mild but it was very stable .The over all region of the OH vibration in USY is very wide, consisting of as

many as 8 types of structural hydroxyl groups. The following are the approximate values of stretching vibrations of such -OH groups and their assignments.

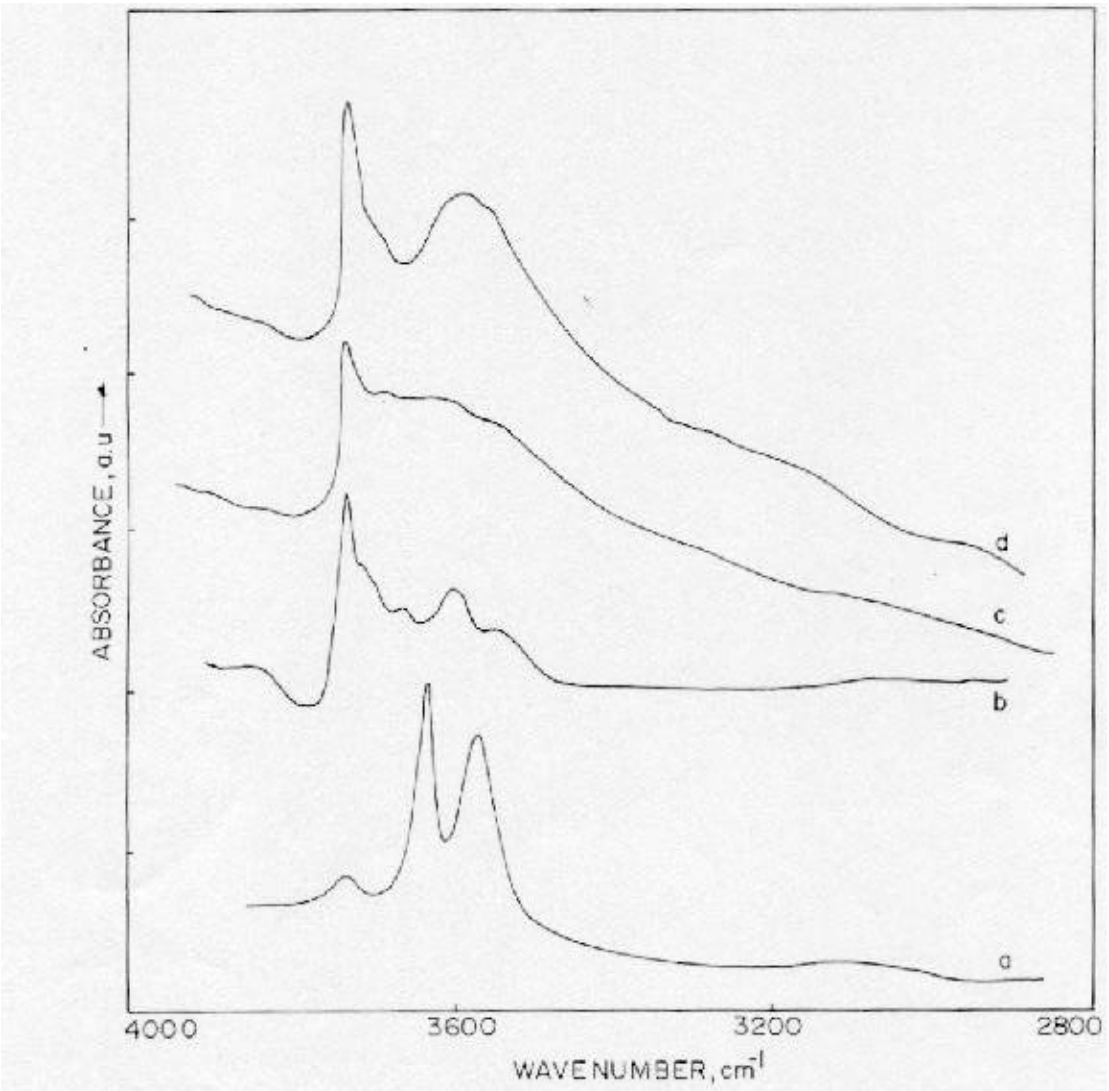

Fig.-5.1 : FTIR spectra of hydrothermally prepared USY samples in the region of structural hydroxyl group vibrations, (a) H-Y, (b) 550- MSTP(high silica USY), (c) 550-700 –850-MSTP (very high silica USY) and (d) 550-700-850 – MSTP-10(acid treated very high silica zeolite)

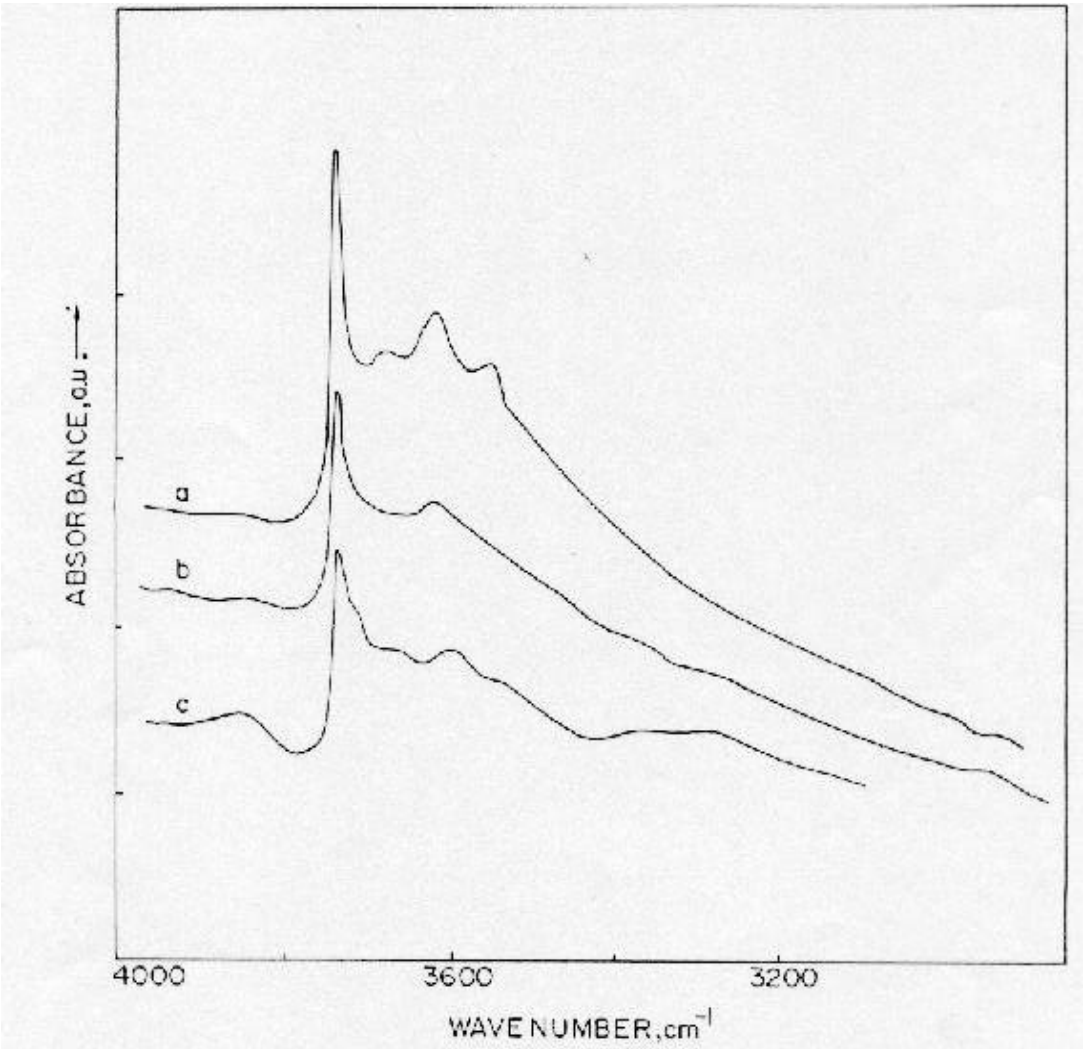

Fig.-5.2 : FTIR spectra of hydro-thermally prepared modified USY samples in the region of structural hydroxyl group vibrations

(a) Oxa-MSTP-200-0.33 (very high silica Ti-USY), (b) Oxa-Fe-Ti-USY (very high silica Fe-Ti-USY) and (c) 550-700-850 –MSTP-10 (acid treated very high silica USY)

	Frequency of -O-H stretch vibrations, cm^{-1}	**nments for –O-H stretch vibrations**	**ence**
1	3745-3740	Terminal Silanol groups (Si-O-H)	115
2& 3	3695, 3675,3700	Extra framework aluminum species, dehydroxylated sites near Na^+ cation	220
4	3640, 3550-3540	High frequency (HF) and low frequency (LF) bridging hydroxyl groups [Si- (O-H) -Al]	115
5&6	3625-3620	High frequency (HF) bridging hydroxyl groups [Si-(O-H)-Al] shifted due to dealumination	219
7	3600	High frequency bridging hydroxyl group [Si-(O-H)-Al] shifted due to perturbation by nearby penta coordinated aluminum species	219
8	3500-3200	Hydrogen bonded silanol hydroxyl groups [Si-(O-H)….(O-H)-Si]	115

Based on the previous reports and the behavior of the bands in different circumstances, we can also make similar assignments for such bands in our samples. Important features observed in the spectra are

(i) The concentration of bands at 3740, 3704 and 3675 cm^{-1} due to Si-O-H, -OH groups attached to dehydroxylated sites near Na^+ cations and extra lattice Al-O-H bands respectively on high silica USY decreases up on Ti incorporation,

(ii) HF and LF bridging hydroxyl groups [Si-OH-Al] at 3640 and 3550 cm^{-1} in H-Y shift to low frequency at 3620 and 3540 cm^{-1} respectively upon ultra-stabilization,

(iii) two new bands appears at 3704 cm^{-1} whose origin is not clearly known and at 3600 cm^{-1} assignable to HF bridging hydroxyl groups(at 3640 cm^{-1})perturbed by most probably penta coordinated extra lattice Al-O-H groups.

In the fig 5.2, FTIR spectra of Fe-Ti-USY and acid leached high silica USY are compared with that of Ti-USY in the region of structural hydroxyl group stretching. The concentration of HF and LF bridging OH groups increases in Fe-Ti-USY compared to Ti- USY and the concentration of all types of -OH groups have decreased in acid leached USY samples.

5.2.2: FTIR Spectra of adsorbed Pyridine on Very High Silica USY, Ti-USY and Fe-Ti-USY

Ever since the pioneering work of Parry (221), the ir spectroscopy of adsorbed pyridine has been used as characteristic tool to detect and measure the presence of Bronsted and Lewis acid centers on the solid surfaces. The ir bands of pyridine of interest to this study are the C-H and N-H stretching as well as the C-C and the C-N stretching in pyridine ring (222,223). In the fig-5.3-5.10, FTIR spectra of adsorbed pyridine at 100,200,300 and 400^0 C on the samples listed in the table 5.1 are depicted. The spectra were normalized with respect to 5 mg/cm^2 weight of the wafer and the relative concentration of Bronsted and Lewis acid sites are presented in the table 5.4 . Similarly, the data on the samples listed in table 5.2 and 5.3 are given in the tables 5.5 and 5.6 respectively. Inspection of the tables 5.4,5.5.and 5.6 reveals the following points

(i) acid site density decreases monotonically with the severity of hydrothermal treatment due to dehydroxylation and dealumination.

(ii) hydrothermally dealuminated H-Y(USY) samples have greater number of Bronsted acid sites than Lewis acid sites at all temperatures other than at 100^0 C, because some amount of loosely physically bound pyridine possibly has remained on the sample at 100^0 C.

(iii) USY samples acid extracted many times have very small number of both Bronsted and Lewis acid sites, but their proportion remains the same at all temperatures up to 400^0 C.

(iv) Ti incorporation in this very high silica USY (Ti-USY) increases both Bronsted and Lewis acid site density and their proportion also remains constant at all temperatures up to 400^0 C.

(v) Fe incorporation in Ti-USY increases the density of both types of acid sites, greater numbers of Lewis sites than Bronsted sites. But Lewis acid sites of Fe-Ti-USY are less thermally stable than those of Ti-USY samples.

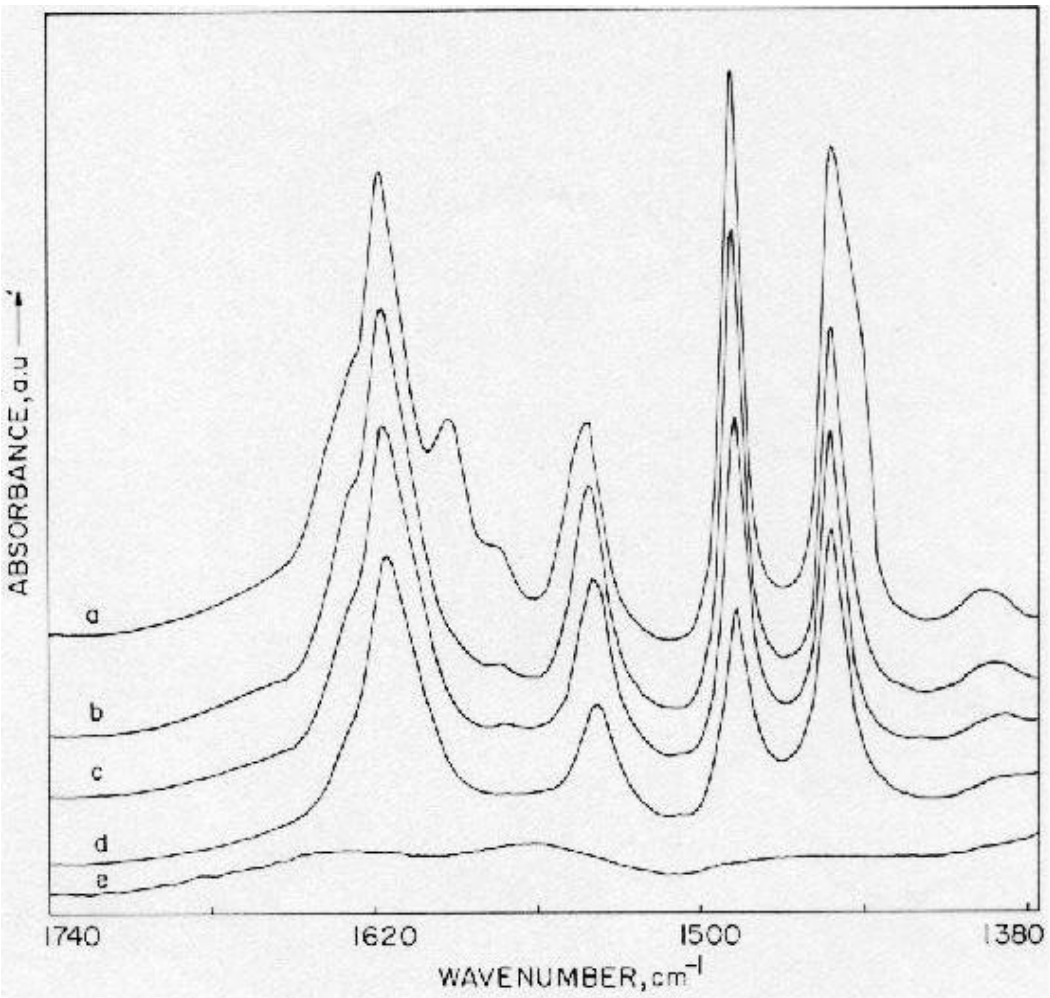

Fig.-5.3 : FTIR spectra of Adsorbed pyridine on H-Y zeolite

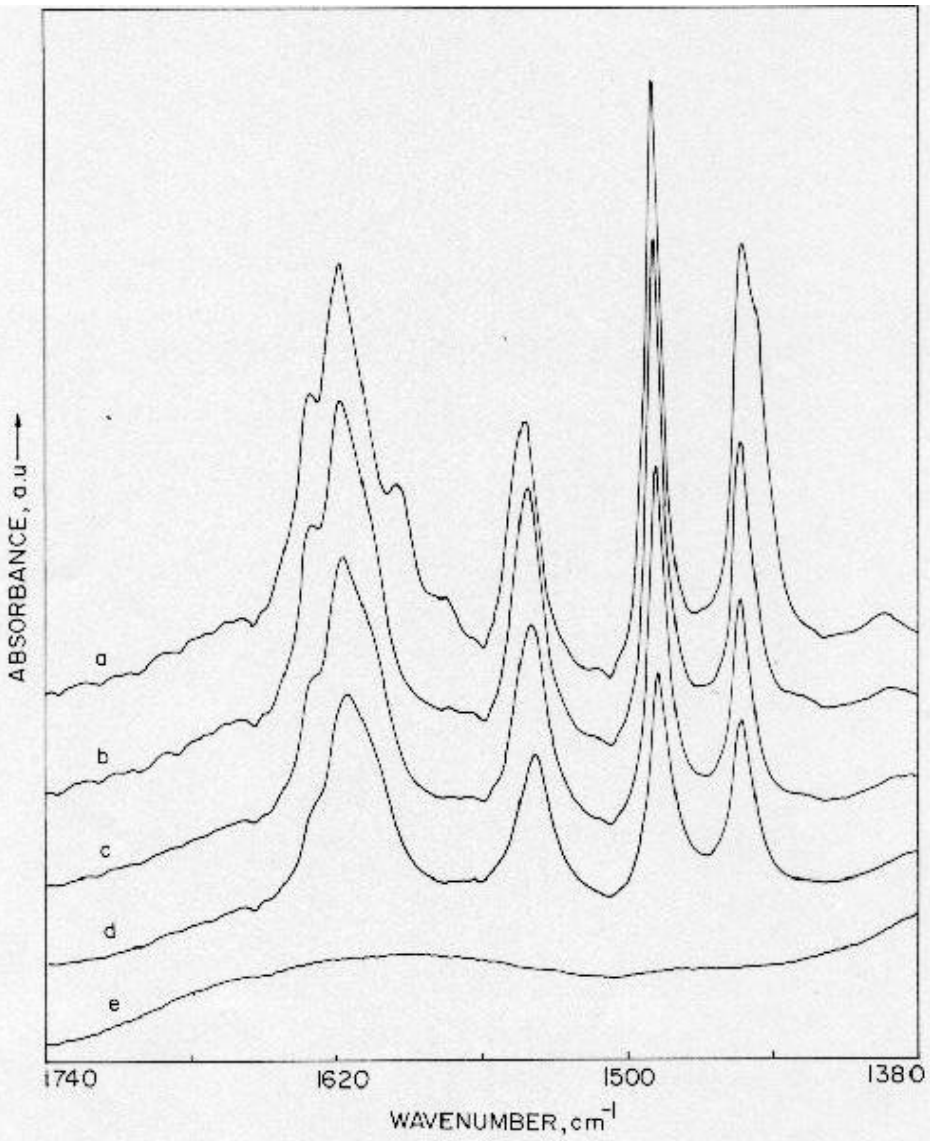

Fig.-5.4 : FTIR spectra of adsorbed pyridine on 550-MSTP sample (high silica USY)

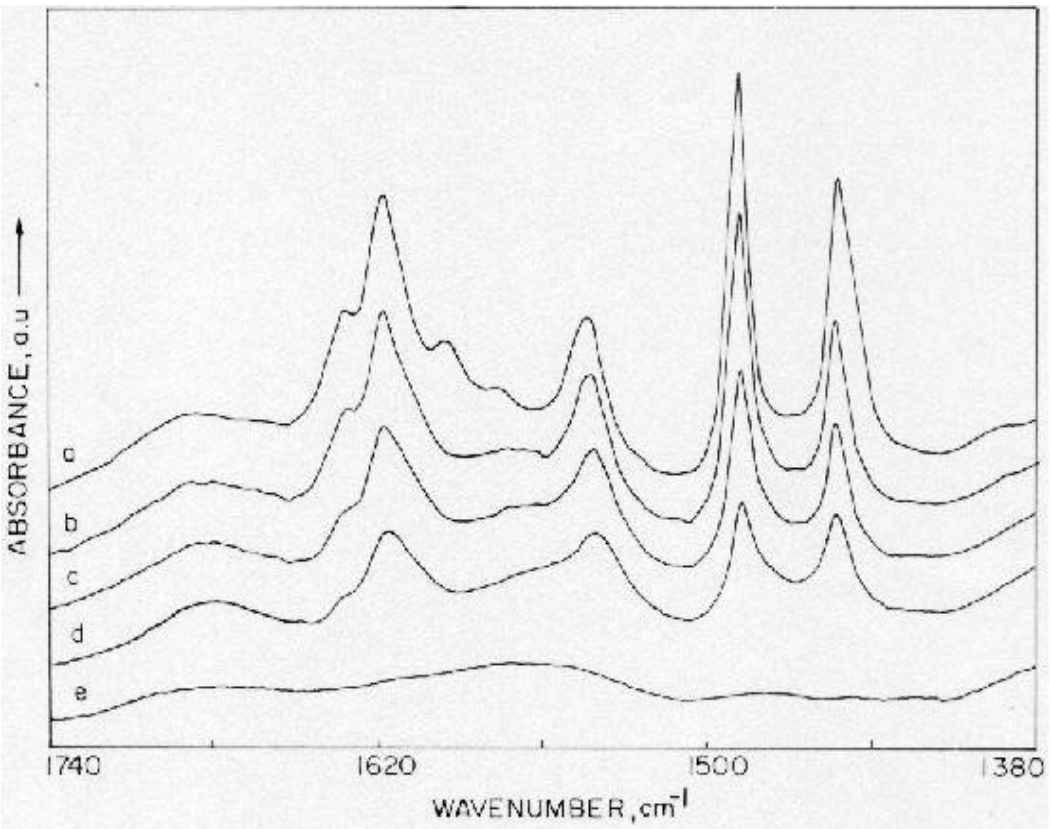

Fig.-5.5 : FTIR spectra of adsorbed pyridine on 550-700 MSTP sample (high to very high silica USY)

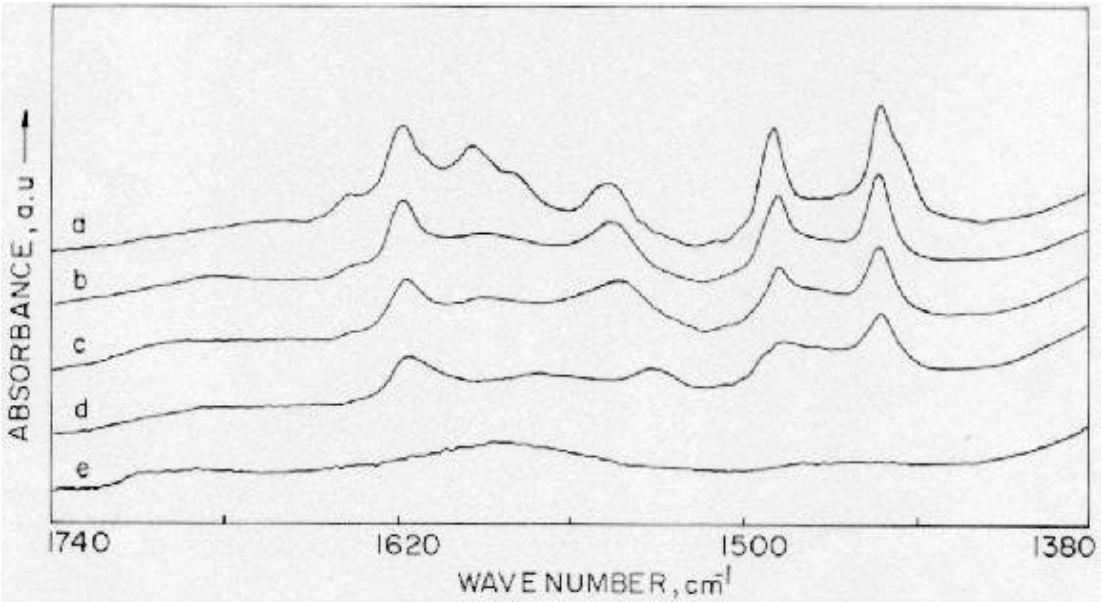

Fig.-5.6 : FTIR spectra of adsorbed pyridine on 550-700-850-MSTP-10 sample (acid treated very high silica USY)

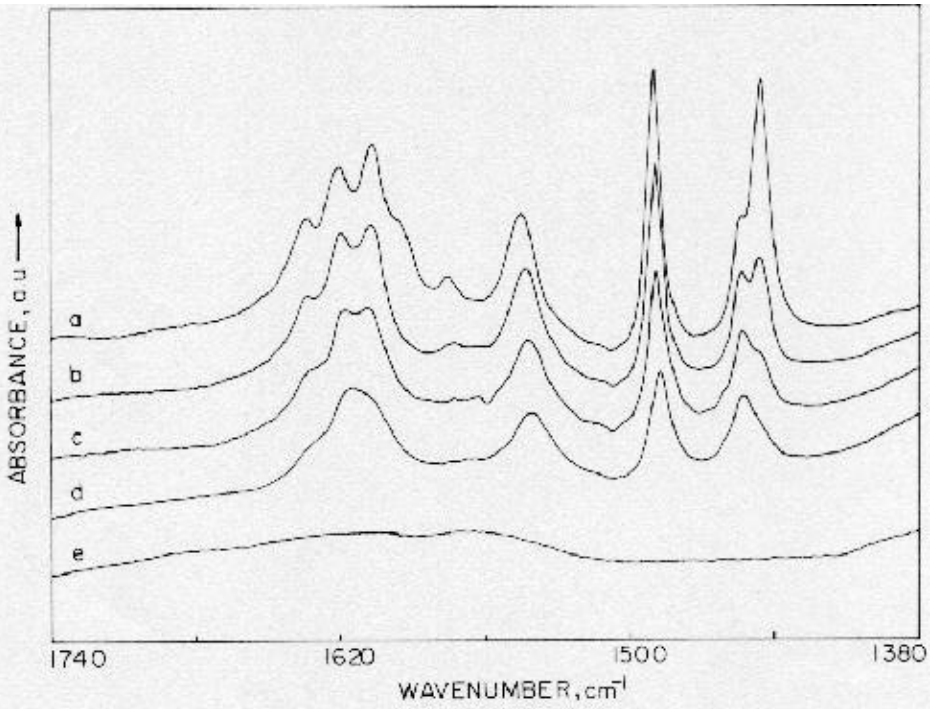

Fig.-5.7 : FTIR spectra of adsorbed pyridine on Oxa-MSTP-200-0.33 sample (very high silica Ti-USY)

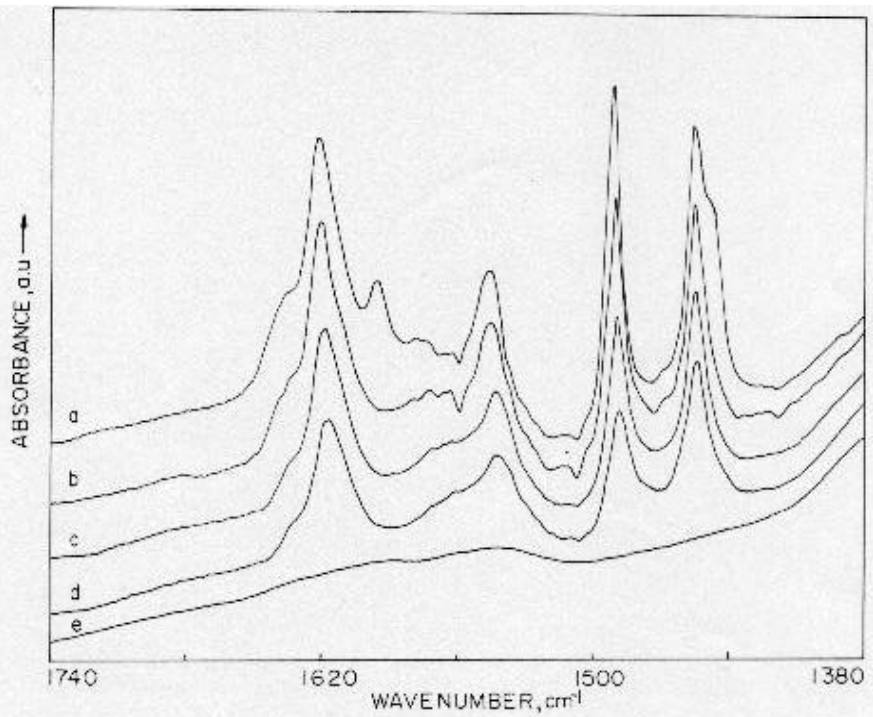

Fig.-5.8 : FTIR spectra of adsorbed pyridine on Oxa-Fe-Ti-USY sample (very high silica Fe-Ti-USY)

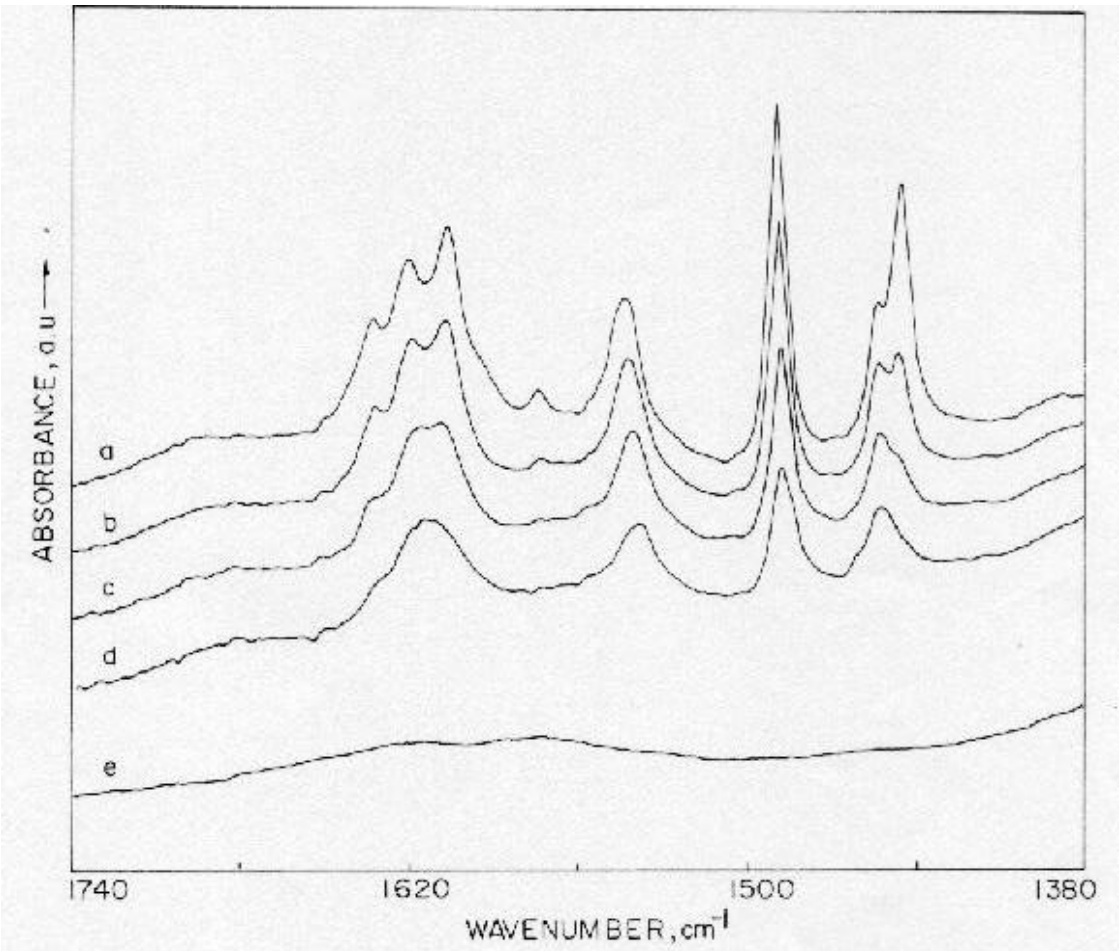

Fig.-5.9 : FTIR spectra of adsorbed pyridine on 550-MSTP -55-0.44-HNO_3 sample (acid treated high silica Ti-USY)

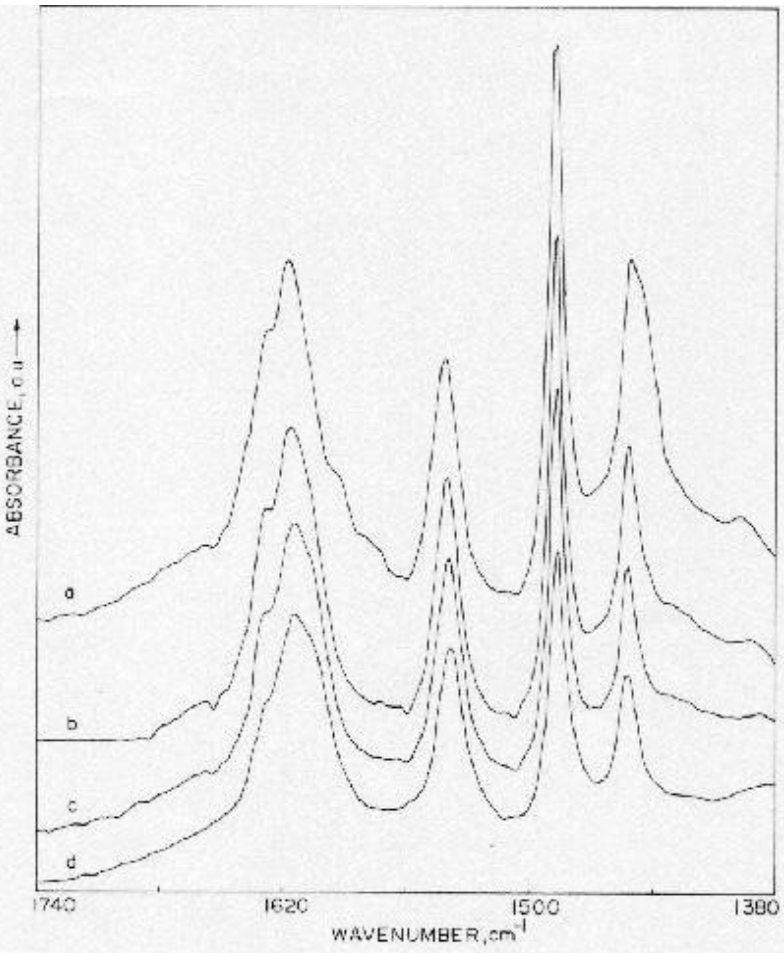

Fig.-5.10 : FTIR spectra of adsorbed pyridine on 550- MSTP-200-0.44- HNO3 (acid treated high silica Ti-USY)

Table 5.4 : Acid strength distribution over USY samples used for alkylation of O-toluidine determined by FTIR spectra of adsorbed pyridine

Name of the sample.	Relative concentration of Bronsted acid sites				Relative concentration of Lewis acid sites				Bronsted / Lewis acid sites, (B / L)			
	100	200	300	400^{0}C	100	200	300	400^{0}C	100	200	300	400^{0}C
H-Y	45	44	39	33	46	28	21	21	0.98	1.56	1.85	1.56
550-MSTP	36	40.6	36	27	42	22	16	15	0.85	1.8	2.2	1.76
550-700-850-MSTP	17	17	17	11	21	9	7	5	0.81	1.87	2.4	2.2
550-700-850-MSTP-10	4	3	3	2	9	6	6	4	0.44	0.5	0.5	0.5
Oxo-MSTP-200-0.44 (Ti-USY)	12	9	5	5	15	10	8	6	0.8	0.9	0.6	0.8

Table 5.5: Acid strength distribution over USY samples for Cyclohexanol Dehydration And Benzoylation of Toluene determined by FTIR Spectra of adsorbed Pyridine

Name of the sample	Relative concentration of Bronsted acid sites				Relative concentration of Lewis acid sites				Bronsted / Lewis acid sites (B / L)			
	100	200	300	400^{0}C	100	200	300	400^{0}C	100	200	300	400^{0}C
Oxo-MSTP-200-0.44 (Ti-USY)	12	9	5	5	15	10	8	6	0.8	0.9	0.6	0.8
Oxo-Fe-Ti-USY (Fe-Ti-USY)	17	17	17	12	29	16	12	10	0..6	1.1	1.4	1.2
MSTP-10 (acid leached USY)	4	3	3	2	9	6	6	4	0.44	0.5	0.5	0.5

Table5.6: Acid Strength distribution over USY Samples for hydroxylation of Phenol determined by FTIR spectra of adsorbed Pyridine

Name of the sample	Relative concentration of Bronsted acid sites				Relative concentration of Lewis acid sites				Bronsted / Lewis acid sites (B / L)			
	100	200	300	400^{0}C	100	200	300	400^{0}C	100	200	300	400^{0}C
H-Y(dry calcined NH_4-Y)	45	44	39	33	46	28	21	21	0.98	1.56	1.85	1.56
550-MSTP-55-0.44-HNO_3	5	4.5	4.0	3. 2	6	3	2	1.7	0.83	1.5	2	1.88
550-MSTP-200-0.44-HNO_3	4.3	4.4	3.9	3	4.7	2.5	1.8	1.5	0.91	1.76	2.2	2

5.3 : Alkylation of O-toluidine over USY, Ti-USY and Fe-Ti-USY zeolites

Alkylated aromatic amines are industrially very important. Ortho-alkylated aromatic amines are used as intermediates for producing dyes, insecticides, resins, stabilizers, rubber processing chemicals and as liquid fuel in missiles. Many solid catalysts have been reported, particularly, clays, bauxite and alumina modified with many metal oxides have been widely used.(224).Microporous materials like zeolites and ALPO-s are also used (225-229). In the alkylation of aromatic amines, the product distribution solely depends up on the preponderance of the interaction of zeolite with the lone pair of đectrons on N in amine group or with the ð electrons of aromatic ring. So, on a series of modified USY zeolites, where in, variety of active sites like Bronsted and Lewis acid sites, defect sites and extra framework Al species are present, the interaction is a very complex process.

5.3.1 : Influence of reaction Temperature

In the table 5.7,the product distributions in methylation of O-toluidine at different temperatures over high silica USY (550-700-850-MSTP) zeolites are presented. Methylation of O-toluidine by methanol gives mainly, N-methyl O-toluidine, N,N-dimethyl O-toluidine, 2,4-xylidine, 2,6-xylidine,N-methyl xylidine, N,N-dimethyl

xylidine and 2,4,6-trimethyl aniline. Among them, the major products are N-methyl-O-toluidine, 2,4-xylidine, N-methyl xylidine and 2,4,6-trimethyl aniline.

Table 5.7 : Effect of temperature on O-toluidine conversion and product selectivity on high silica USY(550-750-850-MSTP) catalyst

Temperature	250	300	350	400	450
O-toluidine Conversion (Wt%)	83.1	92.4	99.9	90.1	82
Selectivity (%)					
Lower Boilers	0.2	0.2	1.6	1.5	1.8
N,N-dimethyl-O-toluidine	6.3	3.1	1.1	0.07	0.01
N,N-dimethyl Xylidine	0	0.01	0.1	0.15	0.4
N-methyl-O-toluidine	37.5	26.5	13.4	0	0
2,4 -Xylidine	31.1	35.6	37.4	43	45.6
N,N-dimethyl-2,4,6-trimethylaniline	0	0	0.07	1	1.2
N-methyl-Xylidine	21.3	12.2	10.5	3.3	5.6
2,4,6-trimethylaniline	2.9	20.4	32.3	37.2	24.2
Others	0.6	1.9	3.4	13.6	21.1
	at 100^0	at 200^0	at 300^0	at 400^0	
Bronsted : Lewis acid site ratio (B/L)	0.81	1.87	2.4	2.2	

Reaction Conditions: Feed : O-toluidine: MeOH = 1:2; catalyst : 550-700-MSTP; TOS = 2h. WHSV = $1h^{-1}$

The complete conversion of O-toluidine was obtained at 350^0 C. The concentration of C-di and trialkylated products (2,4 and 2,4,6-trimethyl aniline) increases and N- alkylated products (N-methyl O-toluidine and N-methyl xylidine) decreases with temperature. The N C conversion increases with temperature. The lower conversion at higher temperature is attributed to the loss of methanol due to the decomposition. In comparison with Bronsted /Lewis acidity ratio in the similar temperature range, which also increase with temperature (table-5.4), we can notice the following significant points: As the B/L ratio increases, N-methyl toluidine decreases,

N-N-dimethyl toluidine decreases,

2,4- xylidine increases,

N-methyl xylidine decreases,

N-N-dimethyl xylidine is not formed at all and

2,4,6-trimethyl aniline increases in the product.

Hence, the role of acid aites is very clear, Bronsted sites favor Galkylation and Lewis acid sites favor N-alkylation. Toluidines can interact with very strong acidic sites on

zeolites through ð electrons of aromatic ring as well as through lone pair of electrons of amine group similar to anilines as described by Singh(230).

5.3.2 : Influence of the type of the catalyst

Considering that both aromatic ring and side chain amine groups interact with zeolite and influence the reaction, we have carried out the reactions on USY and Ti-USY zeolites of which the acid strength distribution varied widely. In the table 5.8, a comparison of the activity over these catalysts is presented and compared with that of ã-Al_2O_3 catalyst.

Table 5.8 : O-toluidine conversion and product selectivity over USY zeolite

Name of the catalyst	ã -Al_2O_3	H-Y	High silica USY	Very high silica USY	Acid treated Very high silica USY	Very high silica Ti-USY
O-toluidine conversion wt%	60.9	36.7	79.6	99.9	85.5	90.9
Selectivity (%)						
Lower Boilers	0.9	3.6	0.1	1.6	0.2	0.4
N,N-dimethyl-O-toluidine	0	0	0.2	1.1	1.8	9.7
N,N-dimethyl Xylidine	1.9	0	0	0.1	0.08	3.5
N-methyl-O-toluidine	71.8	71.6	46.1	6.4	25.4	34.3
2,4 -Xylidine	12.6	14.2	22.7	44.5	21	27.4
N,N-dimethyl-2,4,6-trimethylaniline	1.1	4.6	0	0.07	1.9	1.4
N-methyl-Xylidine	7.8	5.1	7.6	10.5	16.9	11.5
2,4,6-trimethylaniline	0.6	0.5	22.5	32.3	25.4	8.7
Others	3.2	0.5	0.7	3.4	7.3	2.9
Bronsted : Lewis acid ratio (B/L) at 300^0 C	0.2	1.85	2.2	2.4	0.5	0.6

Reaction Conditions: Feed ratio = O-toluidine : MeOH = 1:2; Temp = 350°C; TOS = 2h, WHSV = 1 h^{-1}

The role of Bronsted and Lewis acid sites is further manifested in the product distribution presented in this table.

As B/L ratio increases, N-methyl toluidine decreases

2,4- xylidine increases,

N-methyl xylidine increases,

N-N-dimethyl xylidine is formed in traces and

2,4,6-trimethyl aniline increases in the product.

These observations bring out two important points

N-alkylation increases for the samples which have more of extra lattice Al species and

N-methylation of O-toluidine and xylidines increases inspite of lower B/L acid ratio in acid extracted USY and Ti-USY samples

Only 2,4 xylidine is produced in the reaction, other isomers 2,6 and 2,3 –xylidine were not obtained in detectable quantities.

Inspection of the nature of hydroxyl groups shows a different kind of acidic -OH groups on the samples having excessive extra lattice Al species as discussed previously. The frequency of the "H.F" acidic -OH groups is shifted to lower side which comes back to the original value after removal of extra framework Al species. They are thought to have to have "super acid" nature (219).

5.3.3 : Influence of reactant mol ratio

In the table 5.9, the influence of reactant mole ratio, Methanol : O-toluidine , on the product distribution over USY is presented.

Table 5.9 : Influence of reactant mol ratio (methanol : O-toluidine) on O-toluidine conversion and product yields over USY, (550-700-MSTP)

Mole Ratio (O-toluidine : MeOH)	10	7	5	2	1	0.5	0.2
O-toluidine Conversion (Wt%)	100	100	100	99.9	99.9	46.2	24.8
Selectivity (%)							
Lower Boilers	1.1	0.5	1.3	1.6	0.8	1.9	1.6
Aniline	0	0	0	0	0	4.8	10.1
N,N-dimethyl-O-toluidine	7.7	6.1	9.8	8.1	37.7	0	0
N,N-dimethyl Xylidine	58.8	55.9	0.2	0.1	0.2	0	0.1
N-methyl-O-toluidine	0.7	0.5	0.2	6.4	0.1	0.02	0
2,4 -Xylidine	0.8	1.1	39.6	37.4	42.3	83.9	83.3
N,N-dimethyl-2,4,6-trimethylaniline	8.8	8.6	0.2	0.07	0.09	0.01	0.02
N-methyl-Xylidine	14.9	17.5	2.5	10.5	0.1	0.03	0
2,4,6-trimethylaniline	1.3	2.4	39.3	32.3	6.3	7.2	2
Others	5.6	7.2	6.8	3.4	12	1.9	2.8

Reaction Conditions: Temp: 350°C; catalyst: USY, (550-700-MSTP) ; TOS = 2h. WHSV = 1 h^{-1}

As the concentration of methanol in the feed decreases,

The conversion of O-toluidine is almost 100% except in very low

level of methanol, wherein the quantity of required methanol itself is deficient, N-methyl toluidine is formed in small quantity,

N-N-dimethyl toluidine increases except in very low level of methanol where in

the quantity of required methanol itself is deficient

N-N- dimethyl xylidine is formed in negligible quantity except in very high concentration of methanol,

xylidine increases continuosly,

N-methyl xylidine decreases,

2,4,6 trimethyl aniline decreases continuosly ,

N-N-dimethyl -2,4,6-trimethyl aniline decreases and

Aniline is formed in small amount only at very low concentration of methanol.

5.3.4 : Influence of WHSV

In the table 5.10, the influence of WHSV on the reaction product distribution is depicted.

Table 5.10 : Influence of WHSV on O-toluidine conversion and product selectivity over USY, (550-700-MSTP)

WHSV (h^{-1})	5	3.3	2	1	0.2
O-toluidine Conversion (Wt%)	83.3	92.1	95.1	99.9	83.3
Selectivity (%)					
Lower Boilers	0.4	1.3	0.9	1.6	3.9
N,N-dimethyl-O-toluidine	3	2.1	2.1	1.1	0.2
N,N-dimethyl Xylidine	0.02	0.2	0.04	0.1	0.4
N-methyl-O-toluidine	25	12.9	7.8	6.4	1.2
2,4 -Xylidine	35.5	37.7	38.8	44.4	52.6
N,N-dimethyl-2,4,6-trimethylaniline	0.1	1.2	0.6	0.07	0.2
N-methyl-Xylidine	20.2	25.6	23.9	10.5	0.3
2,4,6-trimethylaniline	13.9	16.9	22.8	32.3	33.5
Others	1.8	2.1	3	3.4	7.7

Reaction Conditions: Feed O-toluidine : MeOH = 1:2; catalyst: USY, (550-700-MSTP) TOS = 2h;Temp: 350°C

The conversion of O-toluidine passes through a maximum of 100% at WHSV of one. As the WHSV decreases, the concentration of N methyl toluidine in the product decreases and that of 2,4-xylidine increases indicating that N C conversion is favored at

low WHSV (at high contact time). Similarly, the selectivity to N-methyl xylidine decreases and 2,4,6-trimethyl aniline increases with the decrease in WHSV, further indicating that N C transformation increases at low WHSV(high contact time).

5.3.5 : Influence of time on stream

In the table 5.11, the effect of time on stream on the product distribution is presented.

As the time on stream increases, the conversion slowly decreases, N-methyl toluidine ,toluidine and N-methyl xylidines slowly increase, where as trimethyl aniline passes

Table 5.11 : Influence of Time on stream on O-toluidine conversion and product yields over USY (550-700-MSTP)

Time on Stream	1h	2h	3h	4h	5h	6h	7h	8h	14h
O-toluidine conversion (Wt%)	99.9	99.9	99.9	92.2	92.5	91.1	90.4	90.4	79.4
Selectivity (%)									
Lower Boilers	3.1	1.6	2.9	1.7	1.3	1.3	1.2	1.1	0.7
N,N-dimethyl-O-toluidine	28.3	8.1	6.1	0.4	0.5	0.7	0.7	0.7	0
N,N-dimethyl Xylidine	0.1	0.1	0.09	0.07	0.05	0.04	0.03	0.02	0.01
N-methyl-O-toluidine	6.3	6.4	6.5	7.3	7.5	8	11.6	13	17.7
2,4 -Xylidine	35.5	37.4	37.3	42.2	42.8	45.7	44.9	45.5	48.4
N,N-dimethyl-2,4,6-trimethylaniline	0.7	0.07	0.25	0.4	0.5	0.6	0.4	0.2	0.01
N-methyl-Xylidine	1.4	10.5	12.9	13.2	12.6	11.9	12.2	12.1	9.2
2,4,6-trimethylaniline	19.4	32.3	30.4	31.2	30.8	28.1	25.7	24.7	21.8
Others	5.2	3.4	3.5	3.4	3.8	3.6	3.2	2.4	1.4

through a maximum. N-N methylated products are formed in very small amount. The trend in product distribution seems to be in line with the demands of acidity levels essential for various transformations.

5.3.6 : Mechanism of methylation of O-toluidine

From the above described analysis of methylation of O-toluidine on USY zeolites, it is clear that the reaction is very complex, consisting of parallel reaction of C-alkylation and N-alkylation and net work of consecutive reactions involving both C- and N- di-alkylation, disproportionation, and N C transformations. The mechanism of methylation of O-toluidine over Bronsted and Lewis acid sites over USY can be represented as follows.

1) C-alkylation over Bronsted acid sites: The activation of methanol is initiated by hydrogen bonding of Bronsted acid sites with oxygen of methanol, leading to the protonation of alcohol, dehydration and the formation of carbocation . The

carbocation then reacts with the aromatic ring of O-toluidine forming xylidine. Due to the delocalization of unshared pair of electrons over the amine group into the aromatic ring, the ortho and para positions of the ring becomes susceptible to the electrophile attack and the product is directed to ortho/para position only. The mechanism can be shown as below.

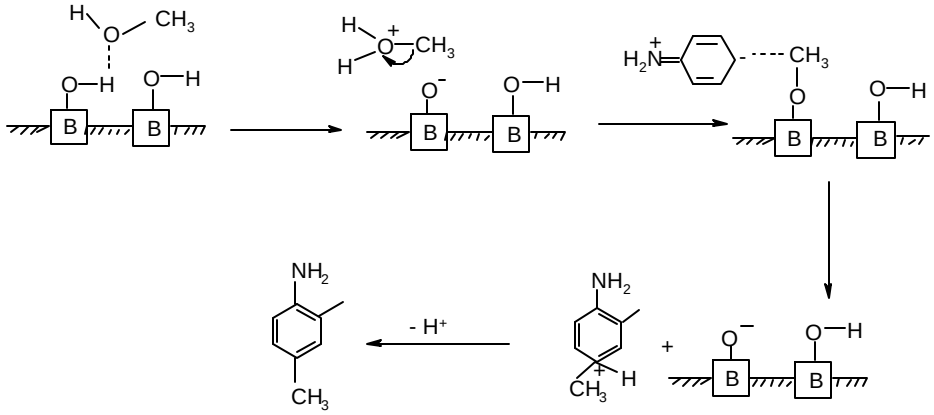

2) N-alkylation over Bronsted acid sites : the carbocation formed over relatively weak Bronsted acid sites will attack electronically rich amine group to form N-alkylated product as can be depicted below.

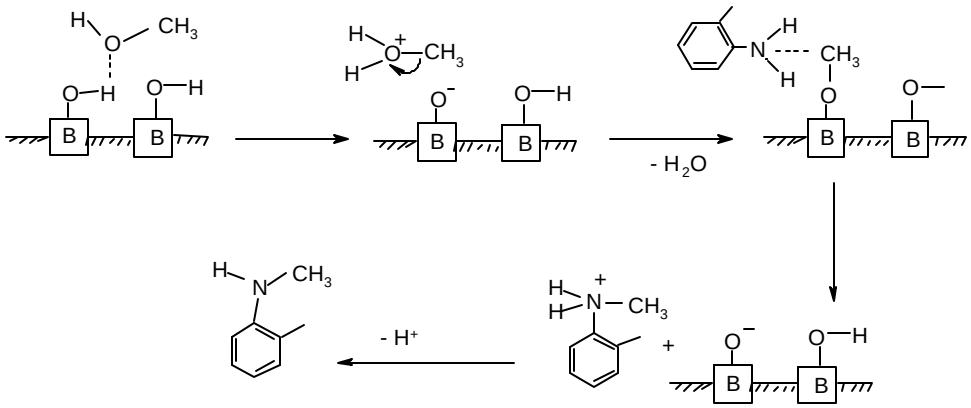

3) N-alkylation over Lewis acid sites : The presence of only Lewis acid sites is very rare, though we may find surfaces very rich in Lewis acid sites. A mechanism of formation of N-methylated toluidine on Lewis acid can be depicted as follows.

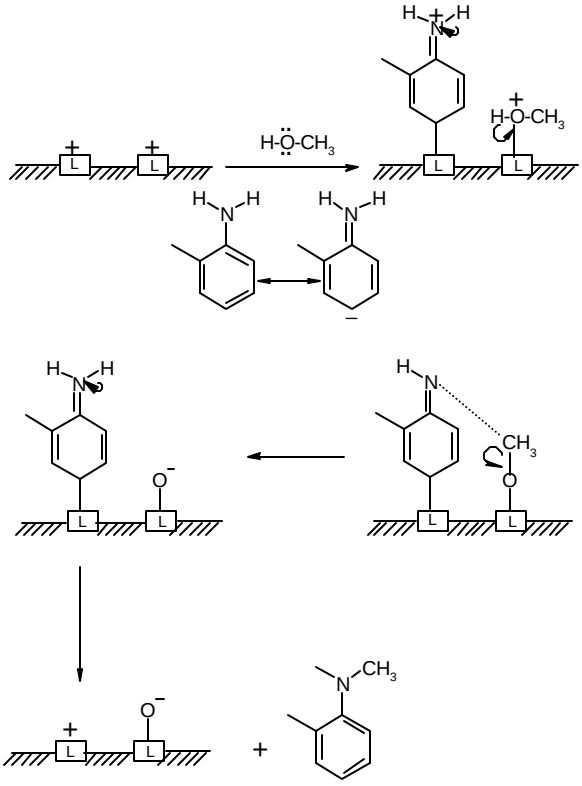

4) O-toluidine methylation over Bronsted and Lewis acid sites: Such examples are most common in zeolite catalysts. Toluidine, being a stronger base than methanol, is preferentially adsorbed on Lewis acid sites, while oxygen of methanol forms strong hydrogen bonds with Bronsted acid protons. The methyl carbocation formed by protonation of methanol on Bronsted acid sites reacts with the conjugate base of Bronsted acid site giving ether of carbocation on the surface. Aniline preferentially gets adsorbed on Lewis sites through lone pair of electrons on amine group, then looses a proton to balance the positive charge developed on Nitrogen. The high electro-negativity of oxygen in ether linkage develops a partial positive charge on the alkyl side chain. This initiates the heterolitic cleavage of polar O-C bond and the shift of alkyl carbocation to nitrogen. It is schematically shown below.

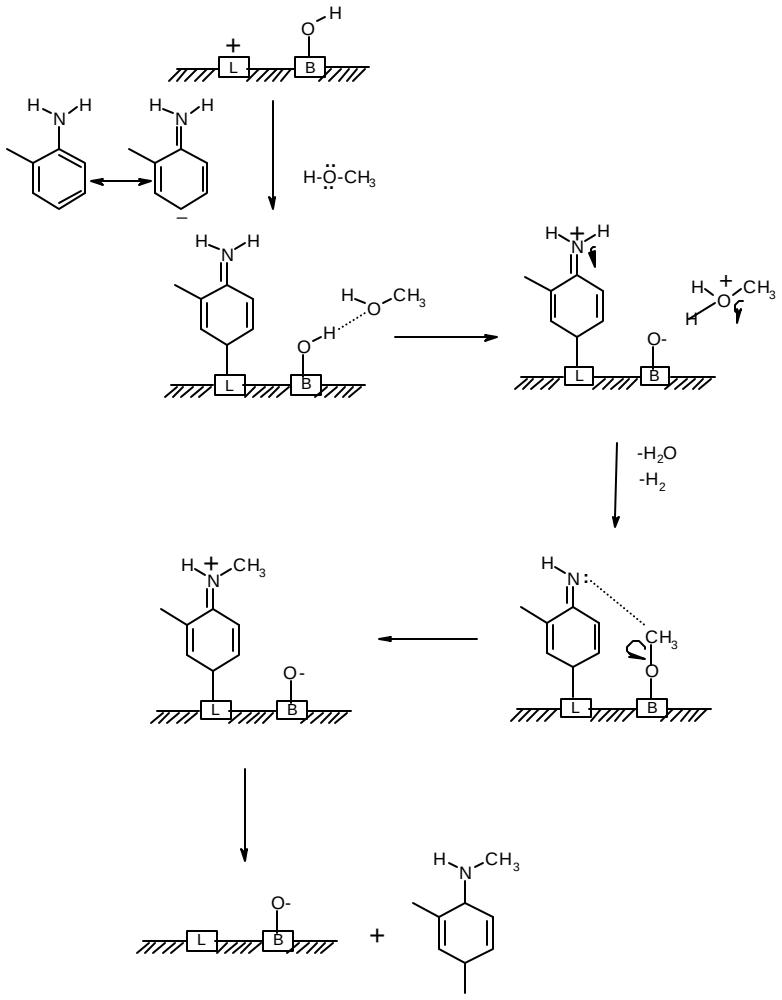

The primarily formed xylidine and N-methyl toluidine further undergo consecutive reaction to form all other products as follows.

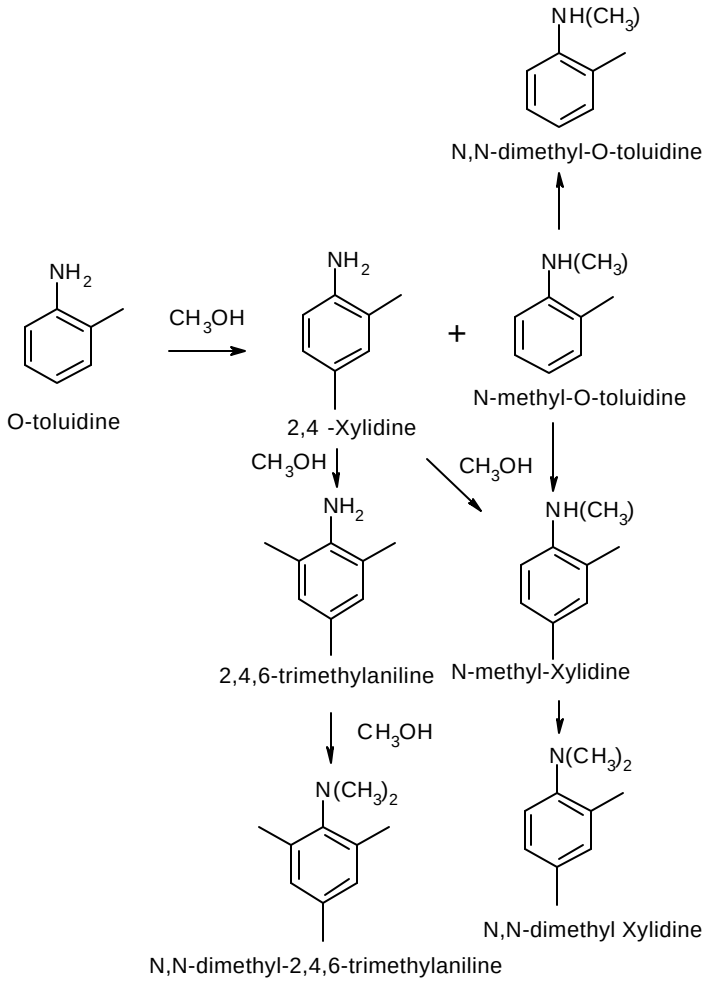

Despite the adsorption of toluidine is electronically most favored through strongly basic amine groups via unshared electrons of N atom, adsorption of methanol over very strong Bronsted acid sites via basic oxygen can also take simultaneously. So C- and N-methylation primarily occur simultaneously, which through further parallel and consecutive reactions leads to other C- and N,N-alkylation products. From these studies, it is demonstrated that USY and Ti-USY are very good catalysts for the selective alkylation of O-toluidine to 2,4-xylidine.

5.4 : Benzoylation of Toluene over modified USY zeolites

USY is reportedly active catalyst for benzoylation of xylene (231).The activity dependeds on the stabilization condition, solvents and acylating agents. Other zeolites like H-Y, Beta, La-Y and Ce-Y are also reported to be useful for reactions like phenyl acetylation of anisole,(232,233) and carboxylation of toluene(234). Singh et al(235) have reported toluene benzoylation by many types of zeolites like Re-Y, H-ZSM-5 and H-Beta and reported the leaching of Al by HCl produced in the reaction and deactivation of the zeolite. Fang et al (231) used mildly dealuminated USY to overcome the leaching of Al and to improve the stability, but found that leached Al species itself acts as the homogeneous catalyst for this reaction. Therefore if we have to use activity and shape selectivity of USY zeolite for acylation reactions, we must obtain very high silica USY and modify that further to increase the acidity and stability. We have tested the activity of such zeolites prepared in this study for benzoylation of toluene to obtain 4-methyl benzophenone in liquid phase. It is industrially very important as perfumary chemical. The activity is compared with the nature of surface acidity. In the table 5.12, and 5.13 respectively, activity of benzoylation of toluene over very high silica USY, Ti-USY and FE-Ti-USY catalysts are presented. The result of a reaction carried out with out any catalyst in the reactor is also presented for comparison.

Studies on benzoylation of toluene by super acids like heteropoly acids, metal sulphated oxides like Al_2O_3, ZrO_2, TiO_2,Fe_2O_3 have been reported(236-238), but they are not shape selective catalysts. USY zeolites show nature of super acidity as demonstrated by FTIR results as well as shape selectivity because of their micropore structure. USY, Ti-USY and Fe-Ti-USY have relative total acidity of 13, 27 and 46 and Bronsted : Lewis acidity ratio of 0.44,0.8 and 0.6 respectively at 100^0C. The Benzoyl chloride conversion of 7, 14 and 15% respectively are obtained over these catalysts. For USY, the selectivity to 4-Methyl Benzophenone (4-MBP) decreases, and for 3- and 4-MBP, it increases with time on stream; for Ti- and Fe-Ti-USY, selectivity for 4-MBP increases with decreasing selectivity to 3- and 2- MBP with time on stream. The Maximum selectivity of 84% for 4-MBP is obtained for Ti- and FE-Ti-USY samples where as it is only 66% for USY. However, it is considerably more than other catalysts reported in the literature. In this reaction, benzoyl chloride is forming acid salt on the surface of acidic zeolite forming

electrophile ($C_6H_5CO^+$) which attacks on the aromatic ring and condenses with toluene liberating HCl as follows. The presence of extra lattice Al, Ti and Fe species in the micropores are responsible for the high activity and selectivity of USY catalysts for the reaction.

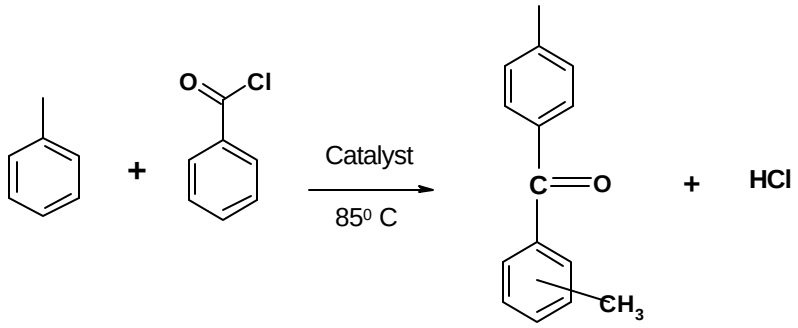

2- (or 3- or 4-)MBP

Schematic presentation of Benzoylation of Toluene over Ti-USY zeolites

Table 5.12 : Benzoylation of Toluene with Benzoyl Chloride over Ti-USY Zeolite

	Ti-USY (Oxo-MSTP-200-0.33)							**eaction**			
TOS	1h	3h	18h	19h	23h	24h	41h	1h	3h	18h	19h
% conv. of BC	4.27	5.99	9.36	9.87	14	15.2	21.3	0.6	1.13	1.9	2.1
% selectivity								As conversion is very less, product distribution could not be estimated .			
2-MBP	13.0	13.6	13.9	14.0	9.7	9.5	9.0				
3-MPB	20.7	19.2	9.1	8.3	5.0	4.9	6.0				
4-MBP	58.2	60.8	76.6	76.7	79.3	84.4	79				
Others	8.15	6.4	1.0	1.0	2.5	1.7	6.1				

Toluene : Benzoyl chloride = 5:1, Reaction temperature = 85^0 C, catalyst= 0.300 mg, Total feed= 10.0 ml

MBP = Methyl Benzophenone

Table 5.13 : Benzoylation of Toluene with Benzoyl chloride over USY and Fe-Ti-USY Zeolites

	Acid treated very high silica USY (MSTP-10)						Fe-Ti-USY (Oxo-Fe-Ti-USY)					
TOS	1h	3h	18h	19h	24h	25h	1h	3h	18h	19h	24h	41h
% conv. of BC	2.5	3	3.2	4.1	7.3	7.6	3.9	5	8.4	9.9	14.7	21.3
Selectivity, %												
2-MBP	8.7	11.0	9.6	9.5	9.6	9.3	4.27	5.04	7.7	7.8	7.9	8.5
3-MBP	14.3	17.6	16.5	17.2	20.2	17.9	6.8	5.6	4.6	4.2	3.8	4.1
4-MBP	83.8	68.4	69.9	69.2	64.2	65.7	81.7	82.8	82.9	84.3	85.6	83.3
Others	10.5	7.5	4.0	4.35	6.1	6.8	7.1	6.8	4.7	3.8	2.7	4.0

Toluene : Benzoyl chloride = 5:1, Reaction temperature = 85^0 C, catalyst= 0.300 mg, Total feed= 10.0 ml

5 . 5 : Hydroxylation of Phenol by H_2O_2

Hydroxylation of phenol by H_2O_2 was chosen as a test reaction for evaluation of Ti- incorporation in USY zeolite. In the table 5.14, the results of the reaction over modified USY samples are presented. The product distribution in the reaction over acid leached very high silica Ti-USY samples of two compositions is compared with that over H-Y zeolite. Ti-USY samples give more than 50 % conversion compared to only 2% over H-Y sample The feasibility of oxidation by H_2O_2 itself suggests that Ti is incorporated in the framework of USY. It is now commonly accepted that the active sites in such reactions are Ti which has to be 4-coordinated (239-241) and in case of surface grafted Ti species, it should be attached to 3 silanol groups and has one -OH group as the 4^{th} ligand.(242). Due to larger three-dimensional pores of USY with secondary pores, that allow bulky transitional state species, the selectivity in the reaction is not observed. The mechanism and scheme of the reaction may be represented as follows.

Mechanism

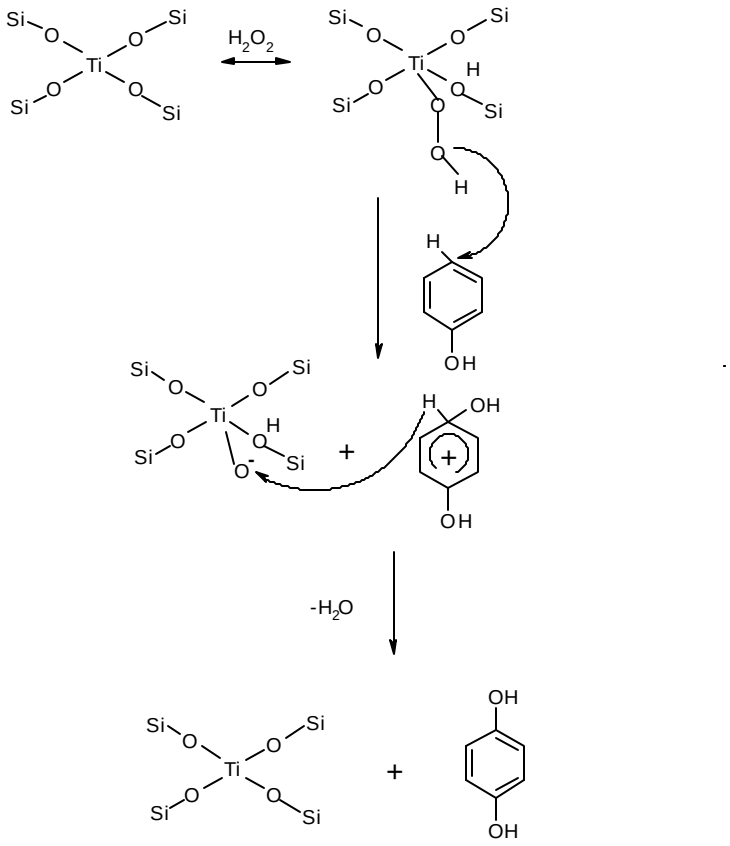

Scheme

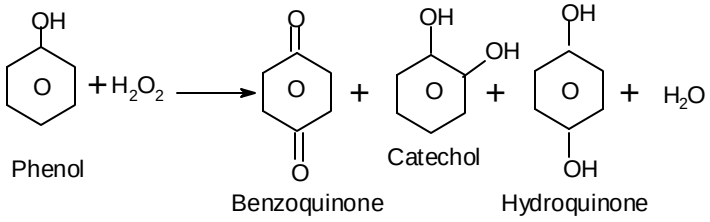

Table 5.14 : Phenol hydroxylation by H_2O_2 over Ti-USY zeolites

Sample used	Conversion, %	Benzoquinone	Hydroquinone	Catechol	Others (tar)	Time (h)
very high silica Ti-USY	43.6	1.64	52.34	45.1	2.56	0.5 h
do	47.9	0.41	43.38	54.773	1.44	1.0 h
do	58.6	0.21	40.4	57.19	2.2	1.5 h
Acid treated very high silica Ti-USY	51.33	1.3	38.44	56.34	3.92	1.5 h
H-Y	2.2	23.18	2.6	5.27	9.92	1.5 h
do	3.467	14.6	57	16.8	11.6	24h

Temperature : 80^0C, phenol/H_2O_2 = 5, Catalyst / Phenol = 0.2, water as solvent

5.6 : Dehydration of Cyclohexanol on acid extracted USY, Ti-USY and Fe-Ti-USY

The catalytic test reactions are one of the methods of determining the strength of acid sites as described by Karge et al (243).This test is the most realistic because, it is carried out under real catalytic reaction conditions. Some of the commonly used test reactions for acidity are alcohol dehydration for weakly acidic sites, n-hexane cracking for strong acidic sites and cyclohexane reaction for determining type of acid sites, whether it is Bronsted or Lewis type(244,245). Cyclohexanol dehydrates to cyclohexene and water on weak acid sites, and cyclohexene undergoes consecutive reaction on stronger acid sites to methyl cyclopentene, cyclohexane, methyl cyclopentane, and benzene. The reaction of cyclohexane will proceed on acid sites as shown in the following scheme

Scheme

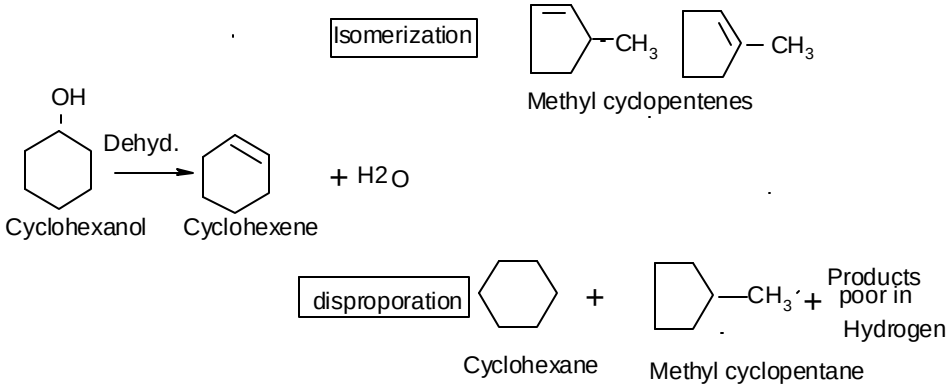

In the table 5.15, results of cyclohexanol dehydration at different temperatures on Ti-USY samples are presented. The data in the table indicate a striking difference in the product distribution at low, medium and high temperature regions of the reaction.

Table 5.15 : Dehydration of Cyclohexanol over Ti-USY Zeolite

Reaction Temp.	Time on stream.	conversion (%)	% Selectivity		
			Cyclohexene	Cyclohexanone	Others
150^0C	2h	20.8	76.41	8.18	15.4
	3h	21.65	78.25	8.70	13.0
	4h	24.9	79.92	7.73	12.4
	6h	26.2	80.86	7.70	11.4
200^0C	2h	99.93	98.52	0.42	1.1
	3h	99.97	99.72	0.38	-
	5h	99.96	99.69	0.31	-
	6h	99.92	99.66	0.34	-
	8h	99.96	99.71	0.30	-
	22h	98.62	98.7	0.47	0.8
	24h	98.54	98.34	0.58	1.1
250^0C	2h	99.9	85.2	-	14.8
	4h	99.8	89.62	-	10.4
	6h	99.79	96.81	-	3.2
300^0C	2h	99.53	53.36	0.42	46.3
	4h	99.87	65.5	0.40	34.2
	6h	99.88	72.94	0.26	26.8
	8h	99.92	83.63	0.12	16.3

Feed rate : 2 ml / h, amount of catalyst =1.5 g , N_2 as carrier gas = 20 ml / min

(i) In the low temperature region of 150^0C, the conversion is very low (~ 25%), selectivity for dehydration is moderate (~80%), dehydrogenation to cyclohexanone (~8%) and consecutive reactions to other products also occur(~12%).

(ii) In the medium temperature region of 200^0 C, selectivity for dehydration to cyclohexene is dominant (~99%) and dehydrogenation and other consecutive reactions are negligible.

(iii) In the high temperature region of 250-300^{0}C, selectivity for dehydration to cyclohexene decreases (~84%), dehydrogenation activity becomes negligible and other consecutive reactions significantly occur which comes down rapidly with the time on stream.

It is reported that Al_2O_3 that has only Lewis acid sites does only dehydration and amorphous aluminosilicate that has both Bronsted and Lewis acid sites does both dehydration, consecutive isomerization and disproportionation reactions of cyclohexanol (245). So, Lewis acid sites are needed for dehydration and Bronsted acid sites are needed for further consecutive reactions of cyclohexanol. Ti-USY has both Bronsted and Lewis acid sites to the ratio of about 0.8 . It is very well known that the external surface of such zeolite is richer in extra lattice Al and Ti- species due to surface migration. Therefore external surface of Ti-USY has excess of Lewis acid sites and probably some basic sites due to Al_2O_3 and TiO_2. It will block the entry of cyclohexanol in to internal micropores where in Bronsted acid sites are situated. So at low temperature, cyclohexanol can not diffuse in to the micropores and so can not reach Bronsted acid sites to give consecutive reaction products. Therefore dehydration mainly occurs on the external Lewis acid sites. with some dehydrogenation due to some external basic sites. At moderate temperature of 200^{0}C, mainly dehydration activity predominates. At higher temperature, cyclohexanol can diffuse in to the internal Bronsted acid sites and consecutive reactions to form cyclohexene and other products become feasible. Time on stream of the reaction leads to the rapid fouling of these internal Bronsted acid sites and then only dehydration activity prevails.

In the table 5.16, data on dehydration of cyclohexanol at moderate temperature of 200^0 C over Fe-Ti-USY and acid treated USY are presented. The data show that Fe-Ti-USY has further improvement giving almost 100% selectivity to dehydrated product, cyclohexene. It is due to further diffusion constraint for cyclohexanol to reach internal

Table 5.16 : Dehydration of Cyclohexanol over Fe-Ti-USY and acid treated USY

TOS	Selectivity of products, % Catalyst = ('Fe-Ti-USY)				Selectivity of products, % Catalyst = acid extracted USY			
	Conv. (%)	Cyclo-hexene	Cyclo-hexanone	Others	% Conv	Cyclo-hexene	Cyclo-hexanone	Others
2h	99.69	98.6	0.35	1.05	99.28	98.83	0.41	0.76
4h	99.62	99.05	0.36	0.59	97.04	93.24	0.46	6.3
6h	99.9	99.42	0.28	0.3	92.24	86.72	1.19	12.09
8h	100	99.99	-	-	90.24	83.38	1.65	14.97
10h	99.99	100	-	-	80.14	80.14	4.33	15.53
22h	98.8	98.84	0.21	0.95	78.57	76.00	2.86	21.14
24h	98.35	98.35	0.23	1.42	75.56	73.26	2.45	24.29
	98.35							

Feed rate : 2 ml / h, amount of catalyst =1.5 g , N_2 as carrier gas = 20 ml / min, reaction temperature = 200^0C.

Bronsted acid sites. Acid extraction of USY will remove some of the external extra lattice Al species which will generate some external Bronsted acid sites, as well as removes the blockage of the micropores. So more of internal Bronsted acid sites are accessible to cyclohexanol to give consecutive reaction products. This activity also dies fast due to fouling of the Bronsted acid sites in due course of time on stream.

The results presented here on cyclohexanol reaction and acidity data obtained by FTIR of pyridine adsorption amply demonstrate the usefulness of this reaction to characterize the nature of acid sites on USY zeolites.

5.7: Conclusions

1) The FTIR spectra of surface hydroxyl groups and of adsorbed pyridine over Ti-USY indicate the generation of "super acid" hydroxyl groups and very strong, and stable Bronsted and Lewis acidity, richer in Lewis type compared to Bronsted type over USY, Ti-USY, Fe-USY and Fe-Ti-USY zeolites.
2) Cyclohexanol dehydration can be used as a test reaction to determine nature of acidity of Ti-USY zeolites.
3) Ti-USY is moderately active in hydroxylation of phenol to give catachol and hydroquinol, selectively active in methylation of O-toluidine to give 2,4-xylidine and in benzoylation of toluene to 4, methyl benzophenone.

4) Low. High and very high silica Ti-USY is promising catalyst for not only for hitherto known oxidation and photo catalytic reactions but also for hydrocarbon conversion reactions requiring very high acidity Some hydrocarbon reactions are reported here for the first time.

5) The acid strength distribution and catalytic activity show that USY has very strong and more of Bronsted acid sites whereas Ti-USY has very strong and more of Lewis acid sites.

6: REFERENCES

1 (a) R M Barrer, in " Zeolites and Clay Minerals as Sorbants and Molecular Sieves," Academic press, London, (1978).

(b) W M Meier, D H Olson, in, "Atlas of Zeolite Structure Types," Butterworth-Heinemann, London, (1992).

2 Lowenstein W, Am. Mineral, 39, P 92-95 (1954).

3 Barrer R M., "Hydrothermal Chemistry of Zeolites", Academic Press, New York (1982)

4 W M. Meier, and Olson, D H., Atlas of Zeolite Structure Types, 2nd revised edition, Butterworths, London, (1987).

5 Flanigen E M., Proc.of 5^{th} Int. Zeol. Conf, Ed. L.V. C. Rees, Heydon London, June 2-6, P 760 (1980).

6 Bragg W L, The Atomic Structure of Minerals, Cornell University Press, Ithaka, New York (1937)

7 Wilson S T, Lok B M , Messina C A , Cannan T R , and Flanigen E M., J. Amer. Chem. Soc, 104,1146-1147 (1982).

8 Davis M E, Saldarriage C, Montes C, Graces J, and Crowder C, Nature, 331, 968 (1988)

9 Estermann M Me, Cusker L B, Bacrlocher Ch, Morrouche A, and Kessler H , Nature, 352, 320 (1991).

10 Montes C, Davis M, J. Phys. Chem. 94, 6431 (1990).

11 Wilson S T, and Flanigen E, A C S Symp Ser, 298, 329 (1988).

12 Kraushaar C B, Horgervorst W J M, Andrea P R, Emeis C A, and Stork W H J, Stud. Surf. Sci. Catal. 69, 231 (1991).

13 Lok M., Messina CA, Patton R L, Gayek R T Cannan, T R, and Flanigen E M, US Pat. 4, 400, 870 (1984).

14 Barrer R M, Pure and Applied Chemistry, 51,1091 (1979).

15 Goldsmith J R, Min. Mag, 28, 952 (1952).

16 Szostak R," Molecular Sieves, Principles of Synthesis and Identification." Van Nostrand Rheinhold, New York, P 211 (1989).

17 Ratnasamy P, Kotasthane A.N, Shiralkar, V P, Thangraj A, and Ganapati S, in 'Zeolite Synthesis" ACS Symp. Ser. 398, 405 (1989).

18 Shizherg L, Wenyang X, Tao D, Yizhao Y, Taiyuang Gongye Daxue Xuebae (China).20, 17 (1989).

19 Kumar R, and Ratnasamy P, J. Catal., 121, 89 (1990).

20 Kumar R, Thangaraj A, Bhat, R. N. and Ratnasamy, P, Zeolites,10, 85 (1990).

21 Szostak. R, "Molecular Sieves, Principle of Synthesis and Identification." Van Nostrand Rheinhold, New York, P. 241 (1989).

22 Perego G, Bellussi G, Corno C, Taramasso M, Buonomo F, and Esposite A, in "New Development in Zeolite Science and Technology", Murakami Y, et. al, (Eds),Elsevier, Amsterdam, P 129 (1986).

23 Tielen M, Geelen M, Jacobs P A, in "Proce. Int. Symp. Zeolite", Siofolk, 1985, Acta Phys. Chem, 31,1 (1985).

24 Hayanshi S, Suzuki K, Shim S, Hayamizu K, and Yamamoto O, Bull. Chem. Soc Japan 59,52 (1985).

25 Scherzer J, in "Catalytic Materials", Whyte T E, et. al. (Eds), ACS Sympo. Ser; 248,157 (1984).

26 Ball W J, Barri S A I, Cartlidge S, Maunders B M, and Walker D W, in "New Development in Zeolite Science and Technology", Murakami, Y et. al, (eds) Elsevier, Amsterdam, P-951 (1986).

27 Shibata M, Kitagawa H, Sendoda Y, and Ono Y, in "Catalytic Materials", ACS Symp. Ser; 248, 717 (1984).

28 Ball W J, Bwyer J, Garforth A A, and Smith W J, in "Catalytic Materials", ACS Symp. Ser ; 248,137 (1984).

29 Chu C T, Chang C D, J. Phys. Chem, 89, 1569 (1985).

30 Coudurier G, and Vedrine J C, Pure and Applied Chemistry; 56, 1389 (1986).

31 Barrer R.M, Baynham J W, Bultitride F W, and Meier W. M, J. Chem. Soc.195 (1959).

32 Notary B, Stud. Surf Sci. Catal. 37, 413 (1988).

33 Ratnasamy P, and Kumar R, Catal .Today, 9,329 (1991).

34 Dyer A, in "An Introduction to Zeolite Molecular Sieves" Soc. Chem. Ind. London,186 (1967).

35 Prasad Rao P H R , Ramaswamy A V, and Ratnasamy P, J Catal. 137, 225 (1991).

36 Rigutto M S, and Van Bekkum H, Appl. Catal., 68, 21 (1991).

37 Li Gang, Guo Xinwen, Wang Xiangsheng, Zhao Qi, Bao Xinhe, Han Xiuwen, Lin Liwu. Applied Catalysis A: General 185, P 11-18(1999).

38 M A Camblor, A Corma, and J Perez-pariente, J. Chem. Soc. Chem.Commun. 557-559 (1993).

39 Charles B Khouw, and Mark E Davis, Journal of Catalysis, 151, 77-86 (1995).

40 R Castillo, B Koch, P Ruiz, and P Delmon, Journal of catalysis 161, 524-529 (1996).

41 M Taramasso G Perego, and B Notary, U.S.Pat.Oct.18 1983 4410501

42 W Holderich, M Hesse, and F Neumann, Angew. Chem. Inst. Ed. Engl. 27, 226(1988).

43 M Chatterjee, D Bhattacharya, N Venkatathri, and S Shivsanker, Catalysis Letters. 35,

P 313-326(1995).

44 M A Camblor, Michel Costantini, Avelino Corma, Laurent Gilbert, Patrica Esteve, Agustin Martinez, and Susana Valencia, Camb. Comm. 1339-1340(1996).

45 Sujit B kumar, S P Mirajkar, Godwin C G Pais, Pradeep kumar, Rajiv Kumar, Journal of Catalysis, 156,163-166 (1995).

46 A Thangaraj, M J Eapen, S Sivasankar, and P Ratnasamy, Zeolites, 12,

P 943-949 (1992).

47 Wilson S T, and Flanigen E M , ACS Symp. Ser. 298, 272 (1988).

48 El. Mekki , Malki Davidson A, Massiani P, Barthomeuf D, Che. M, Am-Chem. Soc, Div. Pet. Chem. 40, 114 (1995).

49 Rschetlowski W, Einicke, W D, Meier B, Brunner E, and Ernst H, Stud. Surf. Sci. Catal, 69 119 (1991).

50 Kucherov A V, and Slinkin A A, (a) Zeolites 8, 110 (1988) (b) 7, 4 (1987) and(c) 7, 38 (1987).

51 Yashima T, Yamagishi K, Namba S, Nakata S, and Asaoka S, Stud. Surf. Sci. Catal. 37, 175 (1988).

52 Sass C E, Chem X, Kevan L J, Chem. Soc. Faraday. Trans. 86, 189 (1990).

53 Kraushaar B, and Van Hoof, J H C, Catalysis Letters, 1, 81 (1988).

54 Hamden H, and Kilnowski J, Zeolite Synthesis, ACS. Symp. Ser; 398, 449 (1988).

55 Pauling, in "The Nature of Chemical Bond " Gaskhimizdat, Moscow (1947).

56 Davis M E, Saldarriage C, Montes C, Graces J, and Crowder C, Nature,329, 968 (1988)

57 Bogdan S, Heterg. Chem. Rev. 3(3), 203 (1996).

58 Van Balmoos R " Collection of Simulated XRD Powder Patterns for Zeolites, " Butterworths, London (1984).

59 Szostak R , " Molecular Sieves, Principle of Synthesis and Identification." Van Nostrand Rheinhold, New York , P 333 (1989).

60 Szostak R, " Molecular Sieves, Principle of Synthesis and Identification." Van Nostrand Rheinhold, New York, P 285 (1989).

61 Szostak R , "Molecular Sieves, Principles of Synthesis and Identification," (Van Nostrand Renold). P 17-18 (1989).

62 Townsend R P, in, "Introduction to Zeolite Science and Practice" ,Eds H.Van Bekkum E M Flenigen, and J C Jansen, (Elsevier) P 359-391 (1991).

63 Kelemen G, Lortz W, and Schoen G, J. of Material Science, 24, P 333-338 (1989).

64 Newsam J M, " Science," 231, P- 1093-1099 (1986).

65 Herron N, Wang Y, Eddy M M, Stucky G D, Cox D E, Moller K, and Bein T, J.Am.Chem. Soc.111, P 530-540 (1989).

66 Turro N G, and Garcia- Garibay M, in "Photochemistry in Organised and Constrained Media, "Ed. V Rammurthy, VCH P1-38(1991).

67 Pool Robert, The Smallest Chemical Plant and Science, 263, 1698-1699 (1994).

68 Charles B Khouw, and Mark E Davis, Journal of Catalysis, (61) P 30-39 (1995).

69 Herron N, Chemtech, P 542-548 (1989).

70 Collins S J, and O Malley P, J. J. Catal. 153, 94-99 (1995).

71 Tilman Beutel, J. Chem. Soc, Faraday Trans 94 (7), P 985-993 (1998).

72 Sankarasubbler Narayanan, K Deshpande, Applied Catalysis , 199, P 1-31 (2000).

73 Thomas J M , " Solid Acid Catalysts ", Scientific American P-112 (1992).

74 Flanigen E M, " Zeolite and Molecular Sieves," (Elsevier) P 13-34 (1991).

75 (a) Feng P, Bu X, and Stucky G D, Nature, 388, P 735-741(1997a).

Feng P, Bu X Tolbert S H and Stucky G D, J. Am. Chem . Soc. 119, P 2497-2504 (1997)b.

76 C V McDaniel and P K Maher, in "Moleculier Sieves", Society of Chemical Industry, London. P 186-195 (1968).

77 Skeels G W, Breck D W, Procedings of 6th International Zeolite Conference; Olson D, Bisio A, (Eds.) Buttesworths, Guilford, U.K , P 87 (1984).

78 Neuber M, Dondur V, Karge H G, Pachco L, Ernest S, Weitkamp Stud. Surf. Sci. Catal. 37, 461 (1988).

79 Cruz J M, Corma A, Fornes V, Appl. Catal. 1989, 50, 287 (1989).

80 Lony F, Lunsford J H, J. Catal . 136, 566 (1992).

81 Keer G T, J. of Phys Chem, Part 5, 72 (7) 2594 (1968).

82 Fejes P, Kiricsi I, Hannus I, Schobel , G Stud. on Surf. Sci. Catal. 10 , 305 , (1985).

83 Fejes P, Kiricsi I, Hannus I, Schobel G, Acta. Phys. Chem. Szegad. 31 , 119 (1985).

84 Derouane E G, Baltius L, Dessau R M, Schmitt K D, Stud on Surf. Sci. Catal , 10 , 305 (1985).

85 M Taramaso, G Perego, and B Notary; US Patent 4410501, (1983).

86 B Notary, Adv. Catal; 41,252(1996), J M Thomos, Philos Trans. R .Soc, 1990, A 333, 173, See also, Nature (London), 368, 289 (1994).

87 J S Reddy, R Kumar, Zeolites, 12 ,95 (1992).

88 D P Serrano, H X Li, M E Davis, J. Chem . Soc. Chem. Commun, 1, P 745 (1992).

89 A Tuel, Zeolites, 15, 236 (1995).

90 T Balasco, M A Cambler, A Corma, J. Perez- Pariente, J.Am. Chem. Soc. 115,11806 (1993).

91 A Corma, M T Navaro, J Perez- Pariente, F. Saricher, "Zeolites and Related Microporous Materials, State of the Art " in " Studies in Surface Science and Catalysis", J Whetcamp, H G Karge, H Pfeifer, W Holderich (Eds) Vol.81 Elsevier, Amsterdam, P 69 (1994).

92 B Kraushaar, J H C Van Hooff, Catal. Letters, 1, 81 (1988).

93 C Ferrini, H W Kouwenhoven,,) " Study in Surface Science Science and Catalysis," Centi , F. Trifiro (Eds), vol. 55; P 53 (1990).

94 G J Kim B R Cho, J H Kim, Catal. Letters, 22, P 259 (1993).

95 M S Rigutto, R de Ruiter, J P M Niederer, H Van Bekkum, in " Studies on Surf. Science and Catalysis, vol. 84, P 2245 (1994).

96 P J Kooyman, P Vander Waal, P A J. Verdaasdonk, K C Jansen, H Van Bekkum, Catal. Letters 13, 229 (1992).

97 J Class, K Kulawic, G Schulz-Ekloff, N I Jaeger, in "Studies on Surf Science and Catalysis, 84, P 2261 (1994).

98 D R C Huybrechts, I .Vaesen, H X Li, P A Jacobs, Catal .Letters, 8, 237 (1991).

99 G W Skeels, E M Flanigen," Zeolite Synthesis , in ACS Symp. Series, (M L Occelli, H E Robson (Eds), 398, American Chemical Society, Wanshington, P 420 (1989).

100 J S Reddy, A. Sayari, J.Chem.Soc, Chem. Comm, P 23 (1995).

101 J S Reddy, A. Sayari ,J .Chem.Soc.Chem.Comm.1, 24 (1995).

102 Hiromi Yamashita, Yo Fujii, Yuichi Ichiashi, Shu Gouzhang, Keita Ikeue, Dal Ryung Park ,Keiko Koyano,Takashi Tatsumi, Masakazu Anpo, Catalysis Today. 45, P 221-227(1998).

103 Xinsheng Liu, Kai-Kong Iu and J.Kerry Thoman J.Chem. Soc. Faraday Trans, 89, P 1861-1865 (1993).

104 Szostak. R;" Molecular Sieves, Principle of Synthesis and Identification." Van Nostrand Rheinhold, New York, P. 333 (1989).

105 Szostak R, " Molecular Sieves, Principle of Synthesis and Identification," Van Nostrand Rheinhold, New York, P. 285 (1989).

106 Mayers B L, Ely S R, Kutz N A, Kaduk J A, and Van Der Bossche E, J. Catal, 100, 555(1986).

107 Szostack R, Thoman T L, J. Catal. 100, 555 (1986).

108 Kraushaar C B, Horgervorst W J M, Andrea P R, Emeis C A, and Stork W.H.J, Stud. Surf. Sci. Catal. 69,231 (1991).

109 Perego G, Bellusi G, Corno C, Taramaso M, Buonomo F, and Esposito A, Stud. Surf. Sci. Catal, 28, 119 (1986).

110 Simmons D K, Szostak R, Agrawal P K, and Thomus T L, J. of Catal, 106, 287 (1967).

111 Klotz M R, U.S. Pat, 4, 299,808 (1981).

112 Pastore H O, Stein E, Davanzo C U, Vichi E J S, Chem. Comm, 772 (1990).

113 Flanigen E M "Zeolite Chemistry and Catalysis," ACS Monograph, (Ed) Rabo et. al, 171, 80 (1976).

114 Flanigen, E.M. and Khatami, H and szymanski, H.A, " Molecular Sieve Zeolite-1".ACS Monograph, 101,201 (1971).

115 Ward J W, Zeolite Chemistry and Catalysis, ACS Monograph, Rabo, J.A. (Ed),171, 118 (1976).

116 Flanigen E M, Zeolite Chemistry and Catalysis,ACS Monograph, Rabo J A, (Ed.) 171, 80 (1976).

117 Ward J W in "Zeolite Chemistry and Catalysis", ACS Monograph, Ed. Rabo et. al. 171, 181 (1976).

118 McDaniel C V, and Maher P K "Zeolite Chemistry and catalysis, ACS Monograph, (Ed) Rabo et. al, 171, 285 (1976) .

119 Kutz N, in " Heterogeneous Catalysis-11" Sharpiro B L, (Ed), P-121 (1984).

120 Szostak R, and Thomas T L, J. Catal. 101,549 (1986).

121 Szostak R, Nair V and Thomus T L, J. Chem. Soc. Faraday Trans-1, 83, 483 (1987).

122 Szostack R, and Thomas T L, J. Chem. Soc. Chem. Commun. 113 (1986).

123 Ward J W, Zeolite Chemistry and Catalysis, ACS Monograph, Rabo, J.A. (Ed);171, 118 (1976).

124 Jacobs P A, Bayer H K and Valyon, J. Zeolites, 1, 161 (1981).

125 Chu, C T-W. and Chang C.D, J. Phys. Chem. 89, 1569 (1985).

126 Jacobs P A and Von Ballmoos, J. Phys. Chem.86, 3050 (1982).

127 Topsoe N Y, Pedersen K and Deronaue E J, J .Catal. 70, 41 (1981).

128 Anderson M W, Klinowski, J. Zeolites, 6,455 (1986).

129 Janin A, Lavalley J C, Macedo A and Raatz F, Zeolite Synthesis, ACS Symp. Ser. 368, 117 (1988).

130 Jentys A and Larcher J A," Zeolites as Catalysts, Sorbents and Detergents Builders",Elsevier, Amsterdam,P 585 (1989).

131 Mirth G, Lercher J A, Anderson M W and Klinowski J, J. Chem. Soc. Faraday Trans –1, 86, 3039 (1990).

132 Jentys A, Warecka G, Derewinski M, and Lercher J A , J. Phys. Chem. 93,4837 (1989).

133 Decanio S J, Sohn J R, Fritz P O, Lunsford J H, J. Catal, 101, 132(1986).

134 Kevan L, in"Time Domain Electron Spin Resonance, Wiley- Inter Science, New York,1979, Chapt-8 (1979).

135 Goldfarb D, Bernado M, Strohmaier K G, Vaughen D E, Thomann H, Stud. Surf. Sci. Catalysis, 84, 403, (1994).

136 Klinowski J," Progress in N.M.R. Spectroscopy ",(Ed. Emsely, et. al.) Pregamon Press, GB. 17, 237 (1984).

137 Englehardt G and Michel D, High Resolution Solid State N.M.R. of Zeolites and Related Systems, John Wiley and Sons, London,(1987).

138 Lippmaa, E, Magi M, Samson A, Engelhardt G and Grimmer A R, J. Amer. Chem. Soc. 102, 4889 (1983).

139 Fyfe C A, Gobbi G C, Hartman J K, Klinowski J and Thomson J M, J. Phys. Chem, 86 , 1247 (1982).

140 Fyfe C A, Gobbi G C, Klinowski J, Thomas J M and Ramdas S, Nature (London), 296,530 (1982).

141 Engelhardt G, Lohase U, Lippmaa E, Tarmark M and Magi, M Z, Anorg. Allg. Chem; 482, 49 (1981).

142 Mastikhin V M, Zamarev K I Z, Phys. Chemie. (Neue Folge),152 ,332 (1987).

143 Muller D, Gessner W, Behrens H J, and Sheler G, Chem. Phys. Lett., 79 ,59 (1981).

144 Thomas J M, Fyfe C A, Ramdas S, Klnowaski J and Gobbi G C, J. Phys. Chem. 86, 3061 (1982).

145 Ramdas S and Klinowski J, Nature (London) 308, 521 (1984).

146 Benn R, Grondey H, Brevard C and Pagelot A, J .Chem. Soc. Chem. Comm. No 2,P102-103 (1988).

147 Whitington B I and Anderson J R, J. Phys. Chem, 95, 3306 (1991).

148 Ratnasamy P and Kumar R, Catal. Today, 9,324 (1991).

149 Kucherov A V and Slinkin A A, Zeolites 7, 43 (1987).

150 G J Ray, A G Nerheim and J A Dhonohue, Zeolites 8, 458-463, (1988).

151 Engelhardt G Z. Anorg. Allg. Chem., 482, 49(1981).

152 Klinowski J, J M Thomas,C A Fyfe and G C Gobbi, Nature 296, 533-536(1982).

153 Kasai P H, Bishop R J , "Zeolite Chemistry and Catalysis," ACS Monograph, (Ed) Rabo et. al, 171, 350-391 (1976).

154 Fajes F, Marsi I, Halas Z, Hannus H, Rockenbeker A, Gy Tasi Korecz L and Schobel Gy, Stud. Surf .Sci. Catal. 69 ,173 (1991).

155 Kornatowski J, Sychev M, Goncharuk V and Baur W H, Stud. Surf. Sci. Catal. 65, 581 (1990).

156 Rigutto M S and Van Becuum H, Appl. Catal. 68 ,L1 (1991).

157 Bocutti M R, Rao K M, Zecchina A, Leofanti G and Petrini G, Stud. Surf. Sci. Catal. 48,133,(1989).

158 Naval Kishor Mal, Ph.D Thesis , The University of Pune, India; Jan. 1997.

159 Centi G, Perathoner S, Trifiro F, Abousaus A, Aissi C F, Guelton M, J. Phys. Chem.. 96, 2617, (1992).

160 Ione K G, Vostrikova L A, Ptrova A V and Mastikhin V M, in Proceedings of 8th International Cong. on Catal, Berlin, 4, P 519 , (1984) .

161 R M Barrer and Langley D A, J. Chem Soc , 3804-3811, 3817, (1958).

162 Breck D W, " Zeolite Molecular Sieves, Structure, Chemistry and Use" Publ. Wiley Interscience, New York ,449 ,(1974).

163 Ga I G, Tankovic O, Makis S, Raoovanov P and Tadorovic M, Trans. Faraday Soc, 67 999, (1971).

164 Flanigen E M and Khatami H, Adv. Chem. Ser., 101, 76, (1971).

165 A I Vogel, Quantitative Inorganic Analysis, 2nd edition, Editor, The English Language Book Society and Longmans Green Company, P- 887-888.

166 Xinsheng Liu, Kai-Kong Iu and J.Kerry Thomos, J. Chem .Soc. Faraday Trans.559, 1861-1865(1993).

167 A A Grinberg, L V Shikheeva, Russian J. Inorg. Chem.5, 287(1960).

168 G Garralon and V Fornes and A Corma, Zeolites, 8, 269 (1988).

169 L J Bellamy in " Infra-red Spectra of Complex Molecules, ed. John Wiley & Sons, New Yark,1960,161-176(1960).

170 Joachim Klass, Gilnter Schulz- Ekloff and Nils I. Jager. J. Phys. Chem. B, 101, P 1305-1311(1997).

171 Shrinivasan S, Datye A K, Hampden-Smith M, Wachs I E, Deo G, Jehng J M, Turek A M, Peden C H F. J. Catal. 131, 260(1991).

172 Anpo M, Aikawa N, Kubokawa Y. Chem; Louis,C; Giamello, E. J.Phys.Chem. 89,5017(1985).

173 Ritala M, Leskela M, Nykanen E, Soininen P N, Jinisto L. Thin Solid Films, 225, 288(1993).

174 A Thangraj, R. Kumar, S P Mirajkar, P Ratnasamy. J.Catal., 130,1 (1991).

175 J S Reddy, R Kumar, P Ratnasamy. Appl.Catal.58, (1990)

176 M A Camblor, A Corma, J Perez-Pariente. J. Chem. Soc, Chem.Commn 557.(1993).

177 P Wu, T Komatsu, T Yashima. J. Phys.Chem.100, 10316(1996).

178 Yangdong Wang, Aimin Zhang, Qinhue Xu, Ranzhang chen. Applied Catalysis A:General 214 167-177(2001).

179 Szostak R, Nair V and Thomos T L. J.Chem. Soc. Faraday Trans 1, 83 ,487(1987).

180 Szostak R, Nair V and Thomos T L. J.Chem .Soc. Faraday Trans 2,83 487(1987).

181 (a)G P Schindler, P Bartl, W F Hoelderich,Applied Catalysis A:General 166 267-279 (1998) (b)H Chen,A Matsumoto, N Nishimiya, K Tsutsumi,157,295-305 (1991).

182 Zi G, Dake T, Ruiming Z. Zeolites, 8, 453 (1988),

182 Wichterlova B, Novakova J, Kukelhova L and Milkusik P, Zeolites 5 ,21(1985).

183 Joshi P N, Awate S V, ShiralkarV P. J. Phys. Chem. 97, 9749(1993).

184 DerouaneE G, Mestdagh M and Vivelvoye L., J Catal.33,169.(1974).

185 Mcnicol B D and Pott G T. J.Catal. 25, 223 (1972).

186 Ball W J et.al. in" Procedings of the 7th International Conference on Zeolites" "(Eds.J.Murakami et,al.) Kodansha,Tokyo, Material Research Society,P.137,(1986).

187 Derouane E G, Mestdaugh and Vielvoye L, J.Catal, 33,169(1974).

188 P J Kooyman, P Van der Waal, PA J Verdaasdonk, K C Jansen, H VanBekkum., Catal. Letters 13, 229(1992).

189 Abraham A. in " The Principles of Nuclear Magnetism." Clarendon Press Oxford,(1961)

190 Ganapati S, Schramm S and Oldfield E.Chem.Phys.Lett.169,301-306,(1990).

191 Engelhardt G and Michel D. High- Resolution Solid State NMR of Silicates and Zeolites ,john willey and sons Ltd; 216 (1987).

192 Frydman L and Harwood J S. J.Am.Chem.Soc.117, P 5367-5368(1995).

193 Llora.and Virlet J. Chem. Phys. Lett.152P-248(1988).

194 L.Frydman and J S Harwood. J. Am.Chem.Soc, 117, P.5379 (1995),

195 AmoureuxJ. P, Fernandez C and Steuernagel S. J of Magn.Reson.123, P 116-118(1996).

196 Bodenhausen G Prog. NMR Spectroscopy 14, P 127(1981).

197 J P Amoureux, C Fernandez and S Steurnagel. J.of Magn.Reson,123, P-116(1996).

198 D States, R Haberkorn and R Ernst. J. of Magn.Resonance;92, P 577(1984).

199 EiichiFukushima and Stephen B W, Roeder. Experimental pulse N.M.R.-A nuts and bolts approach; Addison Wesley ;USA; P 407-415(1981).

200 Colin A, Fyfe J L, Bretherton and L Y Lam. Chem. Comm, P 1575(2000).

201 Colin A, Fyfe J, L Bretherton and L Y Lam. J.Am.Chem.Soc;123, P 5285(2001).

202 G Engelhardt, Berlin and Leiozig. John wiley and sons, P 216(1987).

203 Ian E Maxwell,Wilbert A,Van Erp,Gary R Hays,Ton Couperus,Rob Huis, and A Derek H Clague, J.chemical society, Chem. Comm,Vol-9, P 523-524(1982).

204 Q L Wang, G Ganneto, M Torrealba, G Perot,C Kappenstein, and M Guinset, J. Catalysis, 130, P 459(1991).

205 C Sivadinarayana, V R Choudhary, R Vetrivel, S Ganapati. Solid State Nuclear Magnetic Resonance, 13, 175-182(1998).

206 C A Fyfe, H Grondey, Y Feng, G T Kokotailo. J. Am. Chem. Soc 112; 8812(1990).

207 J Klinowski,J M Thomas,C A Fyfe, and G C Gobbi Nature, 296, P 533-536(1982).

208 Wang Yang-Dong et al. Acta Chimica Sinica, 58, P 656(2000).

209 S M C Menezes, J P Amoureux et al. Applied Catalysis, 207, P 367(2001).

210 M W Anderson, J Rocha, L Orion and A Fereira. Microporous material, 6, P 195(1996).

211 (a)Andrea Labouriau and William L Earl. Chemical physis letters,270, P 278(1997).

(b) A lopez, M H Tuilier, J L Guth, L Delmotte and J M Popa. Journal of Solid State Chemistry,102,P 480-491, (1993).

212 T Blaco, M A Camblor, A Corma and J Perez-Pariente. Ame.Chem.Soc.1993, 115,No.25,11806-11813(1993).

213 Bhelekar A A, Das T K, Choudhar K, Hegde S G, Chandwadker A J. Stud.Surf.Sci.Catal;113, 95-200,(1998).

214 He, Dehua Zhu, Qiming Xu, Qiang Masahiro, Fujiwara Souma, Yoshie SOURCE Ranliao Huaxue Xuebao, 26(3), 197-202 (Chinese) 1998.

215 A R kaur. Ph.D,Thesis Poona University; P 101-113(1999).

216 Z Liu, J Tobora, R.J.Davis. J.Catal; 109, 174(1988).

217 I Willner, Y Eichen, A J Frank. J.Am.Chem.Soc.111; (1989).

218 V Auguqliero, L Palmisano, M Schiavello, A Scalfani. Appl. Catal. 69, 323(1991).

219 Mirodatos C, Barthomeuf D. J.Chem.Soc.Chem.Commun; 39, (1981).

220 O Cairon, K Thomas, T Chevreau. Microporous and Mesoporous Materials, 46; 327-340(2001).

221 Parry E P. J. Cat., 371 (1963).

222 Ocelli M C, Schweizer A.E, Fild C, Schwering G, Eckert H and Auroux. H. J.Cat. P 119-127. (2000).

223 Hegde S.G, Ratnasamy P, Kustov L M, Kazanskey V B. Zeolite, 1,137(1988).

224 B Satyavathi, A Patwari, U T Bhalerao. U.S.Patent, No.5, 986, 138. (1999).

225 P S Singh, R Bandyopadhyay, B S Rao, Applied Catalysis,136(2) 177(1996).

226 Rita H, Hardy and Burtron H, Davis. J.Catalysis; 11,146-151 (1988).

227 S Narayanan, K Deshpande . Applied Catalysis A: General, 199, 1-31(2000).

228 Chen Li-Yu, Zhang, Xiu-Cheng, Dong Wu, Chen Hu-Kui (chines) Fine Chemials, vol.17, No.2; (2000).

229 Chen Li-Yu,Zhang, Hiou-Chang, Dong Wu, (chines) Chemical Reaction Engineering and Technology, vol. 16, No. 2, (2000).

230 P S Singh Ph.D. Thesis, University of Pune, P 227-277(1996).

231 R Fang, G Harvey, H W Kouwenhoven, R Prins. Applied Catalysis A, General, 130,P 67-77 (1995).

232 A Corma, M J Climent, H Garczia and J.Primo. Appl. Catal 49, 109. (1989)

233 G Harvey, A Vogt, H W Kouwenhoven and R Prins in R.von Ballmoos, J.B.Higgins and M.M.J Treacy (editors) Proc.9th Inter. Zeolite Conf; vol.II,Butterworth, Boston, P-363(1992),

234 B Chiche, A Finiels, C Gauthier, P Geneste, J Graille and D Pioch. J. Org. Chem, 51, P 2128. (1986),

235 A P Singh, D Bhattacharya, S Sharma. J.of Molecular Catal.A. Chemical 102, P 139-145(1995).

236 K Tanabe, T Yamaguchi, K Akiyama, A Mitoch, K Iwabuchi and K Isogai, Proc.8th Int.Congress on Catal, Berlin, Verlag Chemi, Berlin, P 601(1984).

237 K Arata and M Hino. Appl .Catal 59, (1990), 197 (1990).

238 K Arata, K Yabe and I Toyoshima. J. Catal, 44, 385(1976).

239 B Notari. Advances in Catal, 41, 252 (1996).

240 J M Thomas, Philos. Trans. of Royal. Soc. A, 333, 173(1990).

241 Bellussi G, Carati A, Clerici M G, Maddinelli G, and Millini R, Journal of Catalysis, 133, 220-230 (1992)

242 T Maschmayer, F Rey, G Sarkar and J M Thomas. Nature, (London) 378,159(1995).

243 H G Karge, H Kosters and Y Wada. In Proc. sixth Int.Conf; O.Olson and A.Bision(Eds) Reno, Butterworths P 308 (1984).

244 J A Lercher, C Grunding and G Edel-Mirth, Catal. Today, 27,353 (1996).

245 J Datka, B Gill, Vogt and Rakoczy. Studies in Surf. Sci. and Catal.vol.125, P 409-415(1999).

SUMMARY

Zeolites are fascinating class of solids, which have played key role in the vigorously growing impact on the world economy in the twentieth century. Among all synthetic and natural zeolites, Faujasite type-Y is the single largest type of zeolite used daily in hundreds of tons in petrochemical industry today. In practice ,Zeolite Y is hydrothermally dealuminated by treating in presence of steam at high temperature to obtain ultra stable Y(USY) and then modified by ion exchange, acid extraction and additives. USY is highly acidic and structurally very stable. Recently, incorporation of Ti in the framework of USY has also been attempted to expand the scope of USY as acid-base catalyst with simultaneous oxidizing activity. Ti-USY can find increasing use as oxidizing catalyst for bigger molecules. The study is limited to very low silica Ti- USY and very preliminary in nature. Therefore, the present study was undertaken. The Ti-USY was prepared by controlled hydrothermal dealumination, then aluminum extraction and treatment with potassium titanyl oxalate. Co-incorporation of Fe also has been attempted. The resulting product contained many types titanium species like Ti^{4+} in the framework, TiO^{+} cations in exchangeable positions, TiO_2 nano particles in the micropores and TiO_2 clusters in the system, all of which have been characterized. Special attempt has been made to prepare very high silica Ti-USY and to characterize them using "Multiple Quantum Magic Angle Spinning (MQ-MAS)" high resolution solid state NMR spectroscopy. In addition, we have also used XRD, SEM, TG/DTA, UV/VIS, FTIR and ESR spectroscopic methods. The catalytic activity for some oxidation and acidic reactions like O-toluidine methylation, phenol oxidation, cyclohexanol dehydration and benzoylation of toluene has been correlated with surface acidity determined by FTIR of adsorbed pyridine.

Three series of Ti-USY samples were prepared : (i) for preparing low silica Ti-USY in single step called SSTP method, NH_4-Y was treated with different proportions of dilute solution of potassium titanyl oxalate. $[K_2TiO(C_2O_4)_2]$ at 25^0C. $K_2TiO(C_2O_4)_2$ establishes ionic equilibrium, $K_2TiO(C_2O_4)_2$ $[K_2]^{2+}\ldots(C_2O_4)^{2-}$ + $(TiO)^{2+}\ldots(C2O4)^{2-}$ under the pH conditions (pH 3 to 4) of the reaction. Oxalate ions react with Al in the

framework extracting Al as soluble aluminum oxalate and sillanol nests in the zeolite. The $(TiO)^{2+}$ ions then react with silanol nests putting Ti in the vacated tetrahedral positions forming Ti-USY. (ii) for preparing high silica Ti-USY, multiple step method called MSTP method, was used. NH_4-Y is dealuminated moderately by steam treatment at 550^0 C, then reacted with $K_2TiO(C_2O_4)_2$ solution at 25,55 and 200^0C to prepare a series of samples. The reactions taking place in MSTP method are similar to those in SSTP method, except that the higher extent of dealumination takes place putting higher amount of Ti in the framework. In this case, $K_2TiO(C_2O_4)_2$ solution was reacted with already considerably dealuminated USY which has more of readily available silanol nests and defect sites.(iii) the very high silica Ti-USY was also prepared by MSTP method and by $K_2TiO(C_2O_4)_2$ solution following similar procedure. The difference is that a very highly dealuminated USY sample was used in this case. Here also, Ti incorporation was much more because of the very highly dealuminated starting USY sample. Fe containing Ti-USY was also prepared similarly using ferric ammonium oxalate $[(NH_4)_3Fe(C_2O_4)_3]$ solution. Two other Ti sources namely titanium butoxide $[Ti[OCH(CH_3)_2]_4]$ and titanium isopropoxide $[Ti[O(CH_2)_3CH_3]_4]$ were also used for preparing very high silica Ti-USY.

The Ti-USY samples were characterized using many spectroscopic techniques all of which were investigations on the nature of Ti species in Ti-USY. XRD patterns of Ti-USY indicated very good crystallinity and the relative intensity of different peaks varied as per the variation in the framework composition. In the table below, the chemical composition of the framework determined by ^{29}Si MAS NMR and the unit cell constant and the unit cell volume determined by XRD patterns of important Ti-USY samples are compared with the parent USY and NH_4-Y samples.

	Name of the sample	Results of XRD		ts of MAS NMR	
		Unit cell const.	Unit cell volume	Framework Si/Al	Framework Si/Al+Ti
1	Na-Y	24.71	15093	2.40	-
2	NH_4Y	24.68	15036	2.56	-
3	Low silica Ti- USY	24.50	14718	-	2.43
4	High silica USY	24.38	14493	8.75	-
5	High silica Ti-USY	24.23	14580	-	6.2
6	Very high silica USY	24.22	14202	26.3	-
7	Very high silica Ti-USY	24.25	14260	-	17.0
8	Very high silica Fe-USY	24.23	14233	12.65	

The values for the samples 2 and 3, 4 and 5, 6 and 7 have to be considered for comparison. The decrease in the unit cell constant inspite of the increase in the number of Al+Ti in the framework compared to that of Al in parent USY indicates that a substantial number of Ti is incorporated in the Ti-USY framework. SEM photographs indicate that Ti-USY samples are highly crystalline. In the UV/VIS spectra of Ti-USY, the strong absorption bands around 215,230 and 280 nm are observed which are attributed to the monomerically substituted Ti in the framework at mono, bi and multi functional silanol, siloxane or defect sites. In addition to the monomeric Ti species, those samples containing high amount of Ti also show the presence of nano-sized TiO_2 species which has absorption in the region of 300-500 nm. FTIR spectroscopic studies provide evidences for Ti substitution in USY. (i) NH_4-Y and USY samples after treatment with $K_2TiO(C_2O_4)_2$ solution but before calcination show the evidence of oxalate species interacted with the surface,(ii) The spectra of calcined samples show a band around 940-960 cm^{-1} characteristic of Si-O-Ti linkages,(iii) Characteristic framework vibrational bands of Ti-USY shift to low wave numbers as per the framework dealumination.(iv) the spectra become sharper and stronger in Ti-USY indicative of high degree of ordering. TG/DTA analysis show the evidence for the presence of oxalate species on un calcined Ti-USY samples. The samples become more and more hydrophobic as indicated by less amount of water loss in Ti-USY samples. The TG/DTA curves also show that the exothermic structural collapse temperature of Ti-USY is higher than that for USY.

Very strong evidence for Ti incorporation in USY was gathered by detailed studies by solid state MASNMR studies. In the present study, we have used ^{27}Al and ^{29}Si MAS NMR, as well as ^{27}Al 3Q-MAS NMR, to study the structural characteristics in relation to the framework stability of the prepared USY materials. We also address the hetero-atom substitution in USY by Ti (using different Ti sources) through ^{27}Al and ^{29}Si MAS NMR and also by ^{49}Ti NMR and compare the results with the Ti free USY. While conventional ^{27}Al MAS NMR can be used to distinguish tetrahedral and octahedral aluminum environments, it is not possible to get information about the nonequivalent aluminum sites within these coordinations (four, six). Moreover, the penta-coordinated aluminum is "invisible" in MAS spectra. In order to characterize the aluminum environments fully, a new technique called "Multiple Quantum Magic Angle Spinning" (MQ-MAS) has been recently discovered. In the present thesis, we have used both conventional ^{27}Al MAS as well as ^{27}Al MQ-MAS techniques to fully study USY and Ti-USY. For ^{27}Si MAS NMR, as the natural abundance of ^{27}Si nuclii is small (4.7%) but sufficient to get resolved spectrum because, homo polar Si-Si dipolar broadening becomes negligible due to low natural abundance of ^{27}Si. The silicon tetrahedral environments designated by the signals of Q_4[4Si], Q_4[3Si,1Al], Q_4[2Si,2Al], Q_4[1Si,3Al] and Q_4[0Si,4Al] are distinctly observable since each aluminum substitution in the zeolite lattice shifts the ^{29}Si signal by approximately 5 ppm in the down field direction. The framework Si/Al is calculated using the formula

$$\left(\frac{Si}{Al}\right)_{FW} = \sum_{n=0}^{4} I_{Si(nAl)} \Big/ \sum_{n=0}^{4} \frac{n}{4} I_{Si(nAl)} \qquad (7)$$

In the literature, there seems to be a lack of unequivocal evidence for the isomorphic substitution of Ti in the lattice of zeolite. In the case of zeolite Y there is only one very recent report by Wang Yang dong *et al* (205) on the preparation and characterization of Ti containing USY zeolites. However, ours this is the first attempt to study Ti-USY using NMR technique.

Ti offers two magnetically active nuclei whose gyromagnetic ratios are close to each other to give a 2% increase in the Larmor frequency for the ^{49}Ti nucleus. Essentially one detects both ^{47}Ti and ^{49}Ti in the same experiment. They are quadrupolar belonging to

n/2 family I = 5/2 for ^{47}Ti and I = 7/2 for ^{49}Ti. When the Ti environment is highly symmetric, as would happen in the tetrahedral framework, the quadrupolar coupling may not be that large due to small value of electric field gradient. With this consideration we have attempted the ^{47,49}Ti static experiments on Ti-USY.

The nature of acidity and catalytic activity for hydrocarbon reactions over very high silica Ti-USY, to our knowledge, has not been published so far.The FTIR spectroscopy of adsorbed pyridine has been used as characteristic tool to detect and measure the presence of Bronsted and Lewis acid centers. The catalytic activity for oxidation of phenol by H_2O_2, cyclohexanol conversion, o-toludine isomerization and benzoylation of toluene were tested and correlated with the acidity. The surface hydroxyl species are drastically modified by dealumination and Ti incorporation as can be seen from the table below.

S.No	Frequency of -O-H vibration, cm^{-1}	Assignment	Reference
1	3745-3740	Terminal Silanol groups (Si-O-H)	115
2& 3	3695, 3675,3700	Extra framework aluminum species, dehydroxylated sites near Na^+ cation	220
4	3640, 3550-3540	High frequency (HF) and low frequency (LF) bridging hydroxyl groups [Si- (O-H) -Al]	115
5&6	3625-3620	High frequency (HF) bridging hydroxyl groups [Si-(O-H)-Al] shifted due to dealumination	219
7	3600	High frequency bridging hydroxyl group [Si-(O-H)-Al] shifted due to perturbation by nearby extra lattice aluminum species	219
8	3500-3200	Hydrogen bonded silanol hydroxyl groups [Si-(O-H)….(O-H)-Si]	115

The decrease in bridging hydroxyl groups and increase in silanol groups in general apart, the formation of new hydroxyl groups at 3700 cm^{-1} attributed to the hydroxyl groups on defect sites near exchangeable cations and 3600 cm^{-1}attributed to Bronsted acid sites perturbed by"NMR invisible"penta-coordinated Al species known to be"super acid sites"are noticed. In addition, HF and LF bridging hydroxyl groups at 3640 and 3540 cm^{-1} are shifted to low wave numbers to 3622 and 3520 cm^{-1} due to perturbation by nearby

extra-lattice Al species. In the FTIR spectroscopy of adsorbed pyridine, the ir bands of pyridine of interest to this study are the C-H and N-H stretching as well as the GC and the C-N stretching in pyridine ring. Due to the unshared pair of electrons, Nitrogen in pyridine accepts a proton of the Bronsted (B) acid sites forming pyridinium ion and shares a pair of electrons with the Lewis (L) acid sites coordinating to it. The combination mode vibration involving C-N stretching and N^{+}-H deformation in pyridinium ring gives a unique band at 1540 cm^{-1} the concentration of which is related to the B acid sites and a band at 1450 cm^{-1} is related to coordinated pyridine on L acid sites. Our results indicate that the number of B acid sites decreases and the strength of it increases by hydrothermal dealumination. For a very high silica USY and Ti-USY, the both B and L acid sites are equally stable, the number of L sites being more than B sites.

In order to characterize the nature of acidity further , Cyclohexanol dehydration as a test reaction was done over USY, Ti-USY and Fe-Ti-USY. Cyclohexanol dehydrates to cyclohexene and water on weak acid sites, and cyclohexene undergoes consecutive reaction on stronger acid sites to methyl cyclopentene, cyclohexane, methyl cyclopentane, and benzene. The comparison of activity with ã-Al_2O_3 shows that L sites give only cyclohexene (dehydration) and B sites give isomerized products like methyl cyclohexene and disproportionated products like cyclohexane and methyl cyclohexane. The influence of temperature in the range 150-300^0 C and time on stream up to 24 hours were studied.

Studies on the benzoylation of toluene by super acids like heteropoly acids, metal sulphated oxides like Al_2O_3, ZrO_2, TiO_2, Fe_2O_3 have been reported, but they are not shape selective catalysts. USY zeolites show nature of super acidity as demonstrated by FTIR results as well as shape selectivity because of their micropore structure. There fore we have tested USY and TI-USY catalysts for Benzoylation of Toluene to produce methyl benzophenones. The Maximum selectivity of 84% for 4-MBP is obtained for Ti- and FE-Ti-USY samples where as it is only 66% for USY. However, it is considerably more than other catalysts reported in the literature. In this reaction, benzoyl chloride is forming acid salt on the surface of acidic zeolite forming electrophile ($C_6H_5CO^{+}$) which attacks on the aromatic ring and condenses with toluene liberating HCl and forms methyl benzophenone. The presence of extra lattice Al, Ti and Fe species in the

micropores are responsible for the high activity and selectivity of USY catalysts for the reaction.

Alkylated aromatic amines are industrially very important. Many solid catalysts have been reported, particularly, clays, bauxite and alumina modified with many metal oxides have been widely used .Microporous materials like zeolites and ALPO-s are also used. In the alkylation of aromatic amines, the product distribution solely depends up on the preponderance of the interaction of zeolite with the lone pair of electrons on N in amine group or with the ð electrons of aromatic ring. So, on a series of modified USY zeolites, where in, variety of active sites like Bronsted and Lewis acid sites, defect sites and extra frame work Al species are present, the interaction is a very complex process. Methylation of O-toluidine by methanol gives mainly, N-methyl O-toluidine, N,N-dimethyl O-toluidine,2,4-xylidine,2,6-xylidine,N-methyl xylidine, N,N-dimethyl xylidine and 2,4,6-trimethyl aniline. Among them, the major products are N-methyl O-toluidine, 2,4-xylidine, N-methyl xylidine and 2,4,6-trimethyl aniline. The reactions ware carried

out on USY,TI-USY and Fe-Ti-USY and compared with ã-Al_2O_3. The influence of temperature from 250^0C to 450^0C, rate of toluidine from 5 to 0.2, mol ratio of methanol to toluidine from 10 to 0.2 and time on stream up to 14 hours were studied. From the results of methylation of O-toluidine on USY zeolites, it is clear that the reaction is very complex, consisting of parallel reaction of Galkylation and N-alkylation and net work of consecutive reactions involving both C- and N- dialkylation, disproportionation, and N C transformations. The mechanism of methylation of O-toluidine over Ti-USY must consider both B and L acid sites. Despite the adsorption of toluidine is electronically most favored through strongly basic amine groups via unshared electrons of N atom, adsorption of methanol via basic oxygen over very strong Bronsted acid sites can also take simultaneously. So C- and N-methylation primarily occur simultaneously, which through further parallel and consecutive reactions leads to other C- and N N-alkylation products. From these studies, it is demonstrated that USY and Ti-USY is very good catalyst for the selective alkylation of O-toluidine to 2,4-xylidine.

Oxydation of phenol by H_2O_2 was chosen as a test reaction for evaluation of Ti-incorporation in USY zeolites. The product distribution in the reaction over acid leached very high silica Ti-USY samples of two compositions is compared with that over H-Y zeolite. Ti-USY samples give more than 50 % conversion compared to only 2% over H-Y sample.The feasibility of oxidation by H_2O_2 itself suggests that Ti is incorporated in the framework of USY. It is now commonly accepted that the active sites in such reactions are Ti which has to be 4-coordinated and in case of surface grafted Ti species, it should be attached to 3 silanol groups and has one -OH group as the 4^{th} ligand Due to larger three dimensional pores of USY with secondary pores , that allow bulky transitional state species, the selectivity in the reaction is not observed.

Important conclusions

1. Preparation and properties of low, high and very high silica Ti-USY from NH_4-Y and $K_2[TiO(C_2O_4)_2$ are reported for the first time. Our MAS NMR studies provide the direct evidence for the Ti substitution in the framework of zeolite for the first time.
2. The substitution of Ti in the framework of low to very highly silicious USY is confirmed from XRD, FTIR, MAS NMR,TG/DTA results and catalytic hydroxylation activity.
3. In the present study, we have used ^{27}Al and ^{29}Si MAS NMR, as well as ^{27}Al 3Q-MAS NMR, and ^{49}Ti NMR to understand the structural characteristics in relation to the framework stability and the heteroatom substitution of Ti (using different Ti sources) in USY and compare the results with the Ti free USY.

4) ^{27}Al 3Q-MAS results not only show that(Al^V) species are not only the stabilization species, but conclusively show that ultra-stabilization is accompanied by the formation of a new tetrahedral Al species in additon to the distribution of a part of the framework aluminum into the non-framework (due to dealumination) and 'invisible' (Al^V) positions.

5) Ti incorporation by reaction with $K_2TiO(C_2O_4)_2$ solution does not creat (Al^V) species

6) In the ultrastabilization process, Si tetrahedra are reinserted in the "silanol nest" defect sites generating a new ^{27}Si resonance, at -110.0 to -111.2 ppm for the siliceous silicon Si(4Si, 0Al) which are different than parent Si sites and are highly distorted.

7) Another new set of resonances occur at -101.38, -95.52 ppm and -90.0 ppm. which we reckon that these new set of resonances must arise from silicon environments of type Q^4(Si,Ti). This observation suggests that Ti substitution probably occurs at the siliceous sites avoiding Al-O-Ti linkages as per Lowenstein"rule. We believe that this is the first direct evidence from ^{29}Si MAS NMR about the presence of lattice titanium in Ti-USY.

8) We have attempted $^{47,49}Ti$ MAS NMR using spin-echo technique for very high silica Ti-USY and pure TiO_2 (rutile). The difference spectrum gives titanium

signal due to titanium incorporated in the zeolite lattice. The observed titanium must correspond to octahedral titanium since tetrahedral titanium gives broad spectra. Coordination of Ti to 4 Si and OH groups can give such an octahedral geometry.

9) The FTIR spectra of surface hydroxyl groups and of adsorbed pyridine over Ti-USY indicates the generation of "super acid" hydroxyl groups and very strong, and stable Bronsted and Lewis acidity, richer in Lewis type compared to Bronsted type.
10) Cyclohexanol dehydration can be used as a test reaction to determine nature of acidity of Ti-USY zeolites.
11) Ti-USY is moderately active in hydroxylation of phenol, selectively active in methylation of O-toluidine to give 2,4-xylidine also in benzoylation of toluene to 4, methyl benzophenone.